ABSTRACT

FUNDERBURK, PHILLIP MICHAEL. Development of High Level Control, Monitoring, and Communication Strategies for Battery Energy Storage Systems (BESS) Integrated with Renewables, Electric Vehicles, and Power Grid Systems. (Under the direction of Alex Huang.)

Energy storage devices are becoming increasingly popular for new age power grids, including smart grids and micro grids, which are adapting to include renewable energy resources and plug in electric vehicles (PEV's). Specifically, batteries of varying chemistries are being investigated and introduced into the existing power and transportation infrastructures. Batteries cannot only accompany a renewable energy source or PEV, but also supply backup power or supplementary support to the existing power grid when in need. For these reasons, batteries will become a huge research and industrial topic over the next few decades, and consequently, infrastructure and control strategies will need to be developed to effectively integrate them into our existing systems.

This dissertation will cover three main topics related to high level integration of Distributed Energy Storage Devices (DESD) and Battery Energy Storage Systems (BESS) into the current power grid. The first topic will investigate the development of a Human Machine Interface (HMI) with bi-directional Electric Vehicle (EV) charger. A lab ready charger was developed by PhD candidate Xiaohu Zhou under the guidance of Dr. Alex Huang at North Carolina State University (NCSU). Previously, no HMI was integrated into the charger's functionality and all control and monitoring processes were facilitated by large oscilloscopes and advanced computer programs. An HMI was developed in National Instruments' LabVIEW and could properly monitor and control a battery charging process, real-time, with zero to little programming knowledge. This thesis investigates the use of the HMI to simplify advanced computational processes for a typical user. The HMI undertakes high level translation between human commands and machine language, and properly monitors and controls high level processes of the charger.

The second topic of this thesis will cover peak shaving and cost cutting algorithms for residential and small scale industrial daily loads. The integration of a BESS with a smaller utility customer can be best utilized for cost cutting through a time of use (TOU) rate structure, which includes different energy rates for peak and off peak demand periods. This dissertation will investigate a dynamic programming (DP) approach which optimizes a daily pre-determined maximum peak to reduce peak demand. Overall, results will show optimal seasonal peaks for all size households and optimal battery capacities. A payback period will be investigated for the initial cost of the DESD. Also, differences in peak and off peak energy rates will be investigated to provide proper savings and incentives for customers to enroll in the TOU option.

The third topic of this thesis will cover dispatchability of solar power with the integration of a DESD. PV power output prediction will utilize an hourly dispatch rate with predictions based on a PV's previous hour power output. Rule based control will command the DESD to either dispatch power to meet a predicted power level, or store extra energy which falls above the dispatch level. Simulations will be based on a Greensmith 6kW DESD [27][28] and the FREEDM 40kW PV array (see fig A.1). Actual real-time experiments will combine these physical devices' in a LabVIEW based environment for monitoring and control. Results will determine the feasibility of dispatchable solar with DESD integration and suggest necessary improvements.

Development of High Level Control, Monitoring, and Communication Strategies for Battery Energy Storage Systems (BESS) Integrated with Renewables, Electric Vehicles, and Power Grid Systems

by
Phillip Michael Funderburk

A thesis submitted to the Graduate Faculty of
North Carolina State University
in partial fulfillment of the
requirements for the Degree of
Master of Science

Electrical Engineering

Raleigh, North Carolina

2011

APPROVED BY:

Srdjan Lukic

Mo-Yuen Chow

Alex Huang
Chair of Advisory Committee

DEDICATION

First and foremost to my advisor Dr. Alex Huang. His support and funding of my work over the past two years has been unwaivering and progressive. He encouraged me to discover a thesis topic and allowed a creative engineering pursuit to my work. To my supportive family and friends who have helped me in uncountable ways during the past two years. Thank you for your unconditional support. Specifically dedicated to Mom, Dad, Katie, Kari, Eric, Olivia, and Pinky. Finally, I dedicate this dissertation to Christopher Stewart, who not only provided me guidance and perspective throughout the process of graduate school, but also taught me with his actions and demeanor to appreciate everyone and everything in life. RIP

BIOGRAPHY

The author, Phillip Michael Funderburk, was born in Raleigh, North Carolina in 1986 to parents Lorna Brooks and William Funderburk, with one older sister, Katie Alice Guess. After attending Athens Drive High School and graduating in 2004 with honors and participation in academic and non-academic clubs, he began attending North Carolina State University in the fall for an undecided engineering major.

NC State played a huge role in Phillip's life. Growing up, he was raised a Wolfpack fan by his father, who also attended NCSU and graduated with a BS and MA in architecture in the 1970's. Phillip realized that he wanted to be an engineer early on with his strong interest in electronic devices, including computers, video games, electronics, and music. For this reason, he decided to focus on computer and electrical engineering as his undergraduate majors.

Highlights of Phillip's undergraduate career include internships and advanced projects. Phillip obtained 2 scholarships during his tenure as an undergraduate. He would like to thank Duke Energy and the TJ Fischer Foundation for their financial support in his studies. Phillip obtained his first internship with Siemens Healthcare in early 2007. He worked with the finance team and was a technical specialist in data management, report optimization, process automation, and networking reports. For his senior design project, Phillip worked with Dr. Stephen Walsh and Dr. Thomas Miller of the Engineering Entrepreneurship Program (EDP) to develop an advanced final project with three of his student colleagues.

During the summer of 2008, Phillip worked as a Research Undergraduate (REU) for The Center for Remote Sensing of Ice Sheets (CReSIS) at Kansas University. During the two month experience, Dr. Chris Allen and other graduate students assisted Phillip in learning the basics of graduate research through large projects, seminars, and a term project. The goal of the center was to study ice sheet behavior to observe the effects of global warming in uninhabited, ice covered areas of the world. The program encouraged Phillip to consider graduate school for studies which not only encompassed engineering, but also satisfied his desire to decrease human consumption of natural resources in order to a preserve a healthy planet.

The Future Renewable Electric Energy Delivery and Management Systems Center (FREEDM), a generation 3 Engineering Research Center based at North Carolina State University, presented an excellent opportunity to study electric power systems, motors, solid state devices, and other power related topics, while also conducting research on the integration of renewable and sustainable energy sources into traditional power grids and residential households. The FREEDM Systems Center not only provided funding, resources, guidance, and training for sustainable grid solutions, but also presented many new leadership opportunities which Phillip naturally fit into. As the Outreach Coordinator of the Student Leadership Council, Phillip worked with

Dr. Lisa Grable to organize renewable energy labs and training sessions for middle and high school students in the dentral North Carolina Region. During the summers, high school and undergraduate students came to the lab for job shadowing and learning experiences similar to the CReSIS REU program which Phillip was involved in. This allowed him to give back to the research community by training up and coming scientists and engineers. Finally, he was able to participate in the North Carolina Science Olympiad, a state-wide event which puts middle schoolers and high schoolers up against each other in science related competitions. The FREEDM Systems Center created the Shock Value event at the Olympiad which awarded scholarships to young engineers.

ACKNOWLEDGMENTS

I would like to thank Dr. Alex Huang, my Primary Advisor, and the following for their help and support:

- Dr. Lukic and Dr. Chow Committee Members
- Dr. Ewan Pritchard - ATEC Manager
- Dr. Lisa Grable and Dr. Leda Lunardi
- National Science Foundation (NSF)
- Xiaohu Zhou - PhD Candidate/Project Partner
- Hulgize Kassa - Lab Manager
- Anousone Sibounheuang - Lab Manager
- AEG and Greensmith Energy Management Systems
- FREEDM Systems Center, ATEC

TABLE OF CONTENTS

LIST OF TABLES

LIST OF FIGURES

Chapter 1

Prior Art

1.1 Battery Energy Storage Systems (BESS)

A battery energy storage system, or BESS, can provide a variety of assets for power systems operation. Namely, they have been considered for power factor correction, frequency control, voltage control, and peak shaving applications. Batteries are easily dispatchable with a flexible AC converter and are considered for emergency power backup operations and even as a spinning reserve, the equivalent of a spinning turbine which is not connected electrically to the grid but can be applied instantaneously for back up.

1.1.1 Dynamic Programming

In 1995, D.K. Maly and K.S. Kwan studied how a BESS system could be used to offset economic loads to save money for residential or large industrial loads [7]. This paper was published in the earlier years of battery-grid integration and discusses some novel techniques in BESS charge/discharge rates for optimal cost reduction of utility rates. Their scheme elaborates on conventional peak shaving logic of charging during non-peak hours and discharging during peak hours as seen in Figure 1.1. Specifically, the authors cite the theory of dynamic programming (DP), in order to test all possible BESS outcomes to find the lowest cost charge/discharge algorithm to implement.

DP theory consists mainly of 'an optimal policy which must contain only optimal sub-policies' [7]. Optimization of a state only includes variables from the previous state, and only considers possible new deviations from this previous state. In regards to a BESS system, if the beginning and end states of the optimal path are the minimum battery charge, the least cost path will be found because the battery has been fully utilized. Maly and Kwan deviate from the possible burdening task of implementing a full scale DP, which computes almost all possible outcomes in order to trace back the optimum route, and suggest a multipass DP approach.

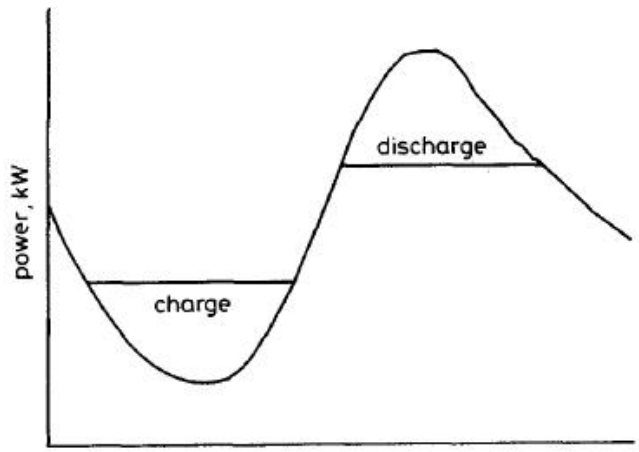

Figure 1.1: Basic Load Redistribution with BESS [6]

Multipass DP involves only taking into account three states at one given time: the previous state, and its upper and lower next step increments [6]. The algorithm moves in the most optimal direction, in this case the least cost, and repeats the three state examination process on the new state. This algorithm continues until it converges on itself, when the upper and lower next increment options are less optimal than the current state. The process can be fine tuned by halving the step increments, in this case charge/discharge current increments, and repeating the process again from the original optimal path [6].

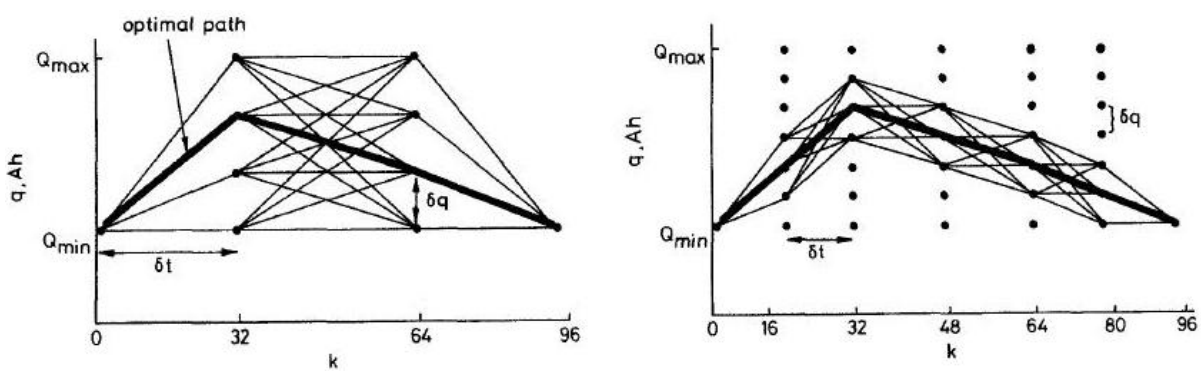

Figure 1.2: An Initial Pass (left) and Second Pass (right) of Multipass DP. The Second Pass Has 1/2 The Step Size and Narrows Down Optimal Path Options Considerably [6]

A DP approach to optimizing a charge schedule must consider the following key variables when making optimization decisions:

1. Utility rates; hourly and peak
2. Typical site load curve; season dependent
3. Limitations of the BESS; see equation 1.1

The limitations of the BESS system include current, voltage, and state of charge (SOC) limits:

$$Vmax < v < Vmin \tag{1.1a}$$

$$Qmin < q < Qmax \tag{1.1b}$$

$$-Imax < i < Imax \tag{1.1c}$$

Maly and Kwan also ran simulations of their DP BESS system considering both large and small battery capacities. Larger capacity battery systems are able to supply more off-grid power during peak intervals, thus saving peak dollars. According to their study, which estimated BESS cost at approximately 400 $/kWh in 1995, with Taiwanese utility rates, a battery sized at 2.0 pu will have a 5-year break even cost, over eight times less than a .1 pu sized system (fig. 1.3). The base being used is the day's maximum kW rating [6].

Battery size (pu)	Power optimised	Energy savings (NT$/kWh/mo)	Power savings (NT$/kWh/mo)	5-year break-even cost (NT$/kWh)
0.1	No	2.55	—	153
0.1	Yes	2.40	642	14800
2.0	No	1.58	—	94.5
2.0	Yes	1.44	74.6	1800

NT$1 = US$0.0375 = £0.0250

Figure 1.3: A Comparison of Small and Large BESS Capacities Using DP Charge Scheduling in Taiwan. [6]

Maly and Kwan presented the idea of dynamic programming for BESS at a relatively early stage in advancement of the US power grid. They did not have a BESS system to test their charging scheme with, and therefore could never verify their results with actual hardware. Their model is not implemented in real time, meaning the charge curve is pre-determined based on a typical load and does not adjust to sudden changes . For example, if there is a snow storm and customers are stranded inside, they will likely use a large amount of heat and appliances if power is available. The load curve would dramatically change from the typical predicted load

where the customers were typically out of the house all day, using no appliances and possibly turning off electric heat. Consequently, the DP charging schedule would need to be adjusted accordingly to pre-planned situations, or implemented on a fast enough computational device so as the charging schedule could be adjusted automatically.

More recently in 2007, ABB published research on peak shaving with a BESS, focusing on BESS sizing and optimal operation [8]. They tested a pre-determined lead-acid BESS with some typical load curves of a large industrial customer. BESS's present financial benefits particularly for TOU based customers such as large industrial plants. In addition to a higher energy (kWh) rate at peak hours, TOU customers are billed per the highest power demand (kW) used over any given interval (usually 15 minutes). A BESS system can be charged at non-peak hours and discharged at peak hours to reduce the peak power demand as well as peak period energy demand, and drastically reduce an electricity bill.

Through setting a reference value (P_{shave}) as the maximum power a user wants to draw from the utility, a user can determine the minimum size of their BESS (B_{pwr}), for a particular day's demand curve [8]. The area determined by the length of the peak power demand (ΔT) and the difference between P_{shave} and the peak power (B_{pwr}) gives the maximum energy the BESS will supply [8]. Integrating this area will give us our BESS size in kWh as seen in equation 1.2a. For a simple rectangular power demand curve, we can represent the BESS size as the product of this difference and (ΔT) as seen in equation 1.2b.

$$B_{cap} = \int_{\Delta T} P_{max} - P_{shave} dt \tag{1.2a}$$

$$B_{cap} = B_{pwr} * \Delta T \tag{1.2b}$$

ABB also used a DP approach to find an optimal charge schedule for the BESS in terms of financial benefit. The authors advance the DP approach by including a battery model into their inputs which could model the battery's internal resistance and number of cycles per year. Using this approach, a varying battery efficiency is used instead of a flat one [8]. ABB's simulation results of a DP for a BESS installed at an industrial site, including modeling of the batteries internal resistance, show a successful charge schedule which charges in between peaks and discharges during power peaks (see fig 1.4). The top chart shows the base load compared with the modified load, revealing that the peak power never exceeds the reference value, P_{shave}. The bottom chart shows the batteries SOC and incremental usage at each hour [8].

Their research contributes to previous DP models with more advanced battery modeling, including internal resistance and limiting the number of cycles per year. In addition to the simple battery sizing technique of peak power area, the ABB contributors also discuss a more advanced battery sizing technique which analyzes monetary costs and payback periods for a

BESS. While ABB did advance the DP approach by adding additional parameters and also including battery sizing techniques for a peak shaving BESS, they still did not test their results on a real time system which has potential to fluctuate and not follow exact load profiles every day. Their studies would be improved with live testing and analysis and comparison of the results.

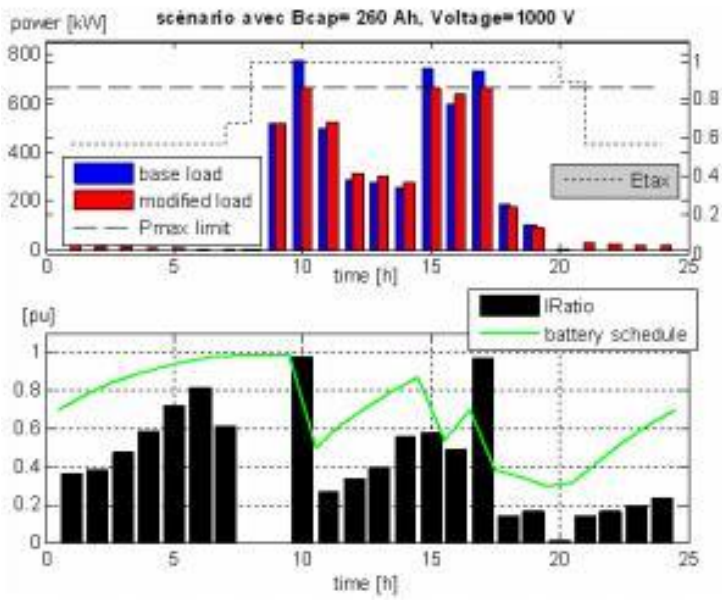

Figure 1.4: BESS DP Results for a Large Industrial Plan Implementing Peak Shaving [8]

1.1.2 BESS Integration in Renewable Resources

BESS's are extremely important as the conventional grid becomes more complicated and relies on reserve power and storage techniques. More recently they have been discussed to help dispatch and integrate renewable energy sources into the power grid..

Predicting Solar Power

Power production in PV arrays is reliant on solar irradiance. In order to implement any kind of predictive charging schedule for a BESS accompanying a PV source, there must be a reliable method to predict solar irradiance, or consequently, output power of the PV array. Historically, scientists have analyzed measured solar irradiance values from locations where measurement technology exists, and applied theoretical models to this data for prediction.

One of the first such models was studied in the 1950's. Whillier used radiation measurement stations in South Africa to predict average hourly distribution of total radiation for those areas and "probably" other local areas in South Africa. At this time period, solar radiation prediction was used primarily for use in air conditioning and solar heating and drying, and potentially power generation [9]. After obtaining a mean hourly radiation value for four specific locations, common solar angle equations were used to correlate the measured data to a specific location.

$$I = K * I_{sc}(cos(\Phi) * cos(\delta)) * (cos(\omega) - cos(\omega_s)) \tag{1.3}$$

where

1. I = intensity of solar irradiation
2. K = fraction of solar radiation arriving at earth's surface
3. I_{sc}= solar radiation external to earth's atmosphere on a normal surface
4. Φ = latitude
5. δ = solar declination
6. ω = hour angle from noon, +/- 15° per hour
7. ω_s = sunset hour-angle

K is assumed a constant quantity in an hourly prediction model for simplicity, but in an actual setting, K would change based on cloud cover. These values can be integrated over an hour or full 24-hour period with respect to the sun hour angle, ω, as the representative of time. Whillier noticed some effects of humidity and smoke-production on different locations and time periods, thus making his analysis more complex than intended. Whillier clarified that except on a clear day, cloud cover extremes preclude any possibility of predicting hourly solar radiation that is not statistical or long term [9].

The Physics department of University of Zambia published a study of the estimation of average hourly irradiance in 1987. Using solar irradiance monthly average values in Montreal between 1964 and 1975, P. C. Jain was able to apply a normal distribution curve he had developed in previous studies from Trieste, Italy to newly acquired data from Montreal (see eqn 1.4) [11].

$$p(t) = \frac{1}{\sigma * \sqrt{2 * \pi}} exp[\frac{t - 12^{12}}{2\sigma^2}] \tag{1.4}$$

The unknown σ is a standard deviation determined through the solar noon measured value if measurements are available (eqn 1.5a), or through a correlation of monthly average daily

maximum sunshine ($\bar{S}_0$) specific to a certain location, in this case Trieste, Italy (eqn. 1.5b) [10]. He also determines a global equation, through averaging, which can be used to fairly accurately model global solar radiation at any location (eqn 1.5c).

$$\sigma = \frac{1}{p(12)\sqrt{2\pi}} \tag{1.5a}$$

$$\sigma = .192 * \bar{S}_0 + .461 \tag{1.5b}$$

$$\sigma = .200 * \bar{S}_0 + .378 \tag{1.5c}$$

Jain noticed a high accuracy correlation from his distribution curve to the actual data from Montreal around solar noon. Closer to sunset and sunrise, there are discrepancies because the distribution curve extends to infinity while actual radiation hits zero when there is no sunlight available. Jain points out that this difference is extremely small compared to radiation values at solar noon and two-thirds to three-fourths of the day surrounding this point [10].

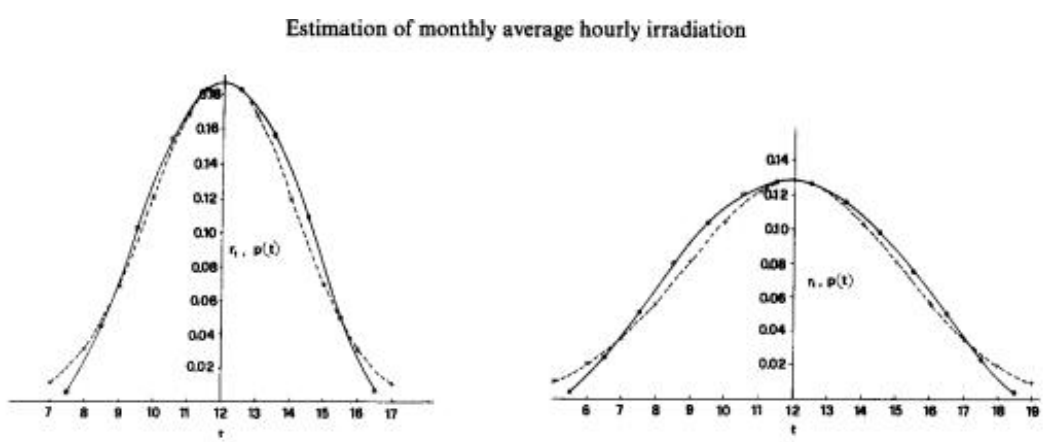

Figure 1.5: Experimental (solid line) and Theoretical (dotted) Curves for Global Radiation of Montreal in January (left) and April (right) [10]

These models offer some long term prediction mechanisms that might be ideal for modeling, but do not address the daily disturbances such as cloud cover or precipitation in an exact plant location. Cloud cover can greatly effect the power output of a PV array, and for all intents and purposes, is not easily predictable due to changing wind speeds and other atmospheric phenomenons. A global model will not be effective, as averaged global trends have the possibility to fluctuate greatly with local radiation models. For this reason, a BESS accompanied with a PV array needs short term predictive modeling which is effective specifically for its location.

A statistical moving model, which updates itself frequently on past measured data, would be ideal for predicting or adjusting to any unexpected disturbances in a typical PV array power output curve.

There are many different predictive models which have already been studied in research papers and compared for accuracy. Recent research from Nanyang Technological University of Singapore in 2009 researches and compares different predictive modeling approaches for solar radiation, and determines that a linear regression model with a 10 to 15 point window size produces the most accurate prediction model for daily solar radiation [12]. Using solar radiation data gathered from Singapore, the authors were able to apply three popular statistical models to the acquired data and compare their results and accuracies. The linear regression model assumes an unknown time series,f_t, is being influence by a known independent input series, z_t (see eqn 1.6).

$$R^2 = 1 - \frac{(\Sigma(z_i - f_i))^2}{(\Sigma z_i - \bar{z})^2} = 1 - \frac{SS_{err}}{TotalSS} \tag{1.6}$$

Where

1. R is the regression
2. $\bar{z}$ is the mean of the observed data
3. f_i is the modeled value

The authors also overview autoregressive models (AR), which determine the number of prior values needed for prediction, and auto regressive integrated moving average (ARMA), which combines the moving average (MA) model by introducing linear combination of noise and the current value of the series. The author's simulations using R statistical software showed some erroneous predictions of solar radiation in Singapore using the AR and ARMA approaches. When there is actually zero radiation at the beginning and end of a day (24th hour), AR and ARMA predicted rising values during these times and were therefore considered not ideal for predicting daily solar radiation [12].

On the other hand, linear regression models successfully predicted the zero radiation times when the sun was not out, as well as modeling the upward and downward trends during the day [12]. In any linear regression prediction technique, a proper window size must be selected as the amount of previous data used in the calculations which will produce the lowest normalized error. The authors test multiple window sizes and determine that somewhere between 10 and 20 data points will give the lowest normalized error (eqn 1.7) in comparison to the actual data seen in Figure 1.5.

$$NormalizedError = \frac{OriginalValue - ForecastedValue}{OriginalValue} \tag{1.7}$$

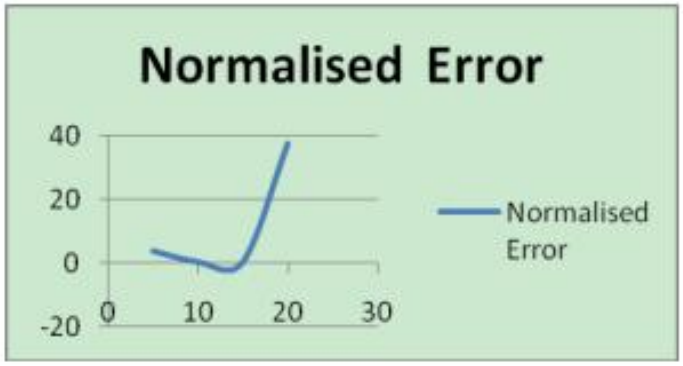

Figure 1.6: Normalized Error of Different Window Sizes in Linear Regression Modeling [12]

Dispatch Length and Control Methods

The interval length of the predictions should be based on utility power dispatch standards. Economic Dispatch (ED) is a very important concept to electric utilities. ED is described as optimal use of generation output from a centralized planning perspective [24], which can save on operation and fuel costs as well as provide accurate power for predicted loads and reserve power. Utilities predict loads, and then accurately determine which generators will operate at certain times to reduce cost and maintain grid stability. Dispatchers must know ahead of time the rated capacity of each generator, which becomes an issue with renewable resources such as solar and wind power. The integration of a DESD provides some control over how much constant power can be drawn at different ED intervals. If the output power of the renewable resource is below or above the desired ED power level, energy can be stored to or extracted from the DESD to compensate the difference. According to other academic studies, this interval can range from 5 minutes to one hour, typically residing in the 15 minute range for more accurate predictions [26].

One previous study performed by S. Teleke, used hourly dispatch intervals of predicted power outputs combined with PV and wind renewable resources in simulations to monitor battery requirements and control methods. P_{set} is defined as the hour's predicted power output, and the amount of power to be provided at any moment by the BESS is defined as:

$$P_{bess,ref} = P_{set} - P_{solar} \tag{1.8}$$

Using hourly forecasts, which coincide with industry dispatch intervals as previously mentioned [26], P_{set} can be calculated as the mean of the hourly forecast in order to keep the battery's SOC change at a minimum (zero) [3]. Teleke describes two successful methods for

BESS control in renewable resource integration: optimal control and rule based control. Optimal control takes into consideration a third battery model and is ultimately open loop control due to its implied reliability and error minimization. Rule based control is closed loop control, which measures system performance real time, adjusts control variables accordingly, and keeps into consideration system rules such as battery SOC, ramp rate, and total power output [3]. Computation time is much less than optimal control, and the feedback, closed loop control keeps the system up to date with real-time system parameters. The system objective, which is that $P_{bess} = P_{bess,ref}$, is satisfied as long as battery constraints and current limits are satisfied, given in 1.1 [3].

Teleke also used a concept known as model predictive control (MPC), which uses shorter control windows over a larger prediction window, or horizon. Thus, closed loop control, where system variables are measured and adjusted to minimize error, occurs multiple times over a prediction horizon, thus increasing system performance over longer horizon windows, such as the one hour window used in this study (see fig 1.7).

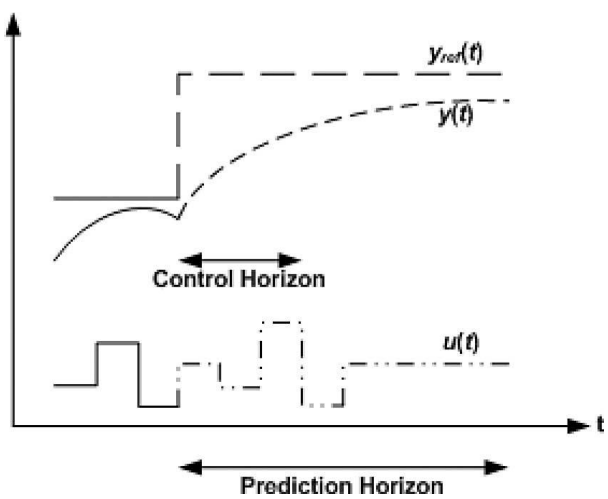

Figure 1.7: MPC Uses Shorter Control Horizons Over Longer Prediction Horizons. The Control Signal, u(t), Changes Multiple Times Over The Prediction Horizon [4]

The results of the study revealed that the rule based control delivered results similar to the optimal control, with less computational time and the absence of a battery model. Finally, a large size BESS, of about 15% to 25% of the renewable resource capacity was required to have an effective hourly dispatch. Teleke used lead-acid batteries in his studies, which might have increased the minimum size of the required batteries due to the small operating window (70%). Lithium Ion batteries have an operating capacity of closer to 93% [5].

1.1.3 Human Machine Interface

Implementing high level control schemes for a BESS integrated power system requires a software side solution that easily integrates with all hardware, including battery chargers, inverters, wires, protection devices, and the batteries themselves. Without a proper software monitoring and control scheme, automation of hardware becomes difficult to implement quickly and properly. Issues such as faults on a power grid, or exceeding limits of a battery system, need to be addressed as quickly as possible through fast electronic communication and reporting in order to prevent equipment damage or potential danger to civilians.

For these reasons, HMIs (Human Machine Interfaces) are a common method of observing and automating hardware to a point where users can monitor systems while the integrated software automatically protects and runs the hardware system. The HMI allows the user to communicate in their native language with devices, while the HMI will convert this information into the proper protocol or programming language for machines, or electronic devices to understand.

One large issue in the power industry is improving the current power grid's ability to communicate and automatically adjust to situations that occur in everyday operation. In one such example in Naperville, IL, the public utility began installing Distribution Automation Systems in addition to their existing SCADA systems in 2001 [13]. These two approaches had no integration methods and required different data centers which had no connection to each other, even though SCADA and DAS systems were sometimes installed at the same location. As with any utility, Naperville wanted reduce faults, improve service time, automate functions, and eliminate unnecessary data centers. HMI's became necessary in the approach to allow personnel to control and configure hardware while also assessing current and post-processing data. The HMI allowed the team to program and monitor devices without having to decode programming languages between themselves and other devices, effectively bringing the "human" portion of the HMI to full life. The automatic control system ran seamlessly beneath the HMI level.

The city selected Siemens SICAM system which integrates protection, monitoring, control, automation, and visualization, to name a few functions, of a substation using a hierarchy design (see fig 1.8). The three phase hierarchy consists of HMI's, Substation Controls, and Intelligent Electronic Devices (IEDs) [13]. The HMI specifically provided present and post-processing data for analysts, and configuration ability of substation controllers for system administrators. The SICAM system understands which kinds of controllers are connected to it and can seamlessly configure and inherit the device and its programming language. The SICAM system allowed administrators and controller to have some control over the system design and functionality, while also having the ability to analyze data and real-time processes [13]. The HMI allowed these personell to perform these tasks without having to understand the protocol or computer programming language of these devices.

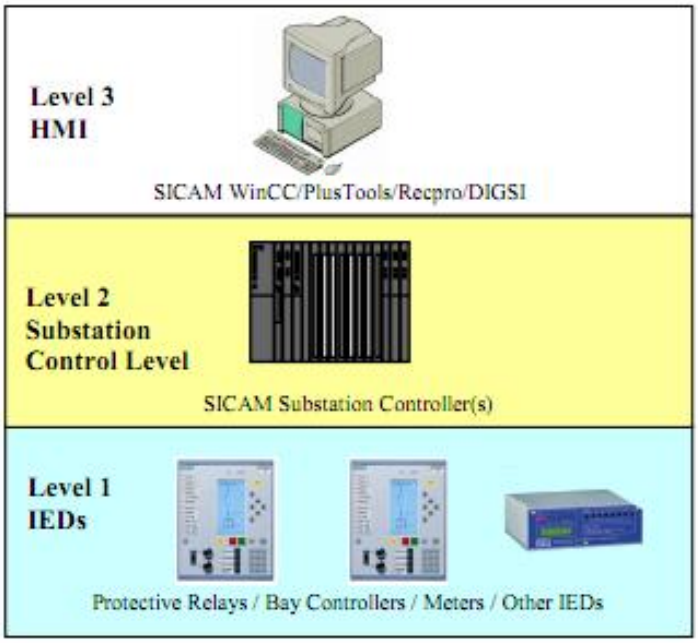

Figure 1.8: SICAM Heirarchial Model Consisting of an HMI Top Level

Researchers at Michigan State University (MSU), published results in 2010 which outlined another example of an HMI system which supplemented a power system. R. Reddi and A. Srivastava included an HMI with their test bed power system to monitor system variables and control generators and loads [14]. The main component of the simulated power system included a Real Time Digital Simulator (RTDS), which is a power system simulator that can perform its simulations real time to mimic a real power grid. The RTDS system includes communication ports which interact with Programmable Logic Controllers (PLCs) via National Instruments PXI system.

LabVIEW was used as the graphical programming tool used for measurements and automation of the system. LabVIEW allows users to develop an easily programmable HMI which reads data and controls devices for test purposes and in some cases, industrial applications. LabVIEW also allowed the MSU research team to work with all of the different input and output hardware interfaces. This allowed the HMI access to all data in the system, regardless of how it is connected. LabVIEW can be run on a computer and connected to advanced data acquisition (DAQ) devices, in this case, a NI-PXI embedded controller [14].

The HMI was connected remotely via Ethernet to communicate with the non-local PCI and directly via Ethernet with the RTDS . A suite of Ethernet and DAQ controls available in LabVIEW allowed the researchers to develop a fully functional HMI which could communicate

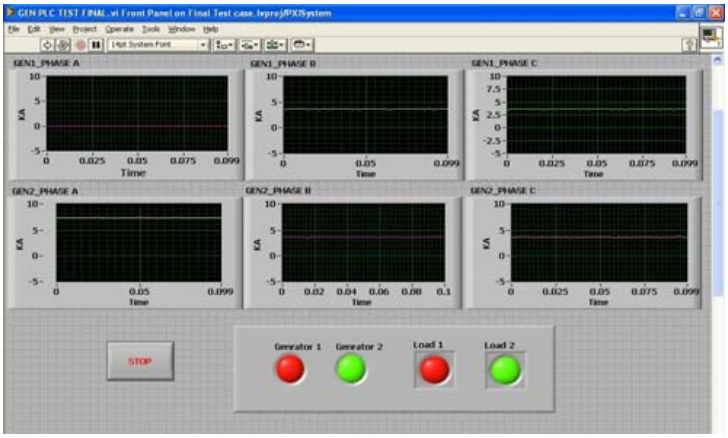

Figure 1.9: HMI of the Power Systems Test Bed Developed at MSU Showing Operational Currents and Generator Status [14]

quickly with the PLC and RTDS.

The LabVIEW HMI displays graphical data while also writing control data to local PLC's (see fig 1.9). The PLC contains all of the logic which tests faults and generates signals for remedial schemes, which are also routed through LabVIEW back to the RTDS. The System was tested with user-induced faults. The LabVIEW program recognized the fault at a generator and sent appropriate logic signals to the PLC while also displaying the data and indicator lights on the HMI for the human operator to recognize the fault.

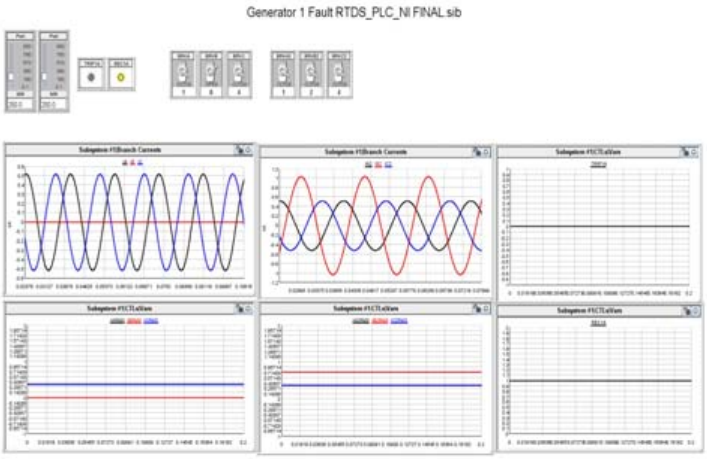

Figure 1.10: RSCAD View of the Simulated Power System with a Single Phase Fault on the C Generator [14]

Chapter 2

Purpose

The concept of using battery technologies for transportation, generation, and grid support has been discussed and researched for decades. User demand for electronic storage technologies must grow for significant industry involvement and subsequent reduction of cost and maintenance to take place. Certain governments and advising committees have placed renewable energy and electric vehicle demands on their markets to help increase this demand. In 2009, wind power and solar PV additions reached record highs in Europe and the United States, with renewables accounting for over half of newly installed power capacity [1]. More than $150 billion was invested in new renewable energy capacity and manufacturing plants up from just $30 billion in 2004 [1]. Also, Europe has a continent wide target of 10 percent sustainable transportation including electric vehicles and biofuels [1]. These numbers indicate a high potential penetration of new energy technologies into a traditional electricity grid.

2.0.4 Renewables and Peak Shaving

This apparent rise in new technology brings great promise to efficient and environmentally friendly energy production, but at the same time introduces many issues. Renewable energy is never predictable as it mostly relies on natural occurrences. Predictability and stability are currently dealt with by alternate forms of generation, in the form of on site generators. The purpose of this paper is to observe energy storage as a complimentary power source to level out unpredictable occurrences and failures. Energy storage also presents the possibility of constant power output for these renewable devices. For example, a day's worth of renewable energy could be stored and measured chemically. The next day, this energy could be dissipated at a constant rate or a variable rate, giving utilities complete control over renewable energy. Batteries and other storage technologies also present the option of peak shaving for all utility customers. Peak shaving benefits users in terms of decreased utility bills, and benefits utilities in terms of lowered peak demand and less dependency on quick start, expensive generation.

There is no doubt that integrating a BESS with an energy source or load will require great research into control methods for functionality, efficiency, and limits. Large scale BESS's are currently not at an affordable market price, and therefore optimally sized BESS's, in terms of battery capacity and inverter size, will need to be determined for peak-shaving and renewable source firming. Not only do these control algorithms need research and results, but any system of this nature would require an HMI solution for operators and customers in order to determine energy generation, storage, and trading preferences.

2.0.5 Electric Vehicles

Electric Vehicles (EV's) and Plug-In Hybrid Electric Vehicles (PHEV's) are BESS's integrated into mobile vehicles which connect to the power grid for charging purposes. These charging sequences will occur mostly when vehicles are idle during the working day or nighttime hours. EV and PHEV technology might require complicated scheduling algorithms for nighttime and daytime charges where cars are parked for multiple hours, and might even be used as grid storage during failures and peak periods. All of these technologies will require some form of high level control by utilities and users as well as graphical displays for users and utility operators. Additionally, protection systems must be included in this high level programming to prevent over or undercharge and to keep battery lifetime optimal.

2.0.6 Control Methods: New and Old

This document will cover BESS control methods for multiple applications, reviewing previously discovered methods and combining optimal parts of each control method in order to create successful control methods with past proven success. Modifications to control methods will also be developed as data and results become available.

2.0.7 Real Time Experiments

One major setback with most of the research available in publications regarding renewable energy firming is that results are simulation based. In the cases of Maly and Kwan [6], Teleke [3], ABB [8], Whillier [9], Jain [11], Nanyang [12], research was conducted using measurements and product specifications in simulation environments to mimic a real-time experiment.

Though effective and useful, the study of BESS technology has very few examples of real-time integration, which puts situation based stresses on batteries, inverters, and control technologies. Until these actual experiments are conducted, the field will be set back by real-time integration results. The purpose of this study will be to introduce some real-time control techniques conducted in an experiment setting. This setting will include DESD's, battery chargers,

and Renewable Energy Sources running and complimenting each other real-time with actual power output values.

Another goal of this study will be to develop graphical monitoring solutions for real time experiments and observe data with a real time HMI coinciding with data storage for statistical analysis. This data will not only be compared to itself, but also to simulated data to reveal discrepancies and new issues not previously found with pure simulation-based research.

2.0.8 Overall Purpose

At this juncture in time, the power grid is mostly instantaneous, relying on the real-time generation with some limited reserve capacity in the form of spinning reserves and potential operational output of generators running at low output. With the addition of BESS's, the grid is no longer instantaneous, and new engineering options are born for utilities and suppliers. These opportunities also present engineering challenges that the US infrastructure has never seen before. Automation, scheduling, and prediction will become just as important as physical infrastructure design.

Chapter 3

Dynamic Programming with BESS Residential System, Cost Cutting

Dynamic Programming (DP) style peak shaving was simulated on typical residential loads using a DESD as a BESS unit. As with Maly and Kwan's DP experiments, the ultimate goal during each simulation day was to start out with a minimum battery charge, and use all energy obtained throughout the day to shave instances where residential power demand exceeded a pre-determined peak [6]. Also considered was the leftover energy after peak shaving, which could be evenly distributed throughout all peak times.

Similar to ABB's research (see sec 1.1.1), a pre-determined peak, P_{shave} was used as a reference for non-peak charging and peak discharging limits [8]. TOU rates from the local utility, Progress Energy, were used for off-peak and peak prices, but also included a peak kW fee which was included in simulations. ABB determines minimum battery size to shave peaks, although in these experiments minimum battery size is determined by maximum energy stored during non-peak hours, assuming that it is cheaper to store non-peak energy and use at peak times. This energy will be used to shave peaks and also be distributed throughout peak hours.

The ultimate goal of these simulations is to determine the proper peak power demand of a residential household during winter and summer months in order for the customer to save the most money.

3.1 Simulation Setup

Simulations were done in MATLAB and included a number of simulated inputs including the BESS, residential load data, and utility rates.

3.1.1 Greensmith 20 kWh DESD

See Subsection 5.1.3

3.1.2 Residential Load Profile Data

Load profile data was unavailable for the Raleigh, NC area, so the most similar climate area with available data was used. The New Hampshire Electric Co-op provides historical load data based on interval metering of each consumer for residential data [33]. Data is given in per unit (pu) basis, and can be scaled based on the typical peak power drawn by a household, by using a multiplying factor ($Factor = ActualPeak_{household}/PUPeak_{profile}$). In order to prove the DP peak shaving theory with a residential household and a BESS, the winter month with the highest PU peak power, February, and the summer month with the highest PU peak power, July, were used in the simulations.

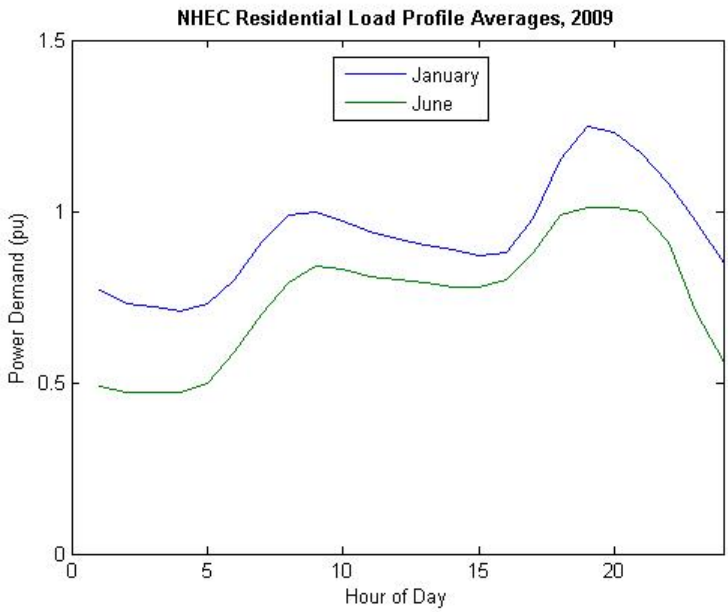

Figure 3.1: NHEC Average Monthly Values for Peak Summer and Winter Months in 2009 [33]

Though no residential load profile data could be found for the NC area through Progress Energy, typical household energy consumption and the corresponding typical winter and summer peaks for different levels of energy consumption were generously provided by Progress Energy through protected material [35]. These peaks could be applied to the peaks associated with the

Table 3.1: Progress Energy TOU Rates (A.13)

Rate Type	**Months**	**Time**	**Cost**
Basic Charge	All Year	N/A	$9.85
On Peak Energy	April - Sept	10 am - 9pm	6.377/kWh
Off Peak Energy	October - May	6 am - 1 pm, 4 pm - 9 pm	5.003/kWh
Max On Peak kW Demand	June - Sept	N/A	$5.02/kW
Max On Peak kW Demand	Oct - May	N/A	$3.73/kW

NHEC residential material and formulated into a potential typical summer/winter load for an east coast resident (assuming NH and NC temperature variations are relatively similar).

3.1.3 TOU Rates

Progress Energy, the local utility for Raleigh, North Carolina, provides public data on different rate structures available to their customers (see Table 3.1). In addition to the general kWh rate offered, a time of use (TOU) schedule is offered which gives customers incentives to use power during non peak times. In addition to a rate difference in peak and non-peak hours, the maximum monthly peak is also taken into consideration.

3.2 Dynamic Programming Simulations

The DP Residential BESS simulations coincided with previous studies mentioned before, and also included limits associated with the Greensmith 6 kW DESD system in order to incorporate industry standard limits on batteries and power electronics (see figs A.7 and A.5). The following were basic rules followed during the simulation, some which were incorporated from previous studies. A complete flow diagram of the simulation sequence can be seen in Figure A.12, located in Appendix A.1.

1. Start with a minimum battery charge, store as much energy as possible, including energy left over from the previous day after on-peak hours [6]
2. Use all of the stored energy over the course of the day
3. Pre-determine a peak to charge up to and discharge down to [8]
4. First, discharge all above peak demand instances to peak level.

5. Evenly distribute any remaining charge across all on-peak hour energy demand in order to reduce demand on equipment
6. For all battery charges, costs and power demand calculations do not include efficiency degradations, but charge stored does
7. For all battery discharges, costs and power demand calculations include efficiency degradation, but charge removed does not
8. Calculate the cost of energy for that day, and coinciding month (assumed 30 days)

By combining Table 5.2 and Equations 1.1, basic DESD limits can be stated for charges and discharges:

$$.05 < SOC < .95 \tag{3.1a}$$

$$-30 < I_{DESD,AC} < 30 \tag{3.1b}$$

3.2.1 Integration of Dynamic Programming

DP theory must consist of sub-policies which make up an optimal policy, choosing most optimal paths along the way which deviate from a previous state. The beginning and end states of this DP approach will be the minimum operating battery capacity, which coincides with the most recent transition from peak to non-peak hours, and ends on the last peak hour of the day. For example, if the previous day ends with three non-peak hours, those hours will be used to charge the battery up from minimum state obtained from shaving peaks for use during peak hours the following day. The final peak hour of each day, assuming that peak hours end before midnight, will coincide with minimum battery capacity, as all stored energy was used to shave peaks and reduce price during peak times.

3.2.2 Dynamic Programming Assumptions

Some assumptions are made in order to make the DP approach easier to implement. It is assumed that energy stored during non-peak times will be cheaper than energy used during peak times. Therefore, the maximum amount of energy during non-peak hours will be stored in order to use during peak hours. Therefore, the decision at each time interval will be pre-determined, and DP will only be used to determine the optimal daily peak to charge and discharge to. Therefore, the logic of the DP approach for residential BESS integration is fairly simple, and DP decisions are made at the end of the programming cycle for a pre-determined peak, when total daily power costs are calculated. If enough energy was available to shave

all peaks, then the total cost for that specific day is compared to the previous minimal total cost. If this cost is lower, it is the new minimum cost and therefore the most optimal peak to charge/discharge to (see Equation 3.7. Therefore, the DP state is the total daily cost for a pre-determined peak, and the two deviating cases are +/- 10W from the pre-determined peak. An optimal peak is found when it is smaller than both deviations. In all cases, all non-peak hours are completely optimized.

For Off Peak Hours

$$\text{if } P_{Demand} > Peak, \qquad P_{DESD} = \frac{P_{Demand} - Peak}{.88} \tag{3.2}$$

$$\text{else,} \qquad P_DESD = -(Peak - P_{Demand}) \tag{3.3}$$

For On Peak Hours

$$\text{if } P_{Demand} > Peak, \qquad P_DESD = \frac{P_{Demand} - Peak}{.88} \tag{3.4}$$

$$\text{else} \qquad P_{DESD} = -LeftoverEnergy_Distributed \tag{3.5}$$

DP Logic

$$\text{if } Cost(p) > Cost(p+1) \text{ OR } Cost(p) > Cost(p-1), \qquad p = p + 10kW \tag{3.6}$$

$$\text{elseif } Cost(p) < Cost(p+1) \text{ AND } Cost(p) < Cost(p-1), \qquad p = p_{optimal} \tag{3.7}$$

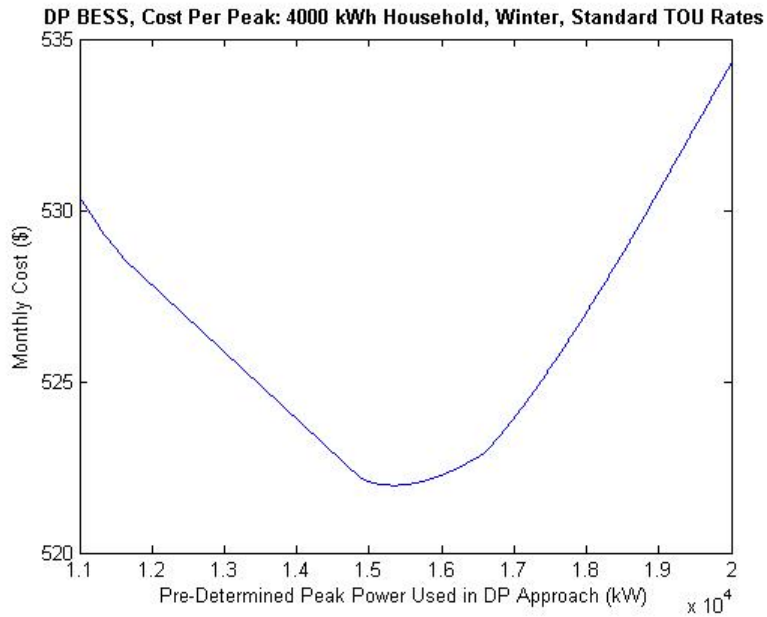

Figure 3.2: DP Results for a Large Residential Household in Winter Time, Using Standard TOU Rates. The Optimal Peak is Easily Determined Based on The Rules Defined in Table 3.7

The assumption that stored off-peak energy will be cheaper than on-peak energy is approximately valid assuming an 88% DESD inverter efficiency given by Greensmith and the prices given by Progress Energy. Inverter efficiency loss will occur during energy charging and discharging, and must be applied twice when non-peak energy is stored, and dispatched at peak times. As we can see in Equation 3.8, off-peak energy will actually cost slightly more (approximately $\frac{1}{10}$ of a penny per kWh) than on-peak energy if stored in the battery and output with 88% losses each way. For the Residential BESS DP Simulations, we can assume these two prices are equivalent.

$$5.003 * (1/.88)^2 = 6.46 \tag{3.8}$$

$$6.377 > 6.46 \tag{3.9}$$

The small difference in price for on-peak and off-peak energy actually renders peak shaving approaches almost useless for cutting cost due to inverter and battery efficiency losses. The inverter efficiency changes depending out commanded power and might be slightly above or below 88%. Reduction of the peak power might reduce a consumer's electricity bill enough to cancel out the efficiency losses of storing the energy in the DESD. For these reasons, simulations were also ran for larger differences in Progress Energy's on and off peak rates. On-peak energy

cost was increased in half penny increments to observe potential cost savings for customers if Progress Energy's tariffs were changed. Also, simulations were run for different size households, ranging from 1000 kWh of monthly energy (a typical single residential household) use to 4000 kWh of monthly energy use (a large family residence).

3.3 Simulation Results

Simulation results were recorded and graphed. Data was first organized by household size, increasing the difference in peak and non-peak hourly energy rates and observing the most optimal peak in terms of daily/monthly energy cost. Finally, the minimum BESS capacity required to perform the daily DP BESS integration was also recorded and plotted for the different households.

3.3.1 Summer Months

In the summer time, peak hours occur in a bunch during mid-day from 10am until 9pm. According to the NHEC data compiled with a typical residential peak in Progress Energy's domain, two peaks occur in this time frame. The first peak at 10am only dips slightly due to summer air conditioning use, and at 4pm shoots up to account for residents returning home. This peak dips back down at 9pm, and therefore the summer peak hours include both day time peaks precisely (see Figure 3.1).

At all residential levels, savings increased slowly from the standard peak price of \$0.06377 to \$0.065, then linearly to \$0.080. At an hourly peak rate of \$0.085 per kWh,a sharp increase in savings occurs (see Table 3.2 and Figure 3.3). This is due to the price difference between stored non-peak energy and peak energy compared to the peak power fee. Stored off-peak energy only costs \$0.0654 per kWh compared to \$0.085, and is apparently enough to offset the peak fee. Therefore, we can increase the pre-determined peak to a much higher value, and our savings will not be completely offset by the peak fee of \$5.02 per kW. In the other cases where stored non-peak energy savings are not enough to offset the peak fee, the savings are limited , and only savings occur when the system peak is lowered substantially. Therefore, all optimal peaks at prices less than \$0.085 per peak kWh are below the original peak in order to obtain peak savings.

Table 3.2: Simulation Results for Summer Residential Households Using Different Peak Prices. Results Include Cost Savings, Optimal Peak, and Minimum Battery Capacity Required

Peak kWh	Peak $/kWh	OptPeak(kW)	OriginalPrice	New Price	Difference	Cap(kWh)
1000.00	$0.0638	3,090.00	$141.41	$137.70	$3.70	7,148.81
	$0.0650	3,130.00	$142.82	$138.88	$3.94	7,606.41
	$0.0700	3,180.00	$148.57	$143.58	$4.99	8,178.41
	$0.0750	3,180.00	$154.32	$148.26	$6.06	8,178.41
	$0.0800	3,450.00	$160.07	$152.83	$7.24	11,267.21
	$0.0850	5,800.00	$165.82	$154.41	$11.41	38,151.21
	$0.1500	5,800.00	$240.63	$164.68	$75.95	38,151.21
1500.00	$0.0638	4,260.00	$195.15	$190.03	$5.11	9,817.26
	$0.0650	4,320.00	$197.10	$191.66	$5.44	10,503.71
	$0.0700	4,390.00	$205.03	$198.14	$6.89	11,304.51
	$0.0750	4,390.00	$212.97	$204.60	$8.36	11,304.51
	$0.0800	4,760.00	$220.90	$210.90	$10.00	15,537.31
	$0.0850	8,040.00	$228.83	$213.05	$15.79	53,058.56
	$0.1500	8,040.00	$331.00	$225.00	$106.00	53,058.56
2000.00	$0.0638	5,060.00	$231.91	$225.84	$6.08	11,637.10
	$0.0650	5,130.00	$234.23	$227.77	$6.46	12,437.90
	$0.0700	5,210.00	$243.66	$235.47	$8.19	13,353.10
	$0.0750	5,220.00	$253.09	$243.15	$9.94	13,467.50
	$0.0800	5,650.00	$262.52	$250.64	$11.88	18,386.70
	$0.0850	9,550.00	$271.95	$253.19	$18.76	63,001.60
	$0.1500	9,550.00	$394.00	$267.00	$127.00	63,001.60
2500.00	$0.0638	5,870.00	$268.68	$261.64	$7.04	13,571.30
	$0.0650	5,940.00	$271.37	$263.88	$7.49	14,372.10
	$0.0700	6,040.00	$282.29	$272.80	$9.49	15,516.10
	$0.0750	6,050.00	$293.21	$281.70	$11.52	15,628.20
	$0.0800	6,550.00	$304.14	$290.37	$13.77	21,350.50
	$0.0850	10,770.00	$315.06	$293.70	$21.36	69,560.32
	$0.1500	11,220.00	$457.07	$310.76	$146.31	73,036.80
3000.00	$0.0638	6,580.00	$301.20	$293.31	$7.89	15,207.52
	$0.0650	6,660.00	$304.21	$295.82	$8.40	16,122.72
	$0.0700	6,770.00	$316.46	$305.82	$10.64	17,381.11
	$0.0750	6,780.00	$328.71	$315.80	$12.91	17,495.52
	$0.0800	7,340.00	$340.95	$325.52	$15.43	23,901.92
	$0.0850	11,200.00	$353.20	$330.25	$22.95	67,988.48
	$0.1500	13,850.00	$512.40	$352.11	$160.29	81,935.36
3500.00	$0.0638	7,220.00	$330.90	$322.23	$8.67	16,606.95
	$0.0650	7,320.00	$334.21	$324.99	$9.22	17,750.95
	$0.0700	7,440.00	$347.66	$335.98	$11.69	19,123.75
	$0.0750	7,450.00	$361.11	$346.93	$14.18	19,238.15
	$0.0800	8,070.00	$374.57	$357.61	$16.95	26,330.95
	$0.0850	11,590.00	$388.02	$363.62	$24.40	66,529.28
	$0.1500	15,270.00	$562.91	$401.09	$161.82	82,370.56
4000.00	$0.0638	7,840.00	$359.18	$349.77	$9.41	18,059.59
	$0.0650	7,940.00	$362.73	$352.76	$9.97	19,203.59
	$0.0700	8,070.00	$377.38	$364.69	$12.68	20,690.79
	$0.0750	8,090.00	$391.98	$376.58	$15.40	20,919.59
	$0.0800	8,760.00	$406.58	$388.18	$18.40	28,584.39
	$0.0850	11,970.00	$421.19	$395.40	$25.79	65,218.56
	$0.1500	15,960.00	$611.00	$448.67	$162.33	82,370.56

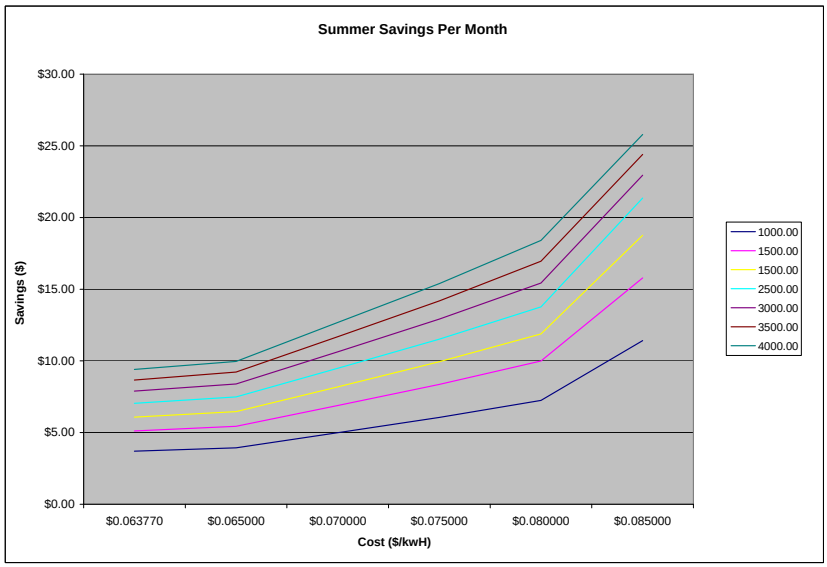

Figure 3.3: Summer Savings for Different Sized Households at Different Peak Rates

Consequently, the amp-hours needed to perform the optimum priced DP BESS integration algorithm remains steady under $0.085 per kWh and jumps rapidly, more than two times the next highest amp-hours' count (see Table 3.2 and Figure 3.4). The highest Ah used during any simulation was 21737.60 Ah, which was not associated with the largest household. After a house size which demands 3500 kWh per month, the total capacity needed to perform an optimal BESS DP algorithm slowly starts to drop, this is due to the current limitations of the specific inverter used in this experiment. The Greensmith 6kW unit cannot output more than 6kW at any moment, and therefore, the peak slowly starts to reach an upper limit with the simulations increasing household size [28]. At this point, shaving the peak hours energy all the way to zero use is optimal, but that required energy level cannot be obtained due to the current limiting restraint of the DESD.

Figure 3.5 shows summer simulation results with standard utility TOU rates. The peak is lower than the previous peak, and at non-peak hours the DESD charges up to the peak demand, and dissipates this charge across the peak-hours once all demand values higher than the pre-determined peak are shaved. Figure 3.6 shows summer simulation results with the highest simulated peak hour costs, which make stored non-peak energy cheaper. The peak is higher

than the previous peak, and at non-peak hours the DESD charges up to the peak demand, and dissipates this charge across the peak-hours evenly until almost zero demand occurs during peak hours. In this case an inverter current limit was not reached. Though in the case of Figure 3.7, a peak inverter current limit is reached, and thus not all of the peak-hour energy can be shaved.

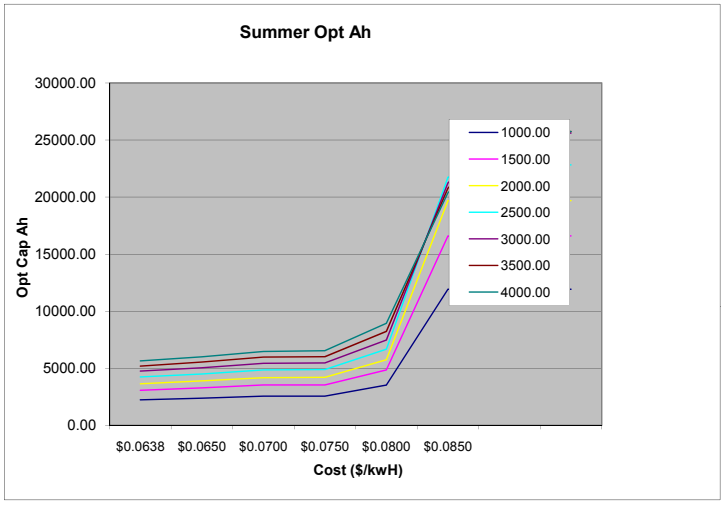

Figure 3.4: Summer OptPeaks for Different Sized Households at Different Peak Rates

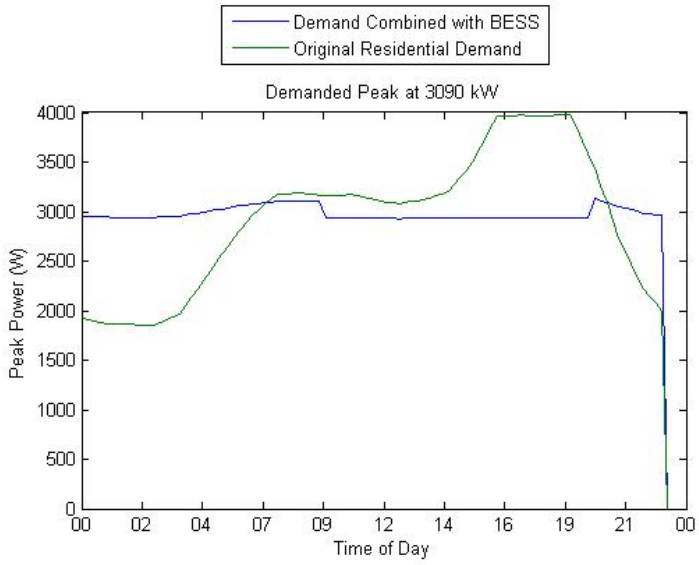

Figure 3.5: Summer Optimum Peak Simulation Results at Standard Utility Rates during Summer

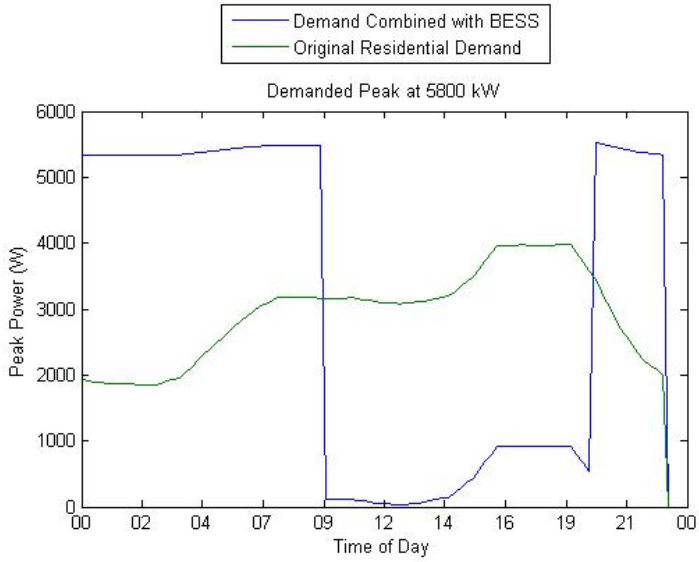

Figure 3.6: Summer Optimum Peak Simulation Results at Maximized Peak Rates during Summer

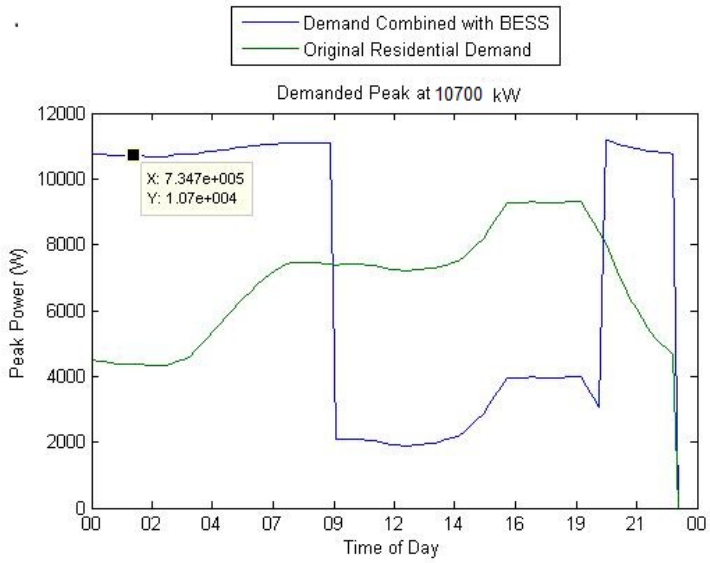

Figure 3.7: Summer Optimum Peak Simulation Results at Maximized Peak Rates during Summer with a Current Limit Reached

3.3.2 Winter Months

In the winter time, peak hours occur in two bunches during mid-day from 6am until 12pm and from 4pm until 8pm. According to the NHEC data compiled with a typical residential peak in Progress Energy's domain, two peaks occur in this time frame. The first peak rises up from 6am and peaks at 9am, then dips moderately due to less air conditioning use in winter time day hours, and after 4pm shoots up to account for residents returning home. This peak stays constant and dips back down at 9pm, and therefore the winter peak hours include both day time peaks precisely (see Figure 3.1).

At all residential levels, savings increased exponentially from the standard peak price of \$0.06377 to \$0.085. At an hourly peak rate of \$0.085 per kWh, a sharp increase in savings occurs (see Table 3.3 and Figure 3.8). This is also due to the savings between stored non-peak energy and peak energy offsetting the even lower peak fee. Therefore, we can increase the pre-determined peak to a much higher value, and our savings will not be completely offset by the smaller peak fee of \$3.73. This lower peak price allows the energy savings to show up more broadly and earlier, as seen in the data at the \$0.80 per peak kWh price level. In the other cases where, the savings are limited, and only savings occur when the system peak is lowered substantially. Therefore, all optimal peaks at prices less than \$0.080 per peak kWh are below the original peak in order to maintain peak savings.

Table 3.3: Simulation Results for Winter Residential Households Using Different Peak Prices. Results Include Cost Savings, Optimal Peak, and Minimum Battery Capacity Required

Peak kWh	Peak $/kWh	OptPeak(kW)	OriginalPrice	New Price	Difference	Cap(kWh)
1000.00	$0.0638	3,450.00	$156.29	$153.05	$3.23	4,861.28
	$0.0650	3,450.00	$157.94	$154.56	$3.38	4,861.28
	$0.0700	3,510.00	$164.66	$160.66	$3.99	5,494.88
	$0.0750	3,800.00	$171.37	$166.45	$4.92	8,557.28
	$0.0800	7,110.00	$178.09	$170.12	$7.96	43,510.88
	$0.0850	7,110.00	$184.80	$171.09	$13.71	43,510.88
	$0.1500	7,110.00	$272.09	$183.72	$88.37	43,510.88
1500.00	$0.0638	4,970.00	$225.06	$220.40	$4.65	7,021.36
	$0.0650	4,970.00	$227.43	$222.57	$4.87	7,021.36
	$0.0700	5,030.00	$237.10	$231.35	$5.75	7,654.96
	$0.0750	5,470.00	$246.77	$239.69	$7.08	12,301.36
	$0.0800	10,250.00	$256.44	$244.97	$11.47	62,776.32
	$0.0850	10,250.00	$266.11	$246.35	$19.76	62,776.32
	$0.1500	10,250.00	$391.82	$264.33	$127.49	62,776.32
2000.00	$0.0638	6,280.00	$284.44	$278.56	$5.88	8,858.09
	$0.0650	6,280.00	$287.45	$281.30	$6.15	8,858.09
	$0.0700	6,360.00	$299.67	$292.41	$7.27	9,702.89
	$0.0750	6,910.00	$311.89	$302.94	$8.95	15,510.89
	$0.0800	11,910.00	$324.12	$310.21	$13.90	68,275.20
	$0.0850	12,180.00	$336.34	$313.31	$23.03	70,364.16
	$0.1500	14,300.00	$495.21	$342.08	$153.13	76,032.00
2500.00	$0.0638	7,390.00	$334.46	$327.55	$6.91	10,477.05
	$0.0650	7,390.00	$337.99	$330.77	$7.23	10,477.05
	$0.0700	7,480.00	$352.36	$343.82	$8.54	11,427.45
	$0.0750	8,130.00	$366.73	$356.21	$10.52	18,291.45
	$0.0800	12,740.00	$381.10	$365.47	$15.63	66,928.64
	$0.0850	13,060.00	$395.47	$370.87	$24.60	69,396.48
	$0.1500	15,550.00	$582.28	$428.43	$153.85	76,032.00
3000.00	$0.0638	8,450.00	$382.91	$374.98	$7.93	11,883.73
	$0.0650	8,450.00	$386.95	$378.67	$8.28	11,883.73
	$0.0700	8,560.00	$403.41	$393.62	$9.78	13,045.33
	$0.0750	9,310.00	$419.86	$407.81	$12.05	20,965.33
	$0.0800	13,540.00	$436.31	$419.00	$17.31	65,587.20
	$0.0850	13,910.00	$452.76	$426.63	$26.13	68,444.16
	$0.1500	16,760.00	$666.63	$512.08	$154.55	76,032.00
3500.00	$0.0638	9,420.00	$426.67	$417.84	$8.83	13,287.13
	$0.0650	9,420.00	$431.18	$421.94	$9.24	13,287.13
	$0.0700	9,540.00	$449.51	$438.61	$10.90	14,554.33
	$0.0750	10,380.00	$467.84	$454.42	$13.42	23,424.73
	$0.0800	14,260.00	$486.17	$467.34	$18.83	64,353.28
	$0.0850	14,680.00	$504.40	$477.00	$27.40	67,599.36
	$0.1500	17,850.00	$742.82	$587.64	$155.18	76,032.00
4000.00	$0.0638	10,280.00	$464.14	$454.64	$9.50	14,476.05
	$0.0650	10,280.00	$470.66	$460.59	$10.07	14,476.05
	$0.0700	10,410.00	$490.63	$478.77	$11.85	15,848.85
	$0.0750	11,320.00	$510.68	$496.03	$14.66	25,458.45
	$0.0800	14,910.00	$530.69	$510.51	$20.18	63,313.92
	$0.0850	15,360.00	$550.70	$521.97	$28.73	66,795.52
	$0.1500	18,830.00	$810.84	$655.10	$155.74	76,032.00

Consequently, the amp-hours needed to perform the optimum priced DP BESS integration algorithm remains study under $0.08 per kWh and jumps rapidly, more than two times the next highest amp-hours' count (see Table 3.3 and Figure 3.8). The highest Ah used during

any simulation was 21988.80 Ah, which was not associated with the largest household. After a house size which demands 2000 kWh per month, the total capacity needed to perform an optimal BESS DP algorithm slowly starts to drop, this is due to the current limitations of the specific inverter used in this experiment. The Greensmith 6kW unit cannot output more than 6kW at any moment, and therefore, the peak slowly starts to reach an upper limit with the simulations increasing household size [28]. At this point, shaving the peak hours energy all the way to zero use is optimal, but that required energy level cannot be obtained due to the current limiting restraint of the DESD.

Figure 3.9 shows winter simulation results with standard utility TOU rates. The peak is lower than the previous peak, and at non-peak hours the DESD charges up to the peak demand, and dissipates this charge across the peak-hours once all demand values higher than the pre-determined peak are shaved. Figure 3.10 shows winter simulation results with the highest simulated peak hour costs, which make stored non-peak energy much cheaper than peak energy. The peak is higher than the previous peak, and at non-peak hours the DESD charges up to the peak demand, and dissipates this charge across the peak-hours evenly until almost zero demand occurs during peak hours. In this case an inverter current limit was not reached. Though in the case of Figure 3.11, a peak inverter current limit is reached, and thus not all of the peak-hour energy can be shaved.

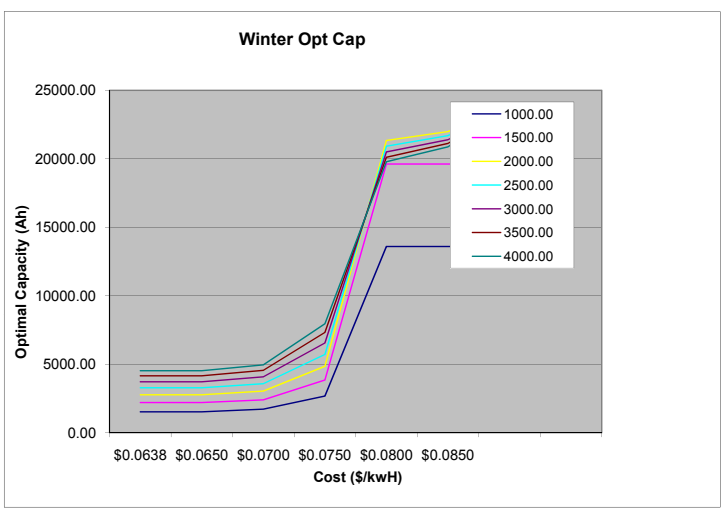

Figure 3.8: Winter OptPeaks for Different Sized Households at Different Peak Rates

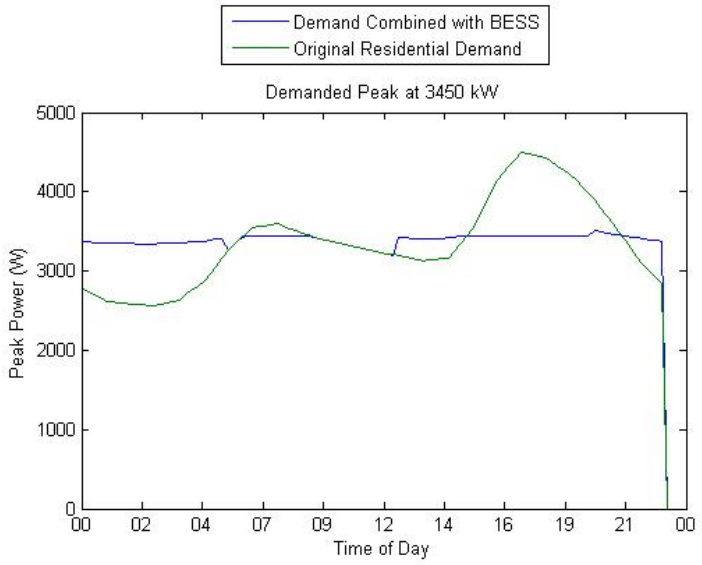

Figure 3.9: Winter Optimum Peak Simulation Results at Standard Utility Rates during Winter

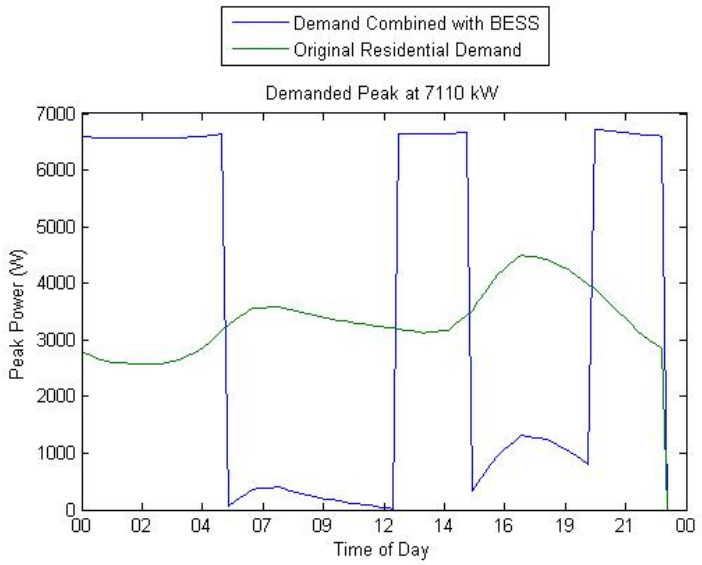

Figure 3.10: Winter Optimum Peak Simulation Results at Maximized Peak Rates during Summer

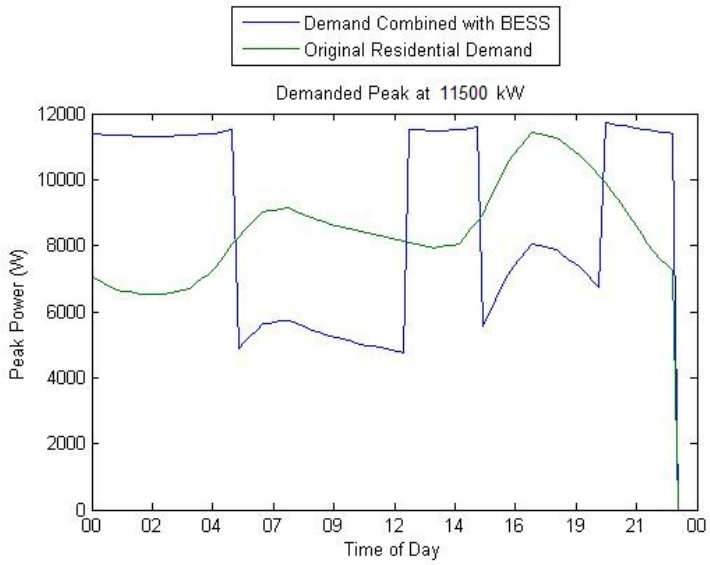

Figure 3.11: Winter Optimum Peak Simulation Results at Maximized Peak Rates during Summer with a Current Limit Reached

3.4 Total Savings

Total yearly savings were calculated assuming six winter months and six summer months, and adding up the total monthly bills for a year. The highest yearly savings were at the 4000 kWh household level and amounted to $327.13. Perhaps though, considering the smaller household of 1000 kWh would be a better indicator. With current prices, only a $41.6292 yearly savings would occur. If peak prices increased (or the difference in off peak and on peak energy costs was greater), more than triple the savings are observed at $150.70 and more reasonably justify the cost of adding the BESS.

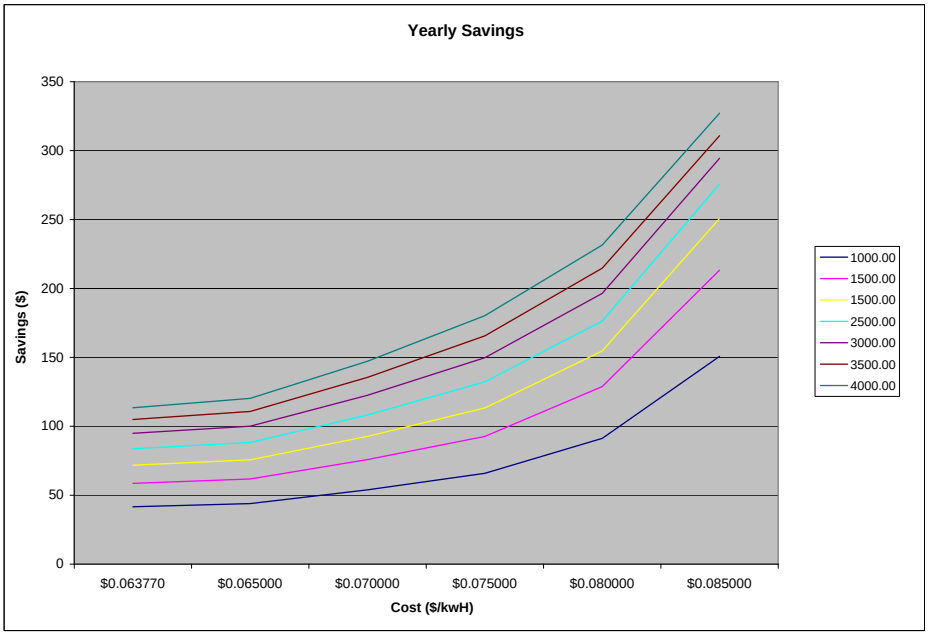

Figure 3.12: Total Savings for Different Sized Households at Different Peak Rates

3.5 Additional Rate Difference Studies

According to the results, households and other utility customers enrolled in the TOU program could see increased savings from approximately $100 to $200 with higher differences in peak and off peak rates. While this is a significant yearly amount, it most likely would not cover the extremely high initial cost of a commercially available BESS. Also, the incentives are not extreme enough to solicit avid customer participation. The savings are approximately equal to one month's energy bill for smaller households.

Therefore, more research was conducted into nationwide TOU rates already deployed in certain regions of the country. The results show that many TOU rates have a high differences in Peak and Off-Peak rates, some even exceeding 30 cents, with most far exceeding the peak price difference provided by Progress Energy (see fig 3.5). The following simulation results include peak price differences of 10 cents and 15 cents to better qualify the simulation results and show

Table 3.4: Yearly Total Savings

Peak kWh	Peak kW	PeakPrice per kWh	Summer	Winter	Year
1000.00	4333.00	$0.0638	$3.70	$3.23	$41.63
		$0.0650	$3.94	$3.38	$43.93
		$0.0700	$4.99	$3.99	$53.91
		$0.0750	$6.06	$4.92	$65.86
		$0.0800	$7.24	$7.96	$91.24
		$0.0850	$11.41	$13.71	$150.70
		$0.1500	$75.95	$88.37	$985.90
1500.00	6000.00	$0.0638	$5.11	$4.65	$58.59
		$0.0650	$5.44	$4.87	$61.82
		$0.0700	$6.89	$5.75	$75.84
		$0.0750	$8.36	$7.08	$92.67
		$0.0800	$10.00	$11.47	$128.83
		$0.0850	$15.79	$19.76	$213.28
		$0.1500	$106.00	$127.49	$1,400.93
2000.00	7100.00	$0.0638	$6.08	$5.88	$71.76
		$0.0650	$6.46	$6.15	$75.69
		$0.0700	$8.19	$7.27	$92.74
		$0.0750	$9.94	$8.95	$113.34
		$0.0800	$11.88	$13.90	$154.69
		$0.0850	$18.76	$23.03	$250.72
		$0.1500	$127.00	$153.13	$1,680.78
2500.00	8250.00	$0.0638	$7.04	$6.91	$83.69
		$0.0650	$7.49	$7.23	$88.28
		$0.0700	$9.49	$8.54	$108.20
		$0.0750	$11.52	$10.52	$132.25
		$0.0800	$13.77	$15.63	$176.39
		$0.0850	$21.36	$24.60	$275.77
		$0.1500	$146.31	$153.85	$1,800.96
3000.00	9250.00	$0.0638	$7.89	$7.93	$94.90
		$0.0650	$8.40	$8.28	$100.08
		$0.0700	$10.64	$9.78	$122.52
		$0.0750	$12.91	$12.05	$149.75
		$0.0800	$15.43	$17.31	$196.46
		$0.0850	$22.95	$26.13	$294.46
		$0.1500	$160.29	$154.55	$1,889.03
3500.00	10125.00	$0.0638	$8.67	$8.83	$104.97
		$0.0650	$9.22	$9.24	$110.75
		$0.0700	$11.69	$10.90	$135.52
		$0.0750	$14.18	$13.42	$165.65
		$0.0800	$16.95	$18.83	$214.69
		$0.0850	$24.40	$27.40	$310.84
		$0.1500	$161.82	$155.18	$1,902.00
4000.00	11000.00	$0.0638	$9.41	$9.50	$113.43
		$0.0650	$9.97	$10.07	$120.24
		$0.0700	$12.68	$11.85	$147.22
		$0.0750	$15.40	$14.66	$180.31
		$0.0800	$18.40	$20.18	$231.50
		$0.0850	$25.79	$28.73	$327.13
		$0.1500	$162.33	$155.74	$1,908.45
		$0.2000	$271.03	$256.06	$3,162.53
		$0.3000	$488.51	$456.87	$5,672.28

Table 3.5: Nationwide TOU Rates With High Peak/Off-Peak Difference

Utility	Season	Peak	PartPeak	OffPeak	Peak Difference
Pacific G&E	Summer	$0.44703	$0.20182	$0.12183	$0.3252
	Winter		$0.16794	$0.12183	$0.04291
O&R	Summer	$0.20368	$0.07288	$0.01311	$0.19057
	Winter		$0.07288	$0.01311	$0.05977
NV Energy	Summer	$0.32013		$0.07866	$0.24147
MGE	Summer	$0.22086		$0.03768	$0.18138
	Winter	$0.19408		$0.03768	$0.15648
Coast EPA	ALL	$0.218		$0.05433	$0.16367

the differences in savings under these conditions. Payback period under these conditions were determined based on the initial cost of the BESS. The initial cost of the BESS system was modeled after the initial cost of the Greensmith 6kW, 20kWh system, which can be priced by contacting an appropriate sales representative. The cost of a system was scaled based on the amount of amp-hours needed to conduct the dynamic programming BESS integration for each simulation.

3.5.1 Higher Rate Difference Results

It can be seen from the results in Figures 3.13 and 3.15 that total savings increase exponentially from the previous maximum savings at 8.5 cents up to an order of magnitude higher at 20 cents. Required capacity levels off at 15 cents for all households due to the large difference in rates being enough to make up for any setbacks provided by the peak fee charged each month. For large households, the optimum capacity is the same due to the limits of the DESD inverter being reached, and therefore maximum potential storage being reached. For smaller households, required capacity levels off even earlier due the complete peak load being small enough to be shaved with a low capacity BESS and small effects on the peak fee (see Figures 3.14 and 3.16).

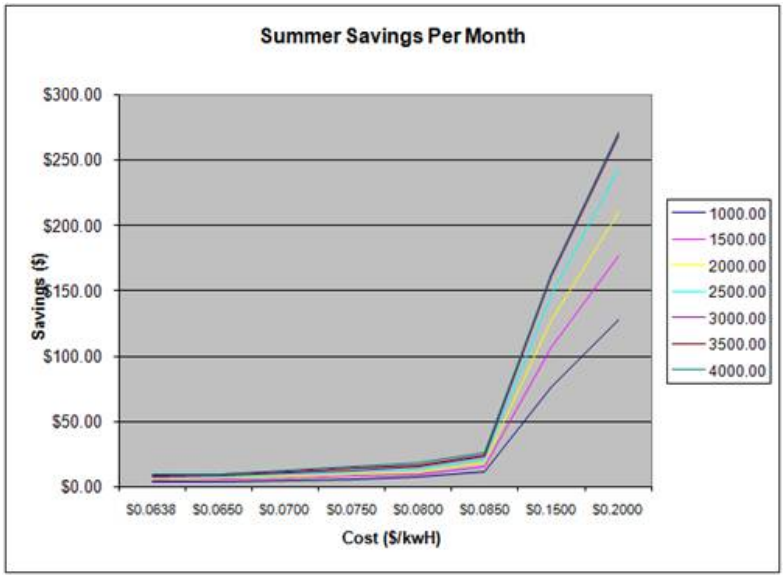

Figure 3.13: Summer Total Savings for Different Sized Households including High Rate Differences of 10 and 15 cents

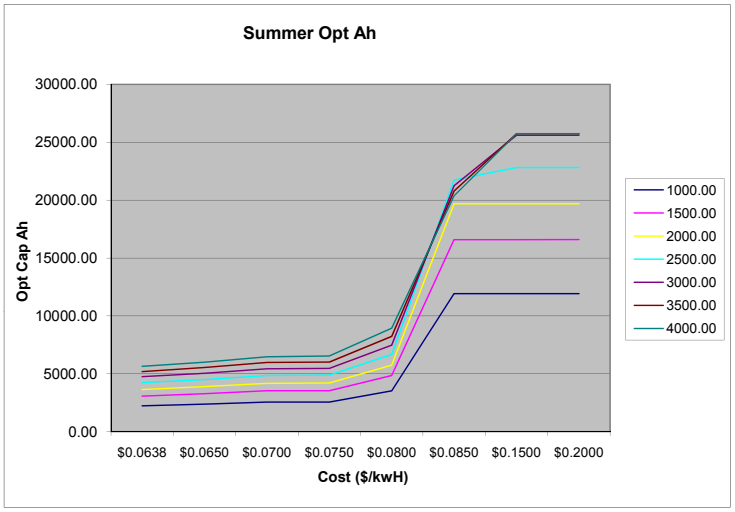

Figure 3.14: Summer Ideal Capacities for Different Sized Households including High Rate Differences of 10 and 15 cents

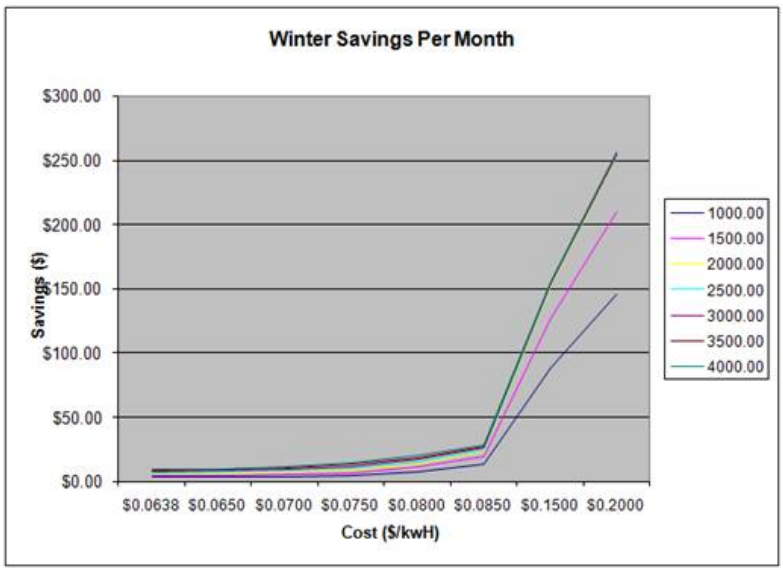

Figure 3.15: Winter Total Savings for Different Sized Households including High Rate Differences of 10 and 15 cents

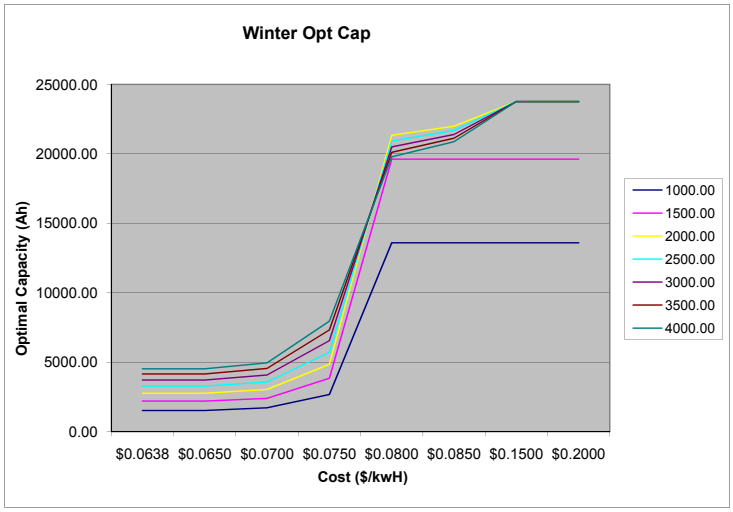

Figure 3.16: Winter Ideal Capacities for Different Sized Households including High Rate Differences of 10 and 15 cents

Yearly savings showed exponential increases at the 15 cents and 20 cents peak rate level (see Figure 3.17). Overall, savings increased an order of magnitude from the mid-level peak price of 8.5 cents to the highest level of 20 cents. Therefore, payback period was reduced greatly for these rates. Payback periods decrease to under 50 years in these cases (see Figure 3.18), which is slightly more feasible than the levels at low and mid rates of 200+ years.

Even though a significant drop off in payback period is shown at 15 and 20 cents per kWh, the payback period is still too large for consumers to see any significant savings over a short period of time. Also, through 30+ years of constant operation, a DESD is likely to require service or replacement parts, therefore reducing the most practical and economic payback period to under 5 or 10 years. Further calculations were performed, and utility peak and off peak rate price differences of greater than 35 cents and beyond are necessary to achieve lower, more practical payback periods. These large rate differences coincide from some utility TOU rate structures shown in Figure 3.5, but it is likely that not all utilities would be willing to try out such large price differentials.

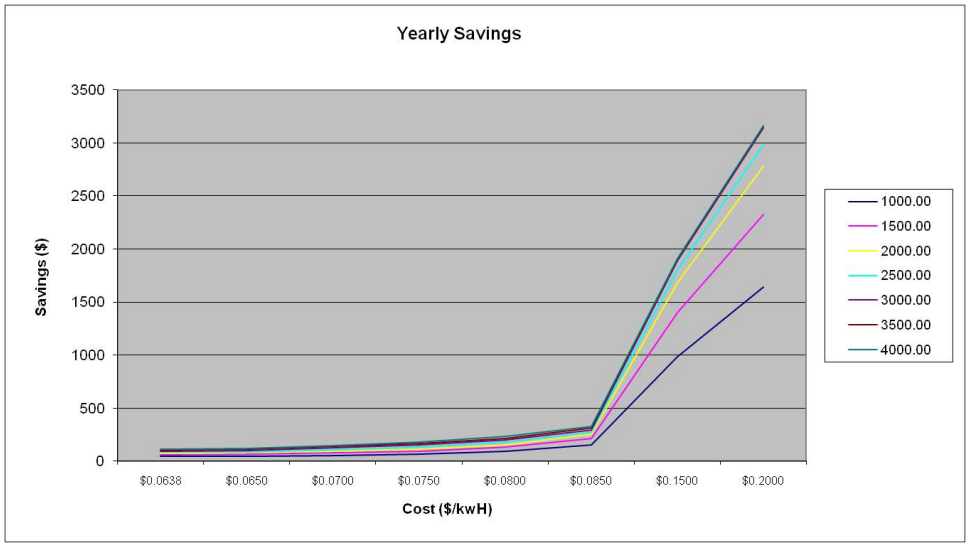

Figure 3.17: Yearly Savings Also Increase Almost Exponentially

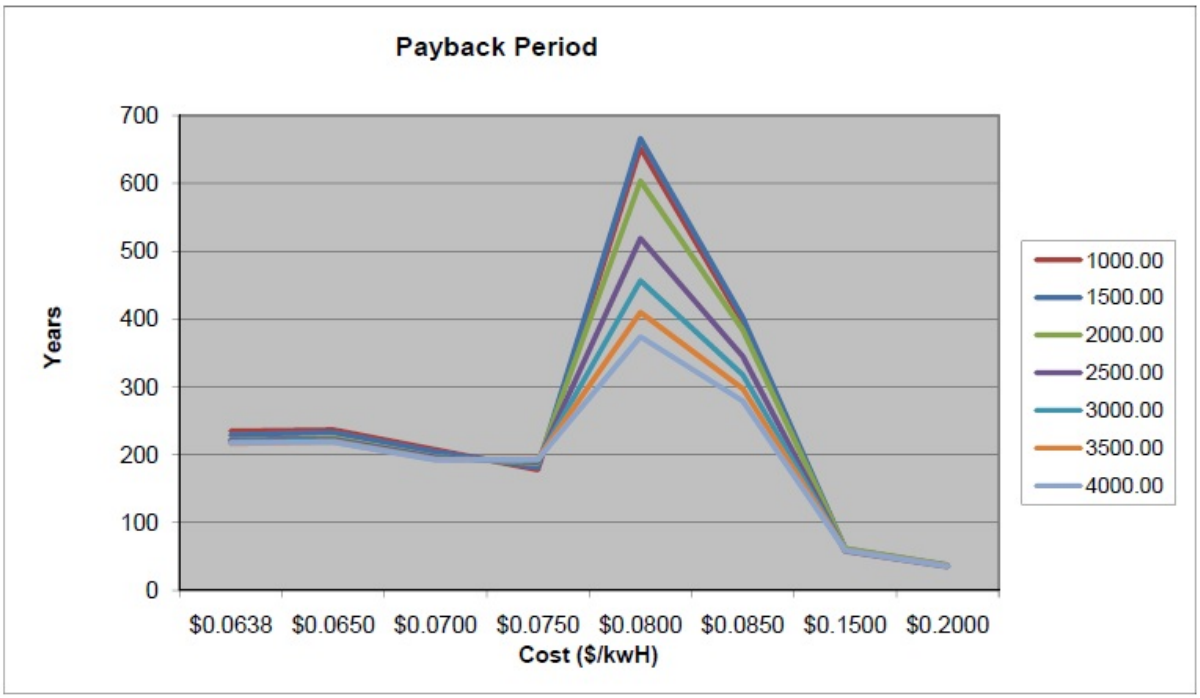

Figure 3.18: Payback Period Starts Off Above 200 Years, and Peaks in Midrange Peak Prices Due to Higher Hapacities Needed to Shave Peaks with a Limited Profit. At High Range Peak Prices, Payback Period Greatly Reduces to Less than 50 Years.

3.5.2 Conclusions

Cost cutting applied to residential and small scale commercial buildings with a BESS was proven successful via simulations and typical residential loads applied to a central NC customer. The combination of a pre-determined peak, rule based BESS control, and dynamic programming proved effective in cutting utility bills in the most optimal manner, taking into account peak fees and rates for different sized households. The only setbacks are the current utility Peak/Off-Peak price structures and the current initial cost of a BESS. There are only minimal savings for 1000-2000 kWH households without price adjustments from the utilities side. BESS integration requires a large kWh system with a large kW inverter. With mild increases in rate structures, payback periods for the initial cost of the BESS are less than 50 years, but also more than 15 to 20 years. A broad based effort to decrease the intial cost of a commercial BESS and increase differences in Peak and Off-Peak prices (while keeping them relative to non TOU customers' rates) would be needed in order for this method of peak shaving to become practical and economical.

Future work includes integration of a PV array for 'Free energy use during peak shav-

ing. Further tests need to integrate the study and DESD into a real time system (FREEDM Hardware) with real time demand monitoring via a smart-meter.

Chapter 4

Human Machine Interface

As previously discussed in the introduction, HMI's are an essential part of any electric power system, including a BESS. Without the proper tools to monitor the battery system and its components, a user has no information on a charge or discharge process and is susceptible to system errors or damage to equipment. Subsequently, without a means of controlling system parameters or processes via communication, a user cannot make changes during a charge or discharge process to react with real-time environmental changes or emergencies. These situations include faults on the power grid or exceeding component limits.

An HMI can directly solve all of these issues. HMI's relay information to a system operator and allow the user to make changes during real-time operation. An HMI can be considered a high-level control and monitoring tool if it is used to monitor and control 'obvious' variables, such as battery voltage and charger current. The HMI usually does not include closed loop controls which use error calculations and PID methods to reduce errors in measurements and outputs.

The main focus of this chapter will be on the design and implementation of an HMI for a 10kW, bi-directional, multi-functional charger (FREEDM Project Y3.C3.E3), developed primarily by Xiaohu Zhou under the guidance of Dr. Alex Huang and Dr. Srdjan Lukic [15]. The charger will be described in more detail in the following subsection. The equipment was built in house by Mr. Zhou with the help of lab managers and other graduate students. The equipment was functional as of September 2009, when the HMI portion of the project was initiated. In order to complete the project, the equipment needed to be commercialized and normalized for demonstrations through the development of an HMI. Previously, all data monitoring took place via temporary oscilloscopes, which are expensive, complicated, and not visually pleasing (see Fig 4.1). All control was encoded via a DSP control card, and real-time alteration of input variables was not possible. The following sections will discuss the background, research, and implementation of the HMI developed for the FREEDM multi-functional, bi-directional

charger.

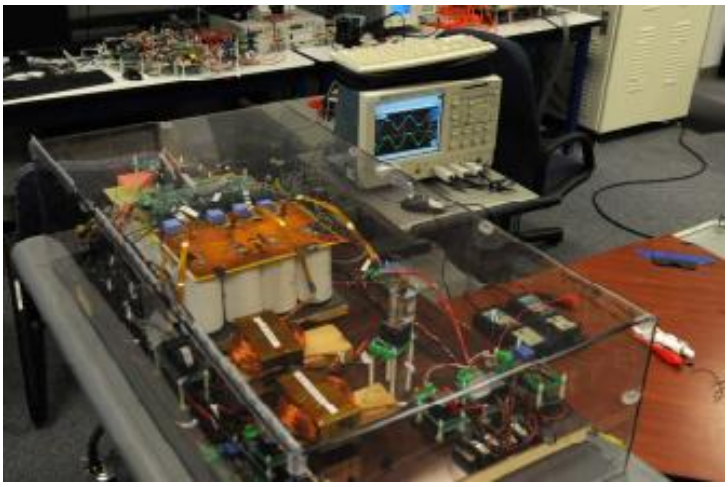

Figure 4.1: Prototype of 10kW Bi-Directional Charger with Oscilloscopes Used for Monitoring [16]

4.1 Multi-Functional Bi-Directional Charger and Initial Stages of Monitoring and Control

The Multi-Functional Bi-Directional (MFBD) charger was initially designed for vehicle batteries of plug-in hybrid electric vehicles (PHEV) and plug-in electric vehicles (PEV), hence the bi-directional quality. The MFBD Charger is designed to operate in three different modes, including battery charging (V2G), vehicle to grid (V2G), and vehicle to home (V2H). PEV's and PHEV's have high capacity battery banks which utilize the electric utility grid for charging, primarily at night. They present the opportunity to utilize electric power during the nighttime and the ability to become energy storage devices to collectively supply the grid during outages , decrease peak load intervals, act as a uninterruptable power supply (UPS) at customer sites, or stabilize renewable energy sources [15].

The charger consists of two power stages, including the grid-side converter (Stage 1), and the battery-side converter (Stage 2) (see Fig 4.2). A half bridge converter operates in boost mode during V2G and V2H and subsequently operates in buck mode during charging. A split phase three-leg converter is used to tap into the to utilize 240V and 120V inputs of a traditional American residential household. The three-leg converter boasts a number of advantages over a split-capacitor H-bridge including lower DC current ripples and smaller output filters [15].

Level I charging is conducted at 120V AC, and Level II charging is conducted at 240V AC. The ratings of MFBD charger exceed typical current and power ratings of residential circuitry boards, but the charger will be connected in the FREEDM laboratory which might require additional testing of high power, fast charging sessions.

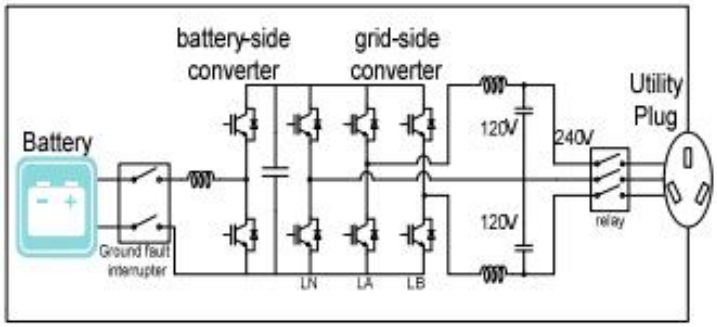

Figure 4.2: Topology of MFBD Charger, Showing Two Phases of Conversion and Connection to Residential Utility Supply [15]

One of the main benefits of this charger is the low harmonic distortion introduced to the grid via a closed-loop, current mode controller operating in V2G mode. A third order filter is created when the LC filter of the H-bridge converter connects to grid impedance, forming an LCL filter. Resonance created due to this filter can compromise the performance of a controller and yield low power quality which does not meed standards and codes. Resonant peaks can also damage equipment [16]. Mr. Zhou proposes an active damping control structure to counteract resonant peaks. The filter capacitor current is sensed, multiplied by the damping factor, and added up to the PWM output. This resonant current is used to eliminate the PWM output components at the resonant frequency. Mr. Zhou's initial experiments were successful using MATLAB Simulink to implement code onto a TMS320f28335 DSP for the open loop control and elimination of harmonics at the resonant frequency (see Fig 4.2). Initially, Mr. Zhou observed a resonant frequency between the 25th and 27th harmonics, giving a total harmonic distortion (THD) of 9.77%. After active damping control, almost no high frequency resonance occurs and the THD reduces to 3.58% [16]. His results were verified in his experiments (see Fig 4.3)

The charger is transformerless, and among other advantages reduces the system weight while increasing efficiency. The absence of a transformer also decreases complications in control algorithms. In order to counteract the effects of the missing transformer, a ground fault interrupter (GFI) was used for safety requirements concerning the vehicle being used as a ground during a battery short. Proportionate and resonate (PR) control is used to reduce output error and

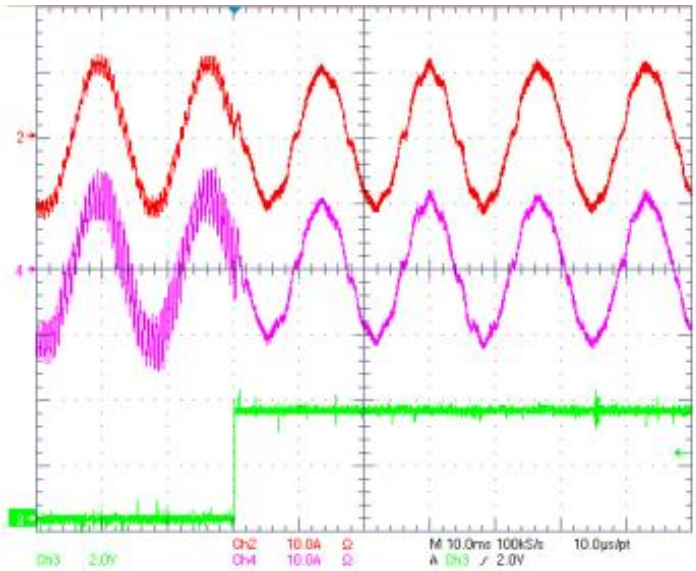

Figure 4.3: The Converter's LC Current (top), and The Grid Current (middle) Before and After Active Damping is Enabled (bottom). It Can Be Easily Seen that The THD is Reduced [16]

limit any DC current injection to the grid, which may damage transformers. Finally, passive EMI filters are used to reduce high frequency leakage current via common-mode voltage [15].

4.1.1 Charger Operation and Software Environments Background

The MFBD charger relied on multiple development programs for algorithm programming and internal controls. A Texas Instruments (TI) TMS320f28335 DSP was used as the brains of the charger, allowing dynamic programming using Code Composer Studio v3.3 in combination with MATLAB Simulink.

Software Environments

The software environments used in the algorithm generation for the MFBD charger are all related and work with each other. The initial code is designed and generated graphically via MATBLAB Simulink and the Target Support Package. The Embedded Coder then coordinates with Code Composer Studio (CCS) v3.3 to build this code and load it onto the hardware (DSP). Anytime the charger needs to be operated, the CCS v3.3 Studio needs to be operated to run and stop the process. The code generation via MATLAB only needs to take place once. If variables need to be adjusted, such as a reference current, control variables, or port settings, the code will need to be altered via graphic programming and regenerated.

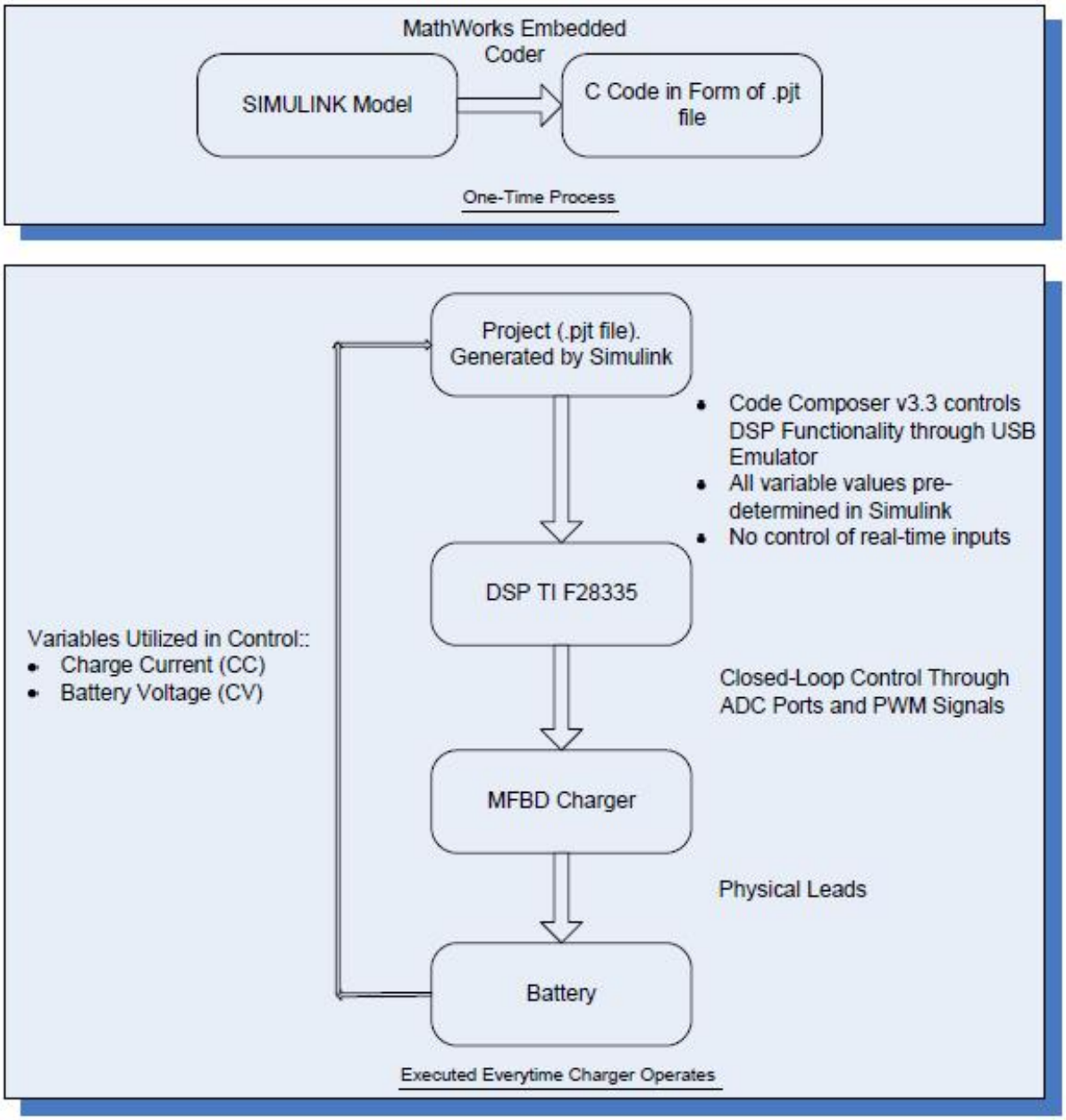

Figure 4.4: Flow Diagram Illustrating The Code Generation and Execution for The MFBD Charger

Initially, all algorithm programming took place via MATLAB R2009B Simulink, a graphical programming tool usually used to simulate hardware and other processes, but also with the capability to run hardware in the loop (HIL) via specific toolboxes. In this case, the Target Support Package was used to generate C code for the TI DSP (embedded system).

The Target Support Package provides an integrated development environment (IDE) Link Target to TI Code Composer Studio (CCS) version 3.3 MathWorks defines the functions of this portion of their Embedded Coder product as follows, "It generates code for compilation and deployment using a supported third-party integrated development environment such as Texas Instruments' Code Composer Studio." [17] Using the 'Chip Support' drop down menu from the 'Texas Instruments C2000' drop down under 'Supported Processors', one can find a variety of graphical programming tools to develop hardware and software algorithms for all C2000 DSP's. There are other supported embedded system products under the 'Supported Processors' drop-down menu (see Fig 4.5). The first step into the graphical programming is to select the proper DSP board number from the 'Chip Support' drop down menu. This menu lists all available options for the TI C2000 boards, including the C28x3x, which coincides with the C28335 board which we are using for this project. A modified board was programmed by Arvind Govindaraj. Many options for ports and memory allocation are available in this block's properties.

The user can access ADC ports, Digital inputs/outputs, Serial ports, and other features of the F28335 DSP. The inner workings of these blocks contain C code that is specific to the model of DSP you are using. These ports can be utilized in a Simulink model and edited via their properties windows. Other traditional Simulink blocks can be used in between to run calculations, control loops, data conversion, and a plethora of other operations. The Embedded Coder converts all of these operations to C codes as well when a user clicks the 'Incremental Build' button on the top of the page (see Fig 4.6). At this point, you must ensure that CC v3.3 is open and the target is connected (discussed in the following section). The incremental build will run a number of operations on the MATLAB home page, and will display any errors. CC Studio will open up, compile and build the code onto the DSP board, and then run the program immediately. You must stop the program via CC Studio 'Halt' operation if you do not wish to run the program [17].

Once the Simulink .mdl file has been converted to C code via the Embedded Coder, you can see the .pjt files as well as the C files in the navigation menu of CCS Studio. You can also Run, Halt, Debug, and edit the code (see Fig 4.7). All errors, including issues with connectivity between MATLAB and TI products and hardware issues should be consulted through the proper Customer Support or other FREEDM lab members who are trained in the appropriate fields. Most FREEDM hardware has a DSP interaction for control.

Charger Operating Algorithms

Xiaohu Zhou was the primary designer of the closed loop control algorithms implemented in MATLAB Simulink via the Target Support Package. The three modes of operation each have a specific model developed for their specific operation.

The battery charging mode utilizes constant current (CC) and constant voltage (CV) charg-

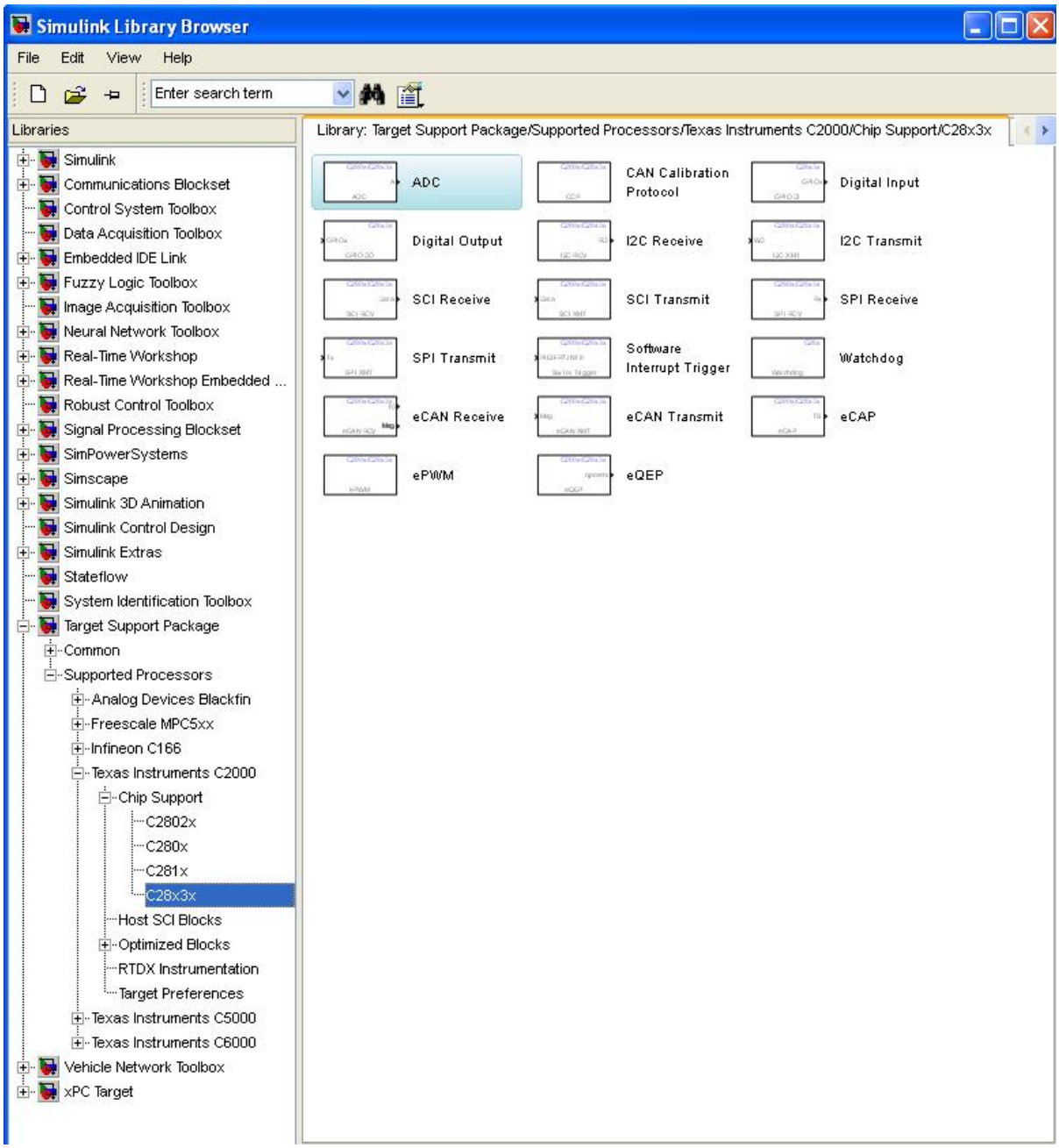

Figure 4.5: The Target Support Package Lists a Variety of Embedded Systems It Is Compatible With. Specifically, The TI C2000 F28335 Graphical Programming Tools Are Shown Which Were Used in This Project [17]

ing loops to safely charge batteries at user defined operation levels. During CC mode, a closed loop control is implemented in the following structure (see Fig 4.8):

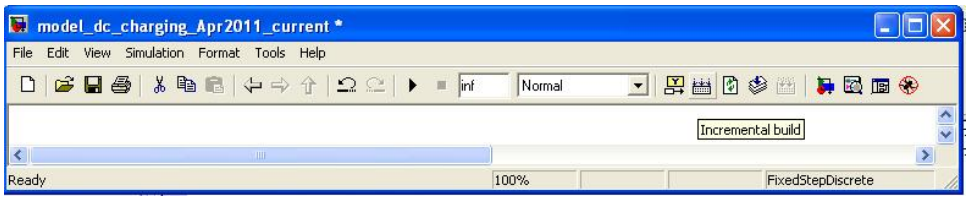

Figure 4.6: Incremental Build Operation Located in The Top of The Simulink Window

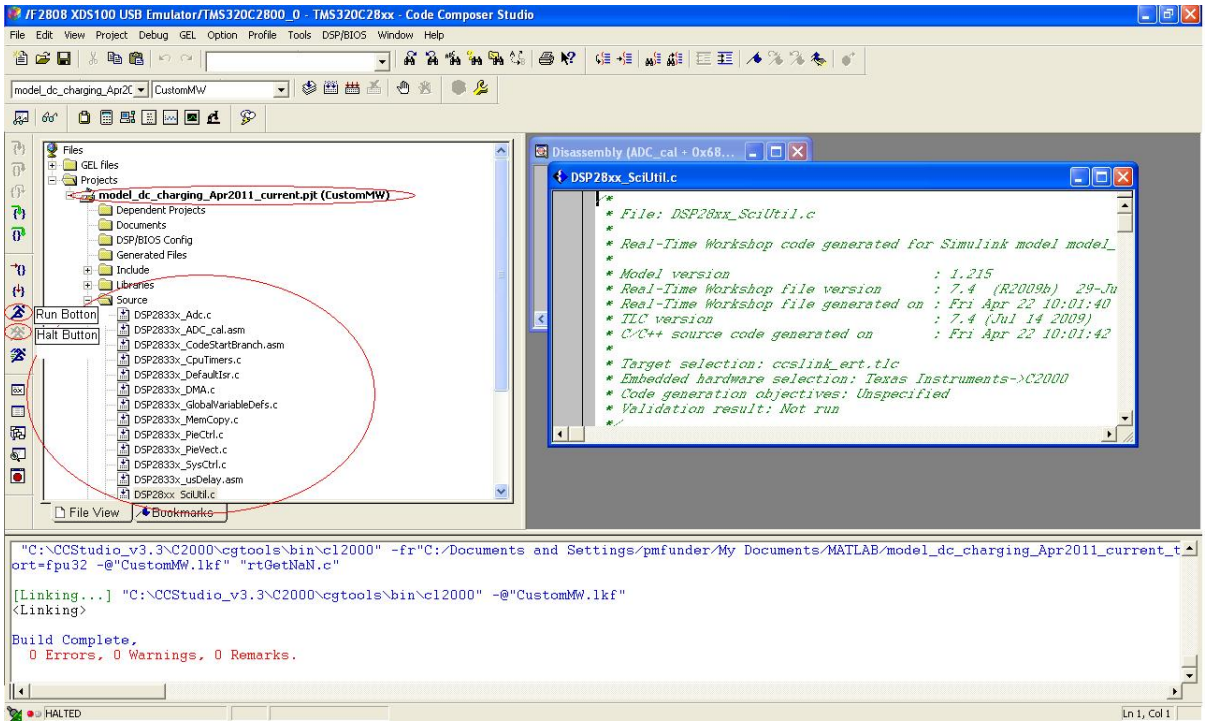

Figure 4.7: CCS Window Displaying a Successfully Converted Simulink .mdl File as a Project File (top). All Available C Code Conversions are Displayed in The 'Source' Drop Down Menu and Can Be Modified (bottom). Commands Are Displayed on The Left Pane (middle)

1. Measures battery charging current via and analog to digital converter (ADC) ports on the DSP
2. Modifies the measurement signals to reflect the actual current
3. Compares the measured signal to the reference current specified by the operator
4. Uses PID (proportionate, integral, derivative) control to adjust the output.
5. Feeds the PID output to a pulse-width modulator (PWM) generator which controls the charging current

6. The measuring process begins again, thus forming a closed loop control which ensures the proper charging current

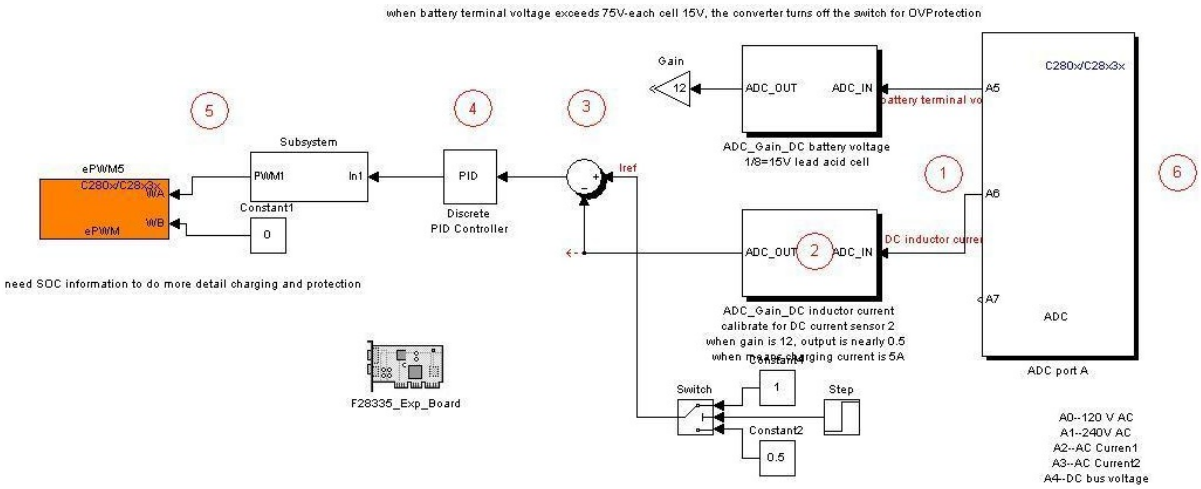

Figure 4.8: Simulink Model of a CC operation. The steps are enumerated and correspond to the list above

The constant voltage charging algorithm is similar in that it utilizes battery voltage measurements instead of charging current measurements. The constant voltage (CV), or topping operation, executes when a battery voltage rated value is achieved. According to battery experts, the best way to charge a Lead-Acid battery is to charge the battery at a constant current below the rated value until a rated voltage is achieved, between 2.30 to 2.45 V per cell. A trickle, or topping charge must then be implemented in the form of a CV charging algorithm, which reduces the current until a minimal value is reached (3% of the rated current), and the battery is fully charged. This method of charging reduces damage to the battery with proper voltage limits, and also ensures that the maximum state of charge (SOC) is achieved via the trickle charge. Finally, an optional float charge is implemented if the battery stays connected to the charger. This float charge maintains the battery at a safe operating voltage if the charge has taken at least 48 hours [19].

4.1.2 Monitoring and Control

As discussed earlier, the earlier version of the MFBD charger used external measuring devices for system monitoring relayed to operators (see Fig 4.1). Specifically, a range of Agilient Oscilloscopes were utilized with high amperage current probes and voltage probes to monitor

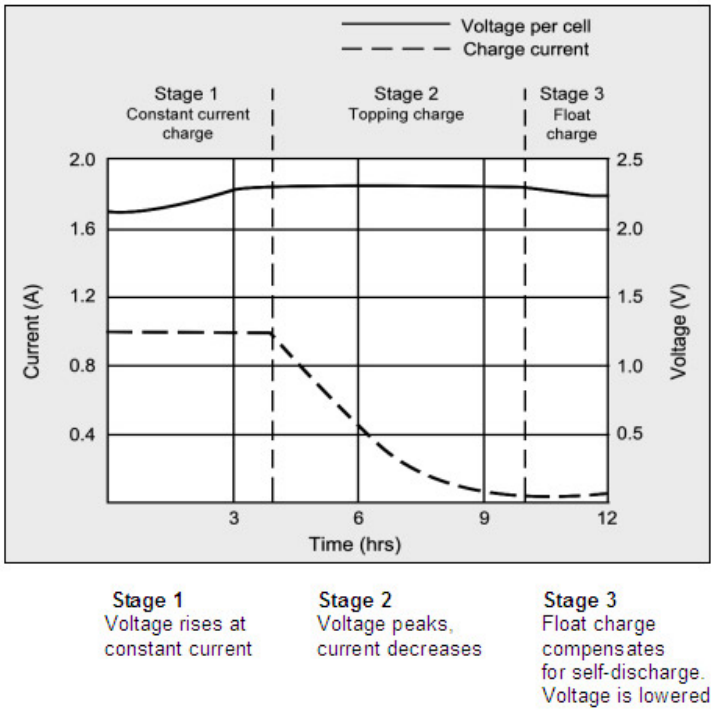

Figure 4.9: The States of Lead-Acid Battery Charging Session Include a CC Stage and a CV Stage (Topping). Optional is the Float Charge Stage Which Maintains the Battery at a Safe Floating Voltage

charge/discharge current, battery voltage, input grid voltage and frequency among other parameters. While providing the proper monitoring purposes, the oscilloscopes rotate frequently between other projects, causing time delays for experiments to be run. The oscilloscopes are also expensive, and would need extra funding if used as the primary means of monitoring a BESS charger. Finally, the oscilloscopes are extremely large and require a number of wires, a mobile cart, and an extra grid connected power supply.

Monitoring the MFBD charger was one of the primary concerns of the FREEDM administration. The other primary concern dealt with how to control the charger, during a real-time operation, to adjust to different scenarios dictated by the operator or environmental changes such as grid outages, SOC deficiencies, or parameter extremes such as current limits and battery voltage limits. The initial version of the MFBD could only be controlled via Code Composer Studio v3.3 through the TI TMS320f28335 DSP.

The FREEDM administration requested that an HMI be constructed to dissolve these issues. The HMI would be required to display and plot important variables which would confirm that the charger is operational and that system parameters are at safe and desired levels. The HMI would also be able to have high-level control over the operation of the MFBD charger. This

subsection will describe the process of determining the which programs and communication methods would be used to develop the HMI. It will also detail the technical aspects of the HMI, successes and failures, and experiments and results.

Choice of Program, Communication Methods

Initially, the programming platform for the HMI of the MFBD Charger was not known. Many options were considered based on Mr. Zhou's initial choice of hardware and software. Numerous options were available, and ultimately the decision was made based on ease of use, compatibility, and aesthetics.

The first option that I looked at was the GUIDE function of MATLAB. GUIDE, which stands for Graphical User Interface Development Environment, was designed by MathWorks for users to create easily implemented GUI's to control m-files and Simulink models. The GUI can resemble a switchboard with knobs and buttons, and can even display variables and graphs, similar to an HMI, but mainly virtually implemented [21]. GUIDE allows easy drop and drag capability as well. While all of these options seemed like an excellent fit, I discovered that GUIDE can only be used on actively running Simulink models. The MFBD charger only utilizes Simulink during the code generation process, then hands over all real-time control to CCS. For this reason alone, GUIDE, and any other program that controls a Simulink model could not be considered as an option for an HMI development tool.

The second program that I looked at was the Simulation Interface Toolkit (SIT). It serves as a direct link between National Instruments LabVIEW and Simulink [20]. Initially, SIT peaked my interest due to its ability to directly connect a user from LabVIEW, a state of the art graphic programming utility which is used in many industrial and research projects [14]. While initially this seemed like a great idea, upon further review I discovered that the SIT can only be used on actively running Simulink models. The MFBD charger only utilizes Simulink during the code generation process, then hands over all real-time control to CCS. Additionally, the SIT could be used in conjunction with the LabVIEW Real-Time Module, which essentially performs the same functions as the Embedded Workshop developed by MathWorks in transforming graphical programming from Simulink and LabVIEW into C code embedded on a real-time target [20]. Though this combination of programs would work in other instances, this additional software would be redundant, cumbersome to obtain and sync with Mr. Zhou's previous work, and also extremely expensive.

Finally, the third program that I looked at was NI's LabVIEW, as suggested to me by faculty and program directors Dr. Srdjan Lukic and Dr. Ewan Pritchard. The two had had previous experience in the HMI field and had personally worked with the graphical programming interface in previous projects. I had also discovered LabVIEW in my research of the SIT. The graphical interface was easy to use and program with, and the amount of input and outputs

for communication were endless. Upon further investigation of LabVIEW and its connectivity to CCS and DSP's, I found the LabVIEW DSP Test Integration Toolkit. LabVIEW lists the first feature of the Toolkit as the ability to automate standard CCS actions such as running, building, and downloading code to a target [22]. This provides the ability to control all of the high level control operations of the DSP via LabVIEW, giving us complete control over all DSP processes via the HMI, which is a great advantage. With this feature, we can rely solely on the HMI for all communications and control without using CCS or Simulink directly. An average user could now use the HMI without knowledge of how the code is processed and run through the DSP.

4.1.3 SCI

NI lists second feature of the Toolkit as the ability to communicate directly to the DSP with Real Time Data eXchange (RTDX) [22]. RTDX uses the USB connection from the DSP to the computer, either via an XDS100 USB Emulator or a Digital Spectrum XDS510 USB Emulator, to send and receive live data for viewing or signal simulation. RTDX uses channels inside the code, and does not effect execution of the code [22] [23]. Simulink also provides blocks for RTDX communication, making the inclusion of RTDX in Mr. Zhou's control code developed in Simulink a very easy fit. With this information, I conducted some initial tests of the RTDX channels, using Simulink and LabVIEW respectively to send and receive data. I was able to observe data on a real-time basis but did have trouble sending signals. I quickly found out that RTDX was not a highly researched protocol and not many help documents were available online for learning and testing.

After further reading, I also discovered that RTDX was not supported anymore under TI as of June 24, 2010 [23]. LabVIEW lists advantages of the RTDX feature as allowing easier understanding of how the DSP responds under different conditions, quickly validating your DSP code, and migrating RTDX channels into real I/O ports [22]. Thus, showing that RTDX is mainly used for debugging complicated programs and using the channels as developmental predecessors to physical I/O ports that are not only more capable of handling data transfer, but also are well documented and have well known protocols. Suggested alternatives are serial port and Ethernet communication [23], which led me to the Serial Communication Interface (SCI). Arvind Govindaraj, a DSP expert in the FREEDM lab, confirmed that I should use the serial port, SCI of the DSP to send and receive data to and from the DSP during real time operation.

The TI Target Support Package contains the function blocks for SCI send and receive as seen in Figure 4.5. These blocks can simply accept or send serial data messages and incorporate the messages into Simulink calculation and data conversion blocks. For simplicity, I relied only

on single 8 bit messages to limit code complexity via data buffers and registers. Using Simulink data conversion blocks to convert numbers sent and received to 8-bit numbers, communication to and from the DSP board became a very simple process. I used a pulse timed switch to send two different variables in 1 second increments (see Fig 4.10). Therefore, multiple messages were sent to the HMI without having to use buffers. Identifiers were used to distinguish the type of data being received by the HMI. Testing of the system was done with Hyper Terminal, Simulink, and other simple RS-232 messaging programs.

In conclusion, the SCI functionality was utilized for communication to and from the DSP which controls the MFBD charger with simple 8 bit messages.

4.2 Implementation of LabVIEW HMI with SCI

LabVIEW was used as the HMI for the reasons discussed in Section 4.1.2. LabVIEW has a simple Serial port sending and receiving function blocks in the form of VISA read and write sessions. A user can set up baud rates, data bits, and all other UART preferences easily on screen.

Messages can be sent by converting to ASCII string values in 8-bit messages. For example, the number 32 must be converted into its ASCII equivalent, while retaining its binary form, and comes out to the ! symbol. This will still transmit as binary 32, and be read by the SCI receive port of the DSP, and used as a current reference during charging.

Vice versa, during DSP operation, the number 32 would be converted to an 8-bit integer, sent to the HMI, received by the VISA Serial Receive function block as the ! string, and converted directly into number format as 32. This would be plotted as current or voltage for monitoring purposes (see Figs. 4.16, 4.12, 4.13).

4.2.1 HMI Results

The combination of Simulink with TI Targets and SCI (see Fig. 4.10), CCS, and LabVIEW culminated through code development and I/O control to become the final version of the HMI (see Fig. 4.16). Only a few setbacks occurred in the form of data type management (strings, bit logic, and conversions) and buffer settings. Primarily with the buffer settings, Simulink's IDE with CCS was producing erroneous buffer code for SCI Tx and Rx blocks which could be seen in the CCS development environment under the SCI block.

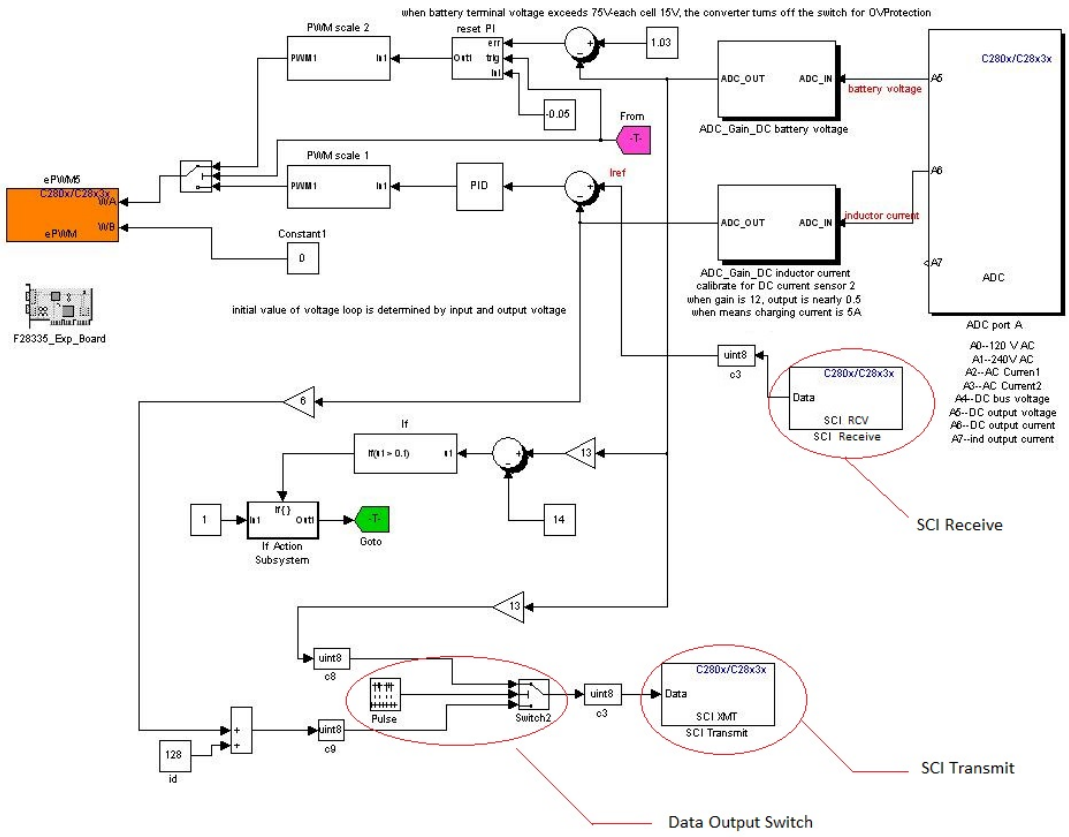

Figure 4.10: Simulink Model Which Generates C Code in CCS 3.3 for the F28335 DSP. SCI Blocks Are Used To Read and Write Data

Data Transfer

For Tx to the HMI from the DSP, the IDE produced buffer checking code in the case of multi-byte messages to allow the serial port to send larger portions of data. I had not included this as part of my communication protocol. The system would stall when checking for a full buffer flag. This flag never changed because a buffer was not included at all (see Fig 4.11). After commenting out the code, the system functioned well for HMI data reception for monitoring system variables, including charging current and voltage. There was some delay from the time of a changed current reference to the visual plotting of a system change on the HMI (see Figs 4.12 and 4.12). Delays were between 5 and 10 seconds due to lack of code optimization and system resources being dedicated to closed loop control and SCI Rx.

```
// Transmit character(s) from the SCIa
void scia_xmit(char* pmsg, int msglen)
{
  int i;
  for (i = 0; i < msglen; i++) {
/*     while (SciaRegs.SCIFFTX.bit.TXFFST == 16) {                 */
/*     }                                   // The buffer is full; */

    SciaRegs.SCITXBUF= pmsg[i];
  }

/*   while (SciaRegs.SCIFFTX.bit.TXFFST != 0) { */
/*   }                                          */
}

int byteswap_L8exp(char* outdata, char* inport ,int inportWidth, int typeLen)
{
  int i,j;
  int k = 0;
  int numWrd = (inportWidth * typeLen)/2;// number of words (16 bit length) to send

  /* Little Endian, 8bit swap */
  for (i = 0; i < numWrd; i++) {
    for (j = 0; j < 2; j++) {
      outdata[k++] = inport[i] >>(8*j);
    }
  }
```

Figure 4.11: SCI Utility Code Commented Out Register Check Values

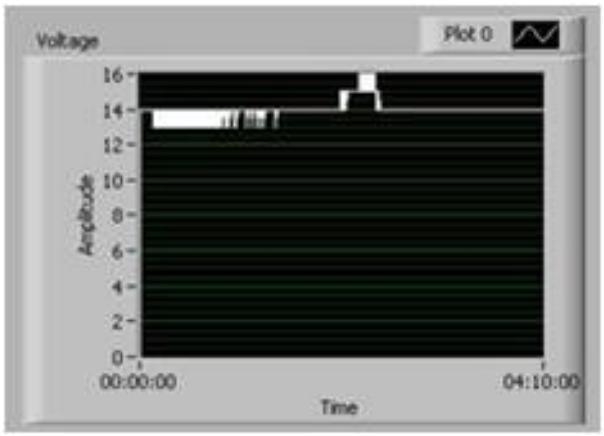

Figure 4.12: Voltage Monitoring of Charging Sequence. Stays at 14 V with Some Integer Error Corrections

Data Receive

For Rx from the HMI to DSP, the IDE produced buffer and register checking code for multi-byte messages. As with the Tx code, the system would stall when checking for a full buffer flag. This flag never changed because a buffer was not included at all (see fig 4.14). After commenting

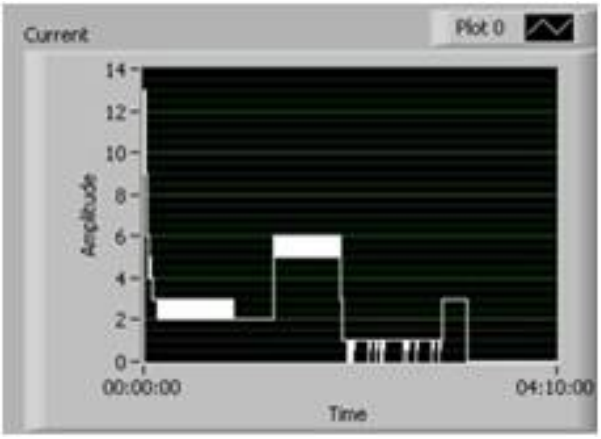

Figure 4.13: Current Monitoring of Charging Sequence. Adjusts According to User Input and Hardware Readout

out the code, the system functioned well for receiving data on the TI DSP and consequently to provide closed loop current or voltage control of the system. User control of constant current or voltage was done via an easy to use, administrator programmable knob (see Fig 4.16). The knob could be programmed to only select certain current reference values to prevent battery damage. System response to changes in charging current reference was almost instantaneous as measured by an oscilloscope (see Fig 4.15).

```
int scia_rcv(char *rcvBuff, int buffLen, int loopMode)
{
  int i;
  unsigned int cnt = 0;
  unsigned int maxcnt;
  if (loopMode == LONGLOOP) {
    maxcnt = RCVMAXCNTL;
  } else {
    maxcnt = RCVMAXCNTS;
  }

  for (i = 0; i<buffLen; i++) {
/*    cnt = 0;                                                          */
/*    while (SciaRegs.SCIFFRX.bit.RXFFST == 0) {// wait until data received */
/*      if (i == 0) {                                                   */
/*        if (cnt++ > maxcnt)                                           */
/*          return TIMEOUT;                                             */
/*      } else {                                                        */
/*        if (cnt++ > RCVMAXCNTL)                                       */
/*          return TIMEOUT;                                             */
/*      }                                                               */
/*    }                                                                 */

    rcvBuff[i] = SciaRegs.SCIRXBUF.all;
    if (SciaRegs.SCIRXST.bit.FE)
      return FRAMERR;
    if (SciaRegs.SCIRXST.bit.PE)
      return PRTYERR;
```

Figure 4.14: SCI Utility Code Commented Out Buffer Check

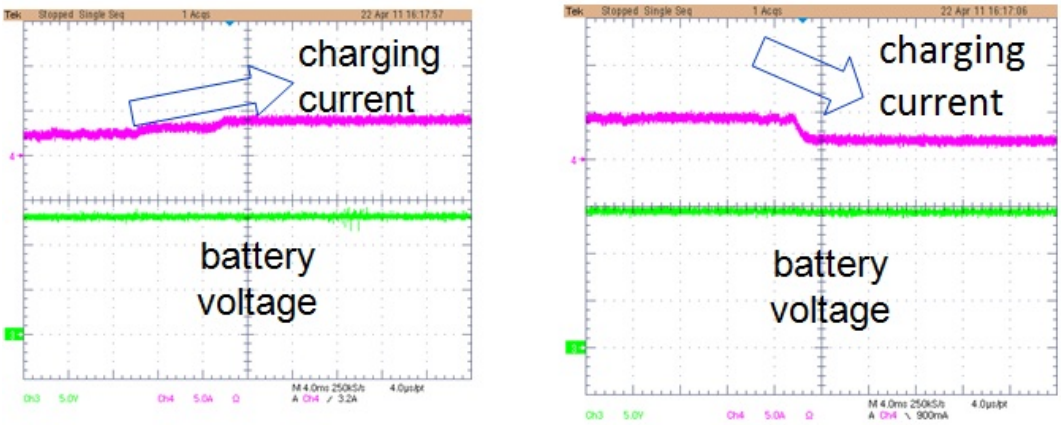

Figure 4.15: DSP Current Reference Update Response to Changes in Increasing Current (left) and Increasing Current (right)

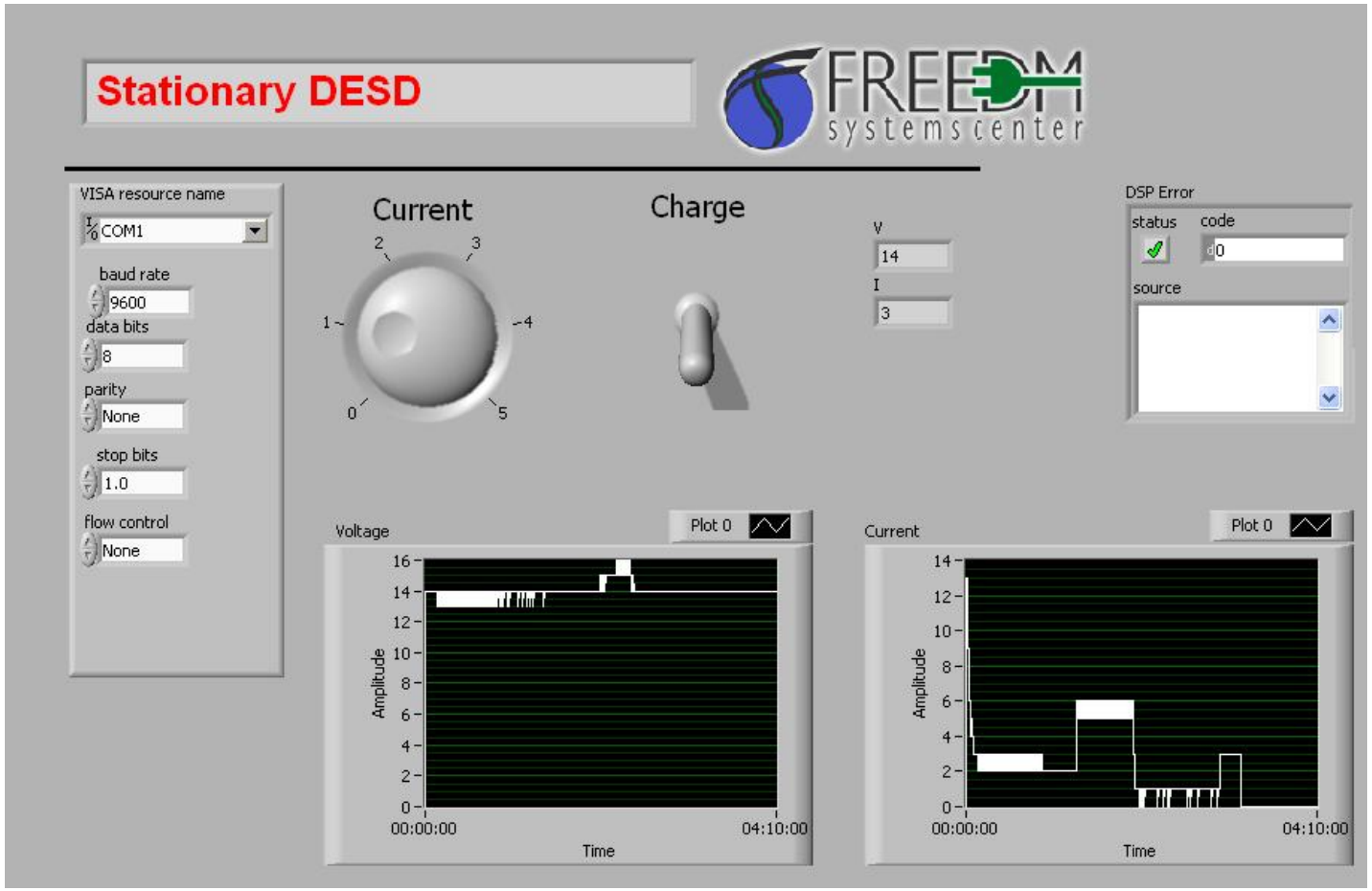

Figure 4.16: Implemented HMI which Controls DC Current, and Monitors DC Voltage and DC Current.

Mode Switch

Additional work on the charger included developing a user controlled switch for selection of the different modes of the MFBD charger, including V2G, V2H, and V2G (see Fig 4.17). For practical purposes, the switch could select a new CCS ready project file created from Simulink to be loaded onto the DSP for a specific mode. This would halt DSP processes for approximately 5-10 seconds for proper loading of C code. This proved the method relatively efficient for future use. The MFBD hardware was not configured for bi-directional ability at the time of HMI development, so no other tests were run with the system hardware.

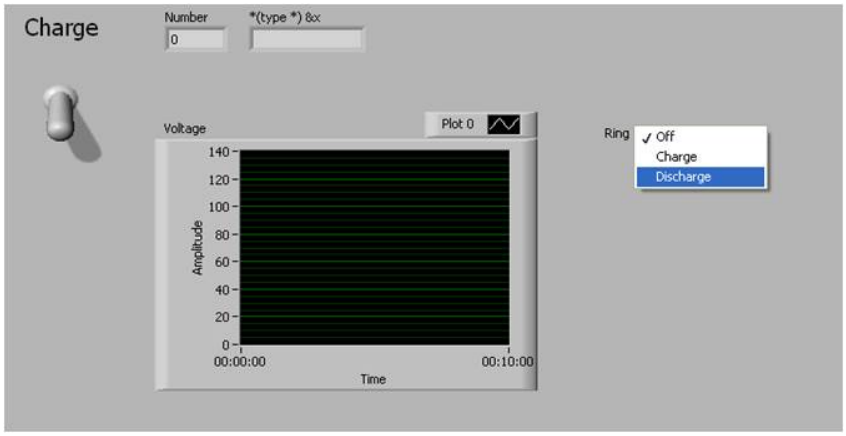

Figure 4.17: HMI With Ability to Switch Charge and Discharge Modes

4.3 Conclusion

A successful HMI was built for the BDMF Charger with real time control and real time monitoring. The HMI is aesthetically pleasing and functional and has the infrastructure ready for multi-function ability built in.

This HMI building process can be applied to other projects utilizing a DSP control approach:

- DC Micro Grid
- Solar Firming
- All other projects with TI DSP Controller

Future Work on HMI Projects related to DSP control should include:

- Graphical studies on user preferences and visual stimuli

- Code optimization methods for SCI Tx and Rx to implement a fully responsive system which does not interfere with system resources
- SCI buffer code development for sending larger messages with multiple data packets for increased variable monitoring

Chapter 5

Predictable and Dispatchable Solar

As discussed in the introduction, a linear regression model will be used to predict solar power output via data collected in the previous time unit. Dispatch times between 15 minutes and one hour will be used based on previous studies and industry standards of dispatch times and the limits of the DESD inverters and control. An averaging technique will be used to limit the effects on the batteries' SOC and keep the total difference close to zero [4]. Also, as discussed in Chapter Two (HMI), I will be using LabVIEW to integrate the physical devices together for control and monitoring.

5.1 Hardware (PV, DESD, and Inverters)

The FREEDM Systems Center has provided an excellent lab environment which not only allows simulation of PV and DESD systems, but also provides real, industry standard hardware to test solar firming algorithms such as the dispatchable solar algorithm described in this chapter. In this section, I will overview the PV array, PV inverters, and DESD hardware/software used for my simulations and actual tests discussed in the following sections. A special acknowledgment should be given to AEG Power Solutions for donating the 40 kW PV system, including wiring and combiner boxes, as well as the Fronius brand inverters and data logging system for enhanced data observation of the PV system over time. The DESD was purchased with FREEDM/ATEC funding provided by the NSF.

5.1.1 REC 215W AE-US PV Panels

A total of 186, Rec 215W AE-US PV panels were used in the 40 kW PV installation at the FREEDM Systems Center. Each panel is rated at 215 Peak Power (Watts), and an efficiency of 13.0% (see Figure A.2). The array was divided up into four primary sub-arrays, which fed into four different inverters with DC inputs of approximately 10 kW a piece. The first three

Table 5.1: FREEDM PV Array Power Total see (A.1)

Module Array	Module Quantity	Power (W)
String - 12 Modules in Series	12	2580
Sub-Array - 4 Strings in Parallel (single inverter)	48	10320
Sub-Array - 3 sets of Sub-Arrays (three inverters)	144	30960
String - 14 Modules in Series	14	3010
Sub-Array - 3 Strings in Parallel (single inverter)	42	9030
Total (4 arrays)	186	39990

consisted of 4 rows of 12 REC 215W panels, totaling 48 panels per each sub-array. A combiner box was used to combine the four rows, for a total output of 10320 W per inverter input, and 30960 W for the three sub-arrays. These panels were all installed at a similar angle of 30, facing SouthWest. The final sub-array, which fed into its own inverter, consisted of three rows of 14 PV panels rated at 215 W, totaling 2 panels and a power output of 9030 W (see 5.1). These panels were installed at a steeper angle due to limited space on the FREEDM building roof. These panels also all faced SouthWest.

The total rated power of the panels peaks at a rated value of 39,990 W (see Figure 5.1), which is simply rounded up to 40 kW for simplifications. Rarely does the total power output of the panels reach this level due to the differing angles between the first three sub-arrays and the final sub-array, but this does occasionally occur on extremely bright days in the afternoon. The first three inverters at 30 degrees have their AC output attached to a separate phase of the three-phase aggregation panel. The fourth inverter's AC output is tied with the first sub-array to add additional power to the first phase.

5.1.2 Fronius IG Inverters

Four Fronius IG Plus, 10.0-1 uni (10 kW), PV Inverters were used as the AC inputs to the three phase, 600 Vac aggregator. They were fed by the four, 10 kW PV sub-arrays described in the previous section and in the one-line electrical diagram (see Figure A.1). The inverters include such features as MPPT tracker, internal combiner, and lockable DC disconnect.

One of the most important aspects of this project, in which real-time PV array data is required to predict future output, and real-time data is also required to determine the necessary DESD power to supply or absorb, is an easy to implement method to extract real-time PV data. Fronius provides a wide variety of data acquisition methods, including a web based datalogger, which stores all relevant data in 5 minute intervals, and a programmable interface card which can

Figure 5.1: Fronius 10 kW IG Plus Inverter used at the FREEDM Systems Center for PV Power inversion [27]

supply user-requested data at a sub-second level. This simple data acquisition was imperative to initial simulations of predictable and dispatchable solar algorithms, comparison of simulated data to actual data, and finally real-time implementation of the algorithm.

5.1.3 Greensmith 20 kWh DESD

Greensmith Energy Management Systems offers a variety of Lithium-Ion (Li-I) Distributed Energy Storage Systems (DESS) which not only include batteries and power electronics, but also include communication for controls and monitoring, high quality BMS which ensures 30,000 life cycles, and internal real-time monitoring which ensures safety and compliance (see Fig. A.7). The FREEDM Systems center invested in a 20 kWh system which included 6 kW rated inverters and chargers, thus ensuring a maximum of 6 kW instantaneous power (30 A at 208Vac) which can be discharged from or charged to the batteries. The 20 kWH storage capacity (16 400 aH, 3.2 V Li-Ion cells) ensures a large amount of energy storage, specifically at a rating of approximately .25C with the 6 kW inverters. The system was connected to a 208 Vac bus which is fed directly from a 12 kV distribution line.

The software system is BOS, Generation 3, which consists of real-time control and monitoring of inverter input/output voltages, currents, temperatures, frequency, SOC, battery voltages, event management, and many more important system parameters. Communication takes place via an Ethernet connection to a local subnet. Once connected to the subnet, a user can read UDP messages sent over the subnet on a local port, and transmit TCP messages directly to the DESS on a specified port to control charge/discharge power of the unit on a real-time basis. The unit has a response time of 5-10 seconds, coupled with a ramp rate that consists of up to

Table 5.2: DESD Calculated Parameters

Parameters	Calculation	Result
16 400 aH cells, Voltage: 3.2 Voc	Energy=kWh=Ah*V	20.5 kWh
AC Voltage: 208, Rated Power: 6 kW	Rated Current=P/V	Rated Current: 28.85 Iac
Rated Energy: 20.5 kWh, Rated Power: 6 kW	Charge Rate=1/h=P/E	.29 C

5-10 seconds based on the amount of power commanded by the user in compared to its current operational. Thus, the actual response time of the unit can range from 10-20 seconds depending on network traffic, and desired power output or input level.

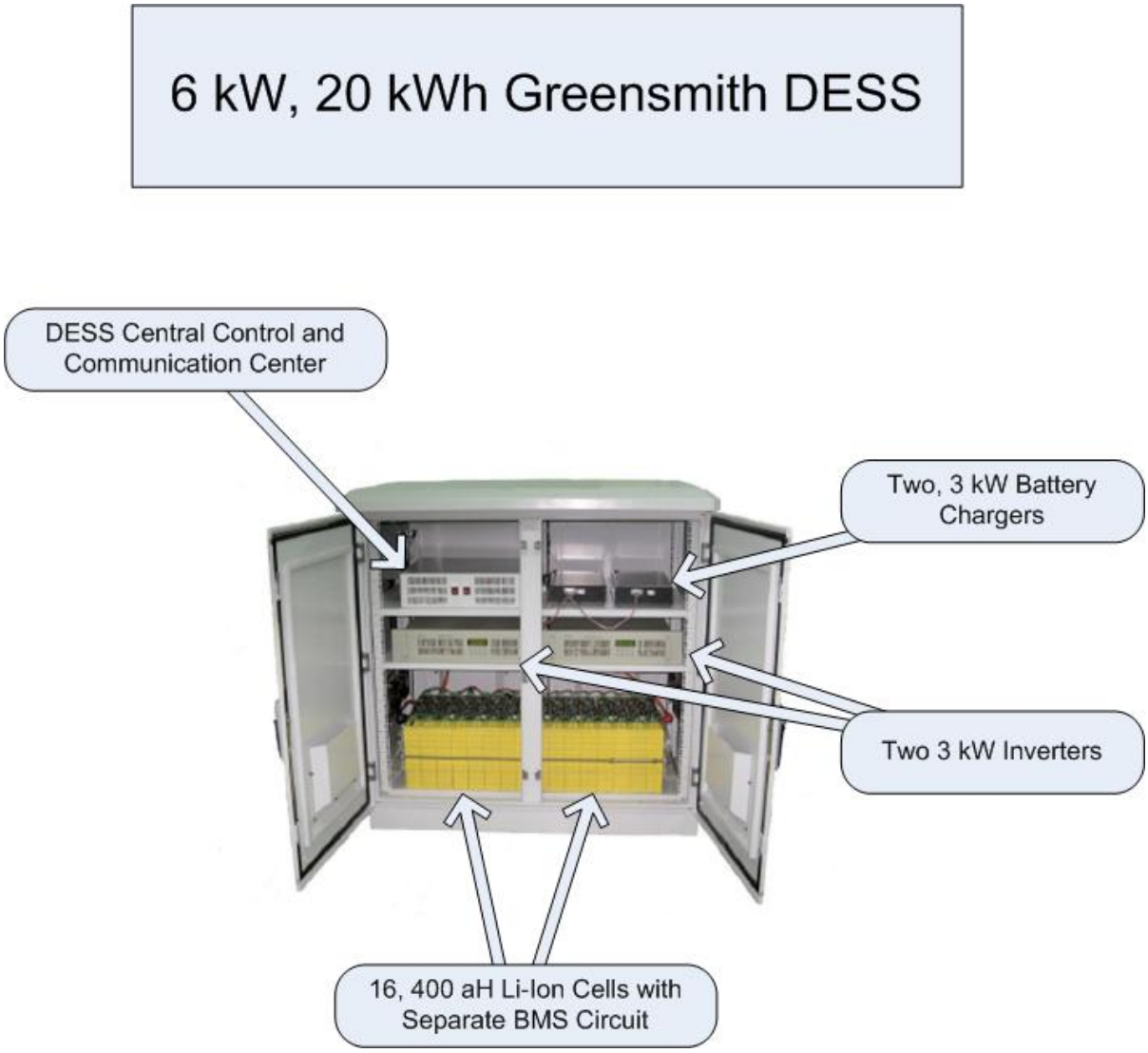

Figure 5.2: The 6 kW Greensmith DESS Consists of Separate Parts Connected via Wires and Communication Cables, Stored in a Vented Cabinet [27]

Data formats for Ethernet communication via UDP and TCP/IP protocols will be discussed in the communications subsection.

5.2 Dispatchable Solar Simulations

Based on previous studies, dispatchable solar simulations were conducted with the following high level system rules:

1. Dispatch/Prediction Horizon intervals of one hour [26] [3]
2. Linear regression model for next interval prediction method [12]
3. Rule based control utilizing closed loop control, neglecting high volume calculations [3]
4. Multiple control horizons per prediction horizon to account for real-time changes [4]

Multiple rules were determined based on system parameters of the DESD and its capabilities. These rules were based on previous studies [3] [6] as well as rules determined for the physical systems described in the previous section. I_{DESD} can be considered the DESD rated inverter current.

$$-I_{DESD_LL} < i_{DESD}(t) < I_{DESD_UL} \tag{5.1}$$

$$SOC_{LL} < SOC(t) < SOC_{UL} \tag{5.2}$$

For $SOC_{LL} = SOC(t)$

$$\text{if } P_{DESD} > 0,\ P_{DESD}(t) = 0 \tag{5.3}$$

$$\text{else,} \qquad P_{DESD}(t) = P_{DESD,ref}(t) \tag{5.4}$$

For $SOC_{UL} = SOC(t)$

$$\text{if } P_{DESD} < 0,\ P_{DESD}(t) = 0 \tag{5.5}$$

$$\text{else,} \qquad P_{DESD}(t) = P_{DESD,ref}(t) \tag{5.6}$$

For $I_{LL} < (I_{BESS,ref}(t)) < I_{UL}$

$$P_{DESD} = P_{DESD,ref} \tag{5.7}$$

For $I_{LL} > (P_{DESD}(t)/V_{bat}(t))$

$$i_{DESD}(t) = I_{LL} \tag{5.8}$$

For $I_{UL} < (P_{DESD}(t)/V_{bat}(t))$

$$i_{DESD}(t) = I_{UL} \tag{5.9}$$

According the Greensmith specification sheet (see Figure A.7), and calculations done (see Table 5.2), a peak inverter current of 30A, both for charging and discharging, was used as

the limit for the DESD instantaneous power available. The SOC limits were defined based on previous studies [5] and information given to us by Greensmith LLC representatives. The lower limit is set at 5%, and the upper limit is sat at 95%, thus giving the DESD a 90% operating capacity, which is still much greater than the typical 70% operatable capacity of lead acid batteries. Also, it should be noted that predictions above the rated 40 kW power output of the PV array should be limited at 40 kW to predict SOC depletion, and predictions below 0 kW should be limited at 0 to prevent negative hourly dispatch.

Total SOC was modified during simulations to determine the minimum SOC needed to carry out the dispatchable solar algorithm. This data was analyzed and compared to the peak solar output of that day.

Table 5.3: Simulation Limits

Parameter	Upper Limit	Lower Limit
SOC	95%	5%
DESD Power	6 kW	-6 kW
DESD Current	30 A	-30A
PV Power	40 kW	0 kW

5.2.1 Simulated Solar Data

Input solar data was obtained in two manners. First of all, initial simulations for future days were done with data from The Green Research for Incorporating Data in the Classroom (GRIDC), a project developed for solar and wind data use and research in the classroom [31]. Technology from the NC Solar Center is analyzed, and data is stored online for the public to use. The project is funded by the NSF. The data was extremely vital because not only is it located approximately one mile from the FREEDM Systems Center's solar array and lab to imitate local conditions, but also because data is provided historically from previous years, and updated daily to include 15 minute interval measurements of power, current, irradiance, and many other important variables.

Specifically, I used data from the 3.07 kW system to replicate the 40 kW system in our lab. The data needed to be compared to data from the FREEDM 40 kW system to accurately determine a close relationship between the two systems. The Fronius Web Datalogger was used in conjunction with Fronius.Access software to download data in five-minute intervals,

including inverter power, current, voltage, solar irradiance, and temperature [30]. To simplify calculations, I only compared total output power. Radiation, temperature, and other variables were assumed negligible due to the close proximity of the two systems. In total, data from GRIDC and the FRONIUS Datalogger were available at matching times from October 2010 to January 2011. This data was compared on a fifteen minute basis (minimum interval time of GRIDC data), and averaged to produce a generic multiplying factor of 12 from the GRIDC 3.07 kW system to the FREEDM 40 kW array (this is relatively close to the actual power multiplying factor between the two systems of 13.03 kW, see Equation 5.10).

$$40kW/3.07kW = 13.03kW \tag{5.10}$$

Normwise Relative Error

Simulated GRIDC data was compared to the FRONIUS datalogger data via normwise relative errors to reveal exactly how close the simulated data matched the actual data. Normwise relative errors are generally used in datasets where individual component-wise errors are not deemed as important [25]. In my case, the day to day errors could widely vary based on cloud cover, and varying conditions between the FREEDM PV 40 kW array and the Solar Center's 3.01 kW array, which were located one mile apart. Component-wise errors were not deemed important for this reason, and a normwise relative error test was conducted to numerically compare simulated GRIDC data and actual FREEDM PV data.

Two types of norms were analyzed to judge the relative error. A one norm was used to give equal weight to all measured errors. A one norm does not square errors, and therefore gives equal consideration to all errors (see Eqn 5.11a). A Euclidean norm, or two norm, was used to include all data points, and the square of the errors to account more heavily for larger errors (see Eqn 5.11b) [25]. Assuming $\widetilde{x}$ is an approximation to a vector x, in our case the simulated GRIDC data being an approximation of the actual FREEDM 40 kW array data, then we can assume a normwise relative error for that data sat as seen in Equation 5.11c [25]. Combining these two equations, we can achieve a normwise relative error for a one norm and Euclidean norm set (see Eqns 5.11d and 5.11e) [25].

$$|x|_1 = \sum_{j=1}^{n} |x_j| \tag{5.11a}$$

$$|x|_2 = \sqrt{\sum_{j=1}^{n} |x_j|^2} \tag{5.11b}$$

$$|x - \widetilde{x}|/|x| \tag{5.11c}$$

$$(\sum_{j=1}^{n} |x_j - \widetilde{x}_j|)/(\sum_{j=1}^{n} |x_j|) \tag{5.11d}$$

$$(\sqrt{\sum_{j=1}^{n}|x_j - \widetilde{x}_j|^2})/(\sqrt{\sum_{j=1}^{n}|x_j|^2}) \tag{5.11e}$$

Using the equation 5.11, and nearly 5500 data points between October 2010 and January 2011 consisting of simulated and actual data in 15 minute intervals, a normwise relative error using one norms was calculated at 35.4%, and a normwise relative error using Euclidean norms was calculated at 38.787%. This error is fairly low given potential geographical, elevation, angle, PV panel characteristics, and shaded surroundings of the two different PV arrays. This low relative error, as well as visual tests comparing similar days, was enough to confidently use the simulated data in dispatchable solar simulations. After these simulations were run, the data could be applied to any solar system using the dispatchable solar algorithm.

Visual Tests

In addition to the normwise relative error test, data points for all days were plotted for quick visual checks in data accuracy. Visually, it could be easily seen that relative daily patterns in the two sets of data matched up perfectly. The only huge differences were in the scales at certain times. At peak hours simulated data might have been overestimated, and during cloudy days simulated data may have been overestimated. Overall, the visual tests checked out extremely well (see Figs 5.3 and 5.4).

Results

The data matched up extremely well according to visual tests and normwise relative errors. Therefore, the simulated data as well as the real data was used for hourly solar dispatch and prediction simulations. As data became available for the simulated months, similar weather patterned days were compared for battery SOC limitations and current limitations to verify the precision of the simulated data. Other daily observations were made between simulated future dates based on GRIDC data and actual dates with similar weather patterns as they occurred. A clear correlation can be seen based on the sample data provided (see Figs 5.5 and 5.6, and thus further proves the validity of the simulated data used for simulations.

5.2.2 Simulation Setup

MATLAB was used to simulate hourly dispatch and prediction of the FREEDM PV array. The parameters described in Table 5.3 were used as limits for current, SOC, and predictions. Simulated GRIDC data was available in 15 minute increments, or four data points per hour, and data from the Fronius Interface card was available in five minute increments, or 12 per hour. Each hour's data points were separated into their own vector, fitted via linear regression

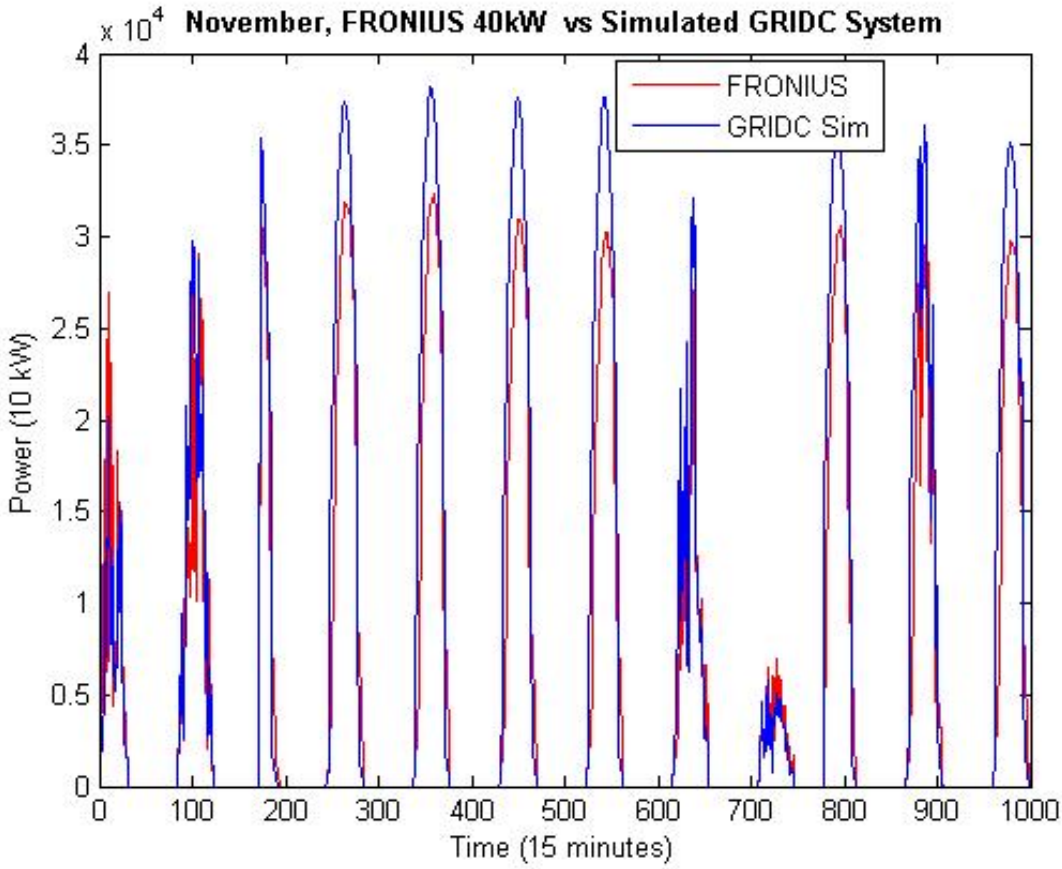

Figure 5.3: Daily Comparisons of Solar Power Output Recorded in November for The FREEDM Fronius System (RED) and The Simulated GRID-C System (BLUE). All Days Have Very Similar Results.

with a 1-degree polynomial equation, and the mean of the polynomial's data points taking place in the following hour was used as a that hour's prediction. Therefore each hour had a new prediction based on the previous hour. No future data was used in predictions to mimic a real-time simulation in which only current and past data is available.

Predictions were limited to values between 0 and 40 kW (see Table 5.3). For each hour, each data point was compared to the predicted value, and calculations were performed to determine if the DESD could absorb or supply the difference. If the DESD did not have enough SOC to perform a discharge or too much SOC to absorb a charge, no actions were taken (see Eqns 5.4 and 5.6). If the DESD's current rating was exceeded, the DESD operated at its maximum charge or discharge rating in order to offset errors as much as possible (see Eqns 5.7 5.8 5.9). The efficiency of the Greensmith Inverter, approximately 88% (see Fig. A.7), was used during any charge or discharge to also mimic real time operation and give proper results as to battery

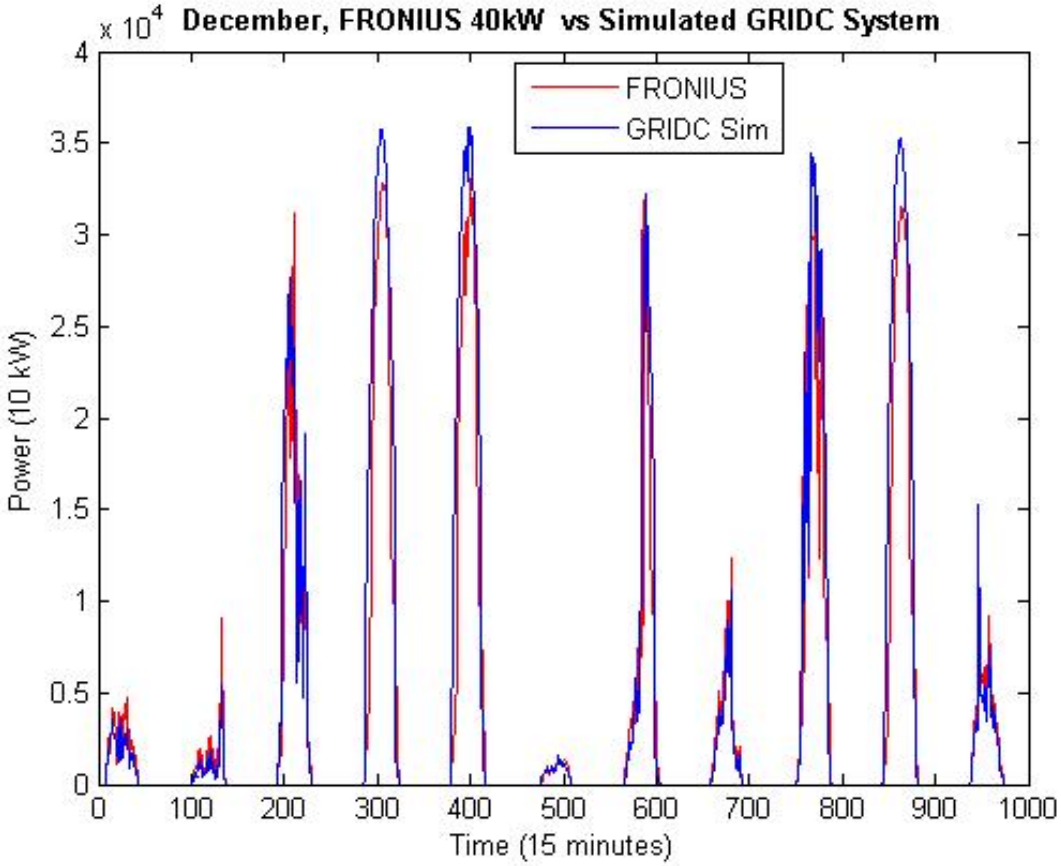

Figure 5.4: Daily Comparisons of Solar Power Output Recorded in December for The FREEDM Fronius System (RED) and The Simulated GRID-C System (BLUE). All Days Have Very Similar Results.

sizes power demands. All values were plotted, including DESD power, SOC, current demands, and predictions. A description of the code operation can be seen in Figure A.9.

5.2.3 Simulation Results

Over 60 different days were used as the input data to the Dispatchable Solar algorithm. The 40 kW solar system connected to a 20 kWh, 6 kW Greensmith DESD and system parameters were used from both of these systems. For research purposes, simulations were also ran with no current or power limits on the DESD inverters, and minimum SOC levels. Selected simulation days varied in month, type of data (real or simulated), and weather conditions. Weather conditions were generalized into clear days, those which have little to zero cloud cover causing minimal output power decreases, and cloudy days, those which have moderate to extreme cloud

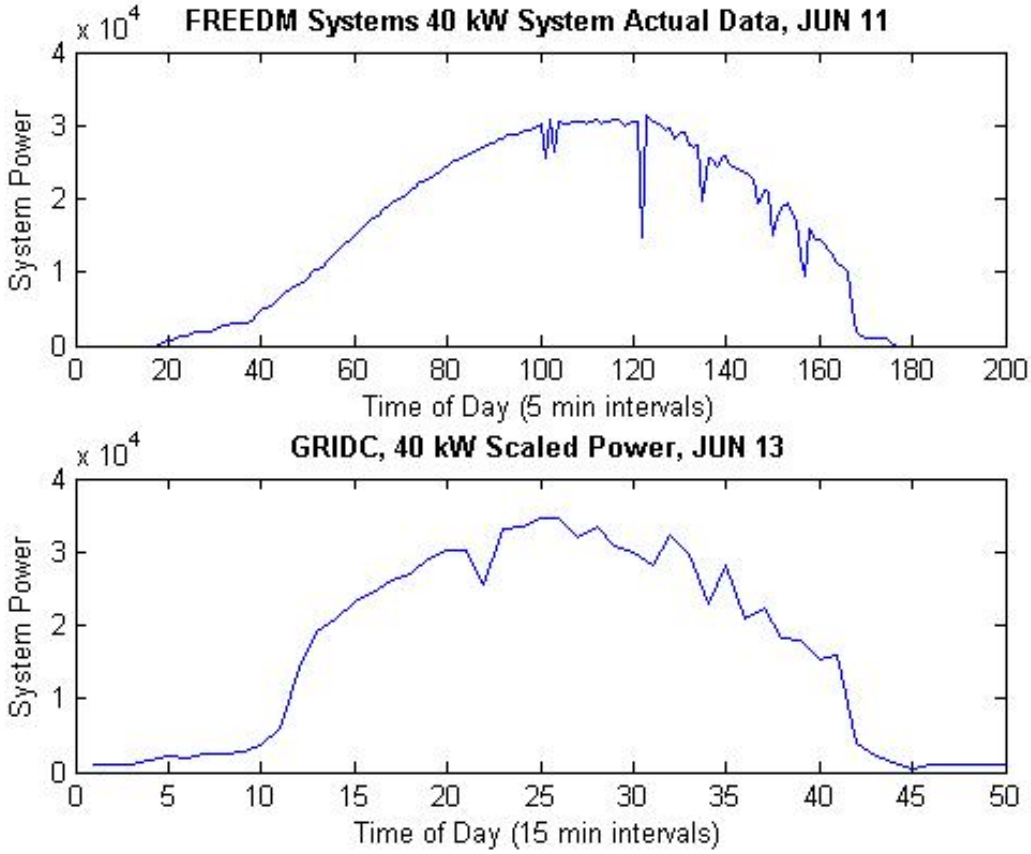

Figure 5.5: Similar Patterns Between The Simulated Data and Actual Data on a Clear Weather Day in June

cover which drastically effects power output curve. Similar days with similar conditions were compared to one another to show trends and once again validate the simulated data with the real data.

Simulations were run in two different scenarios. The first scenario included current limits of the Greensmith 20 kWh, 6 kW system, while a second scenario included no current limits in order to provide useful information on inverter sizing. For all simulations, the minimum battery capacity was observed which resulted in a complete firming of the PV power output without exceeding SOC limits.

Simulation Results for Clear Days

For days where there were little to no cloud cover, the PV power output exhibited its typical parabolic, second order output with minimal digressions. During these clear days, a minor

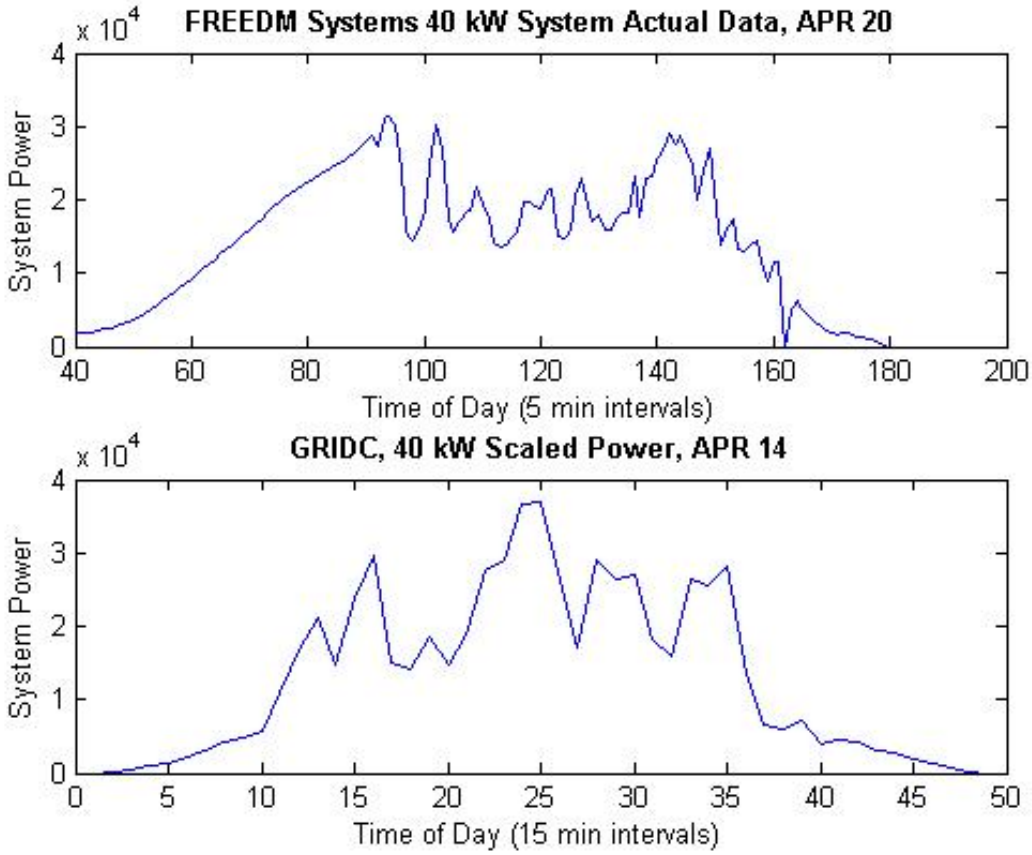

Figure 5.6: Similar Patterns Between The Simulated Data and Actual Data on a Cloudy Weather Day in April

trend could be detected in the minimum battery capacity needed with no current limits (see Table 5.4). Values typically increased during the summer months and fall (June to November) when sunlight is more available for longer portions of the day (typically between 10 and 14 hours).

Table 5.4: Dispatchable Solar Simulation Results for Clear Days. Similar Capacity Results Prove Simulated Data is Comparable to Actual Data. Also, Noticeable Trends Exist Seasonally in Capacity Requirements.

Date	Data Type	Weather	Season	Min aH	Wh	% GSmith	No Lim	Wh	%Solar	Max Amp	Max kW
1/2/2011	Simulated	Clear	Winter	2400	7680	37.5%	3200	10240	25.6%	50	10.4
1/11/2011	Real	Clear	Winter	5600	17920	87.5%	5600	17920	44.8%	50	10.4
2/11/2011	Simulated	Clear	Winter	4000	12800	62.5%	4000	12800	32.0%	100	20.8
2/19/2011	Real	Clear	Winter	4000	12800	62.5%	4000	12800	32.0%	60	12.5
2/27/2011	Simulated	Clear	Winter	6400	20480	100.0%	6400	20480	51.2%	100	20.8
3/4/2011	Real	Clear	Spring	5600	17920	87.5%	6400	20480	51.2%	80	16.6
3/7/2011	Simulated	Clear	Spring	7200	23040	112.5%	9600	30720	76.8%	100	20.8
3/10/2011	Simulated	Clear	Spring	6400	20480	100.0%	9600	30720	76.8%	111	23.1
4/22/2011	Simulated	Clear	Spring	4800	15360	75.0%	4800	15360	38.4%	50	10.4
5/15/2011	Simulated	Clear	Spring	5600	17920	87.5%	5600	17920	44.8%	64	13.3
5/24/2011	Real	Clear	Spring	3200	10240	50.0%	3200	10240	25.6%	85	17.7
6/11/2011	Real	Clear	Summer	6400	20480	100.0%	8000	25600	64.0%	75	15.6
6/13/2011	Simulated	Clear	summer	7200	23040	112.5%	8000	25600	64.0%	55	11.4
7/4/2011	Simulated	Clear	Summer	8000	25600	125.0%	11200	35840	89.6%	89	18.5
8/7/2011	Simulated	Clear	Summer	12000	38400	187.5%	13600	43520	108.8%	76	15.8
8/20/2011	Simulated	Clear	Summer	8000	25600	125.0%	8000	25600	64.0%	80	16.6
9/4/2011	Simulated	Clear	Summer	7200	23040	112.5%	8800	28160	70.4%	77	16.0
10/16/2011	Simulated	Clear	Fall	9600	30720	150.0%	11200	35840	89.6%	85	17.7
11/11/2011	Real	Clear	Winter	5600	17920	87.5%	7200	23040	57.6%	70	14.6
11/12/2011	Real	Clear	Winter	5600	17920	87.5%	6400	20480	51.2%	67	13.9
11/27/2011	Simulated	Clear	Winter	8000	25600	125.0%	8800	28160	70.4%	79	16.4
12/8/2011	Real	Clear	Winter	4800	15360	75.0%	5600	17920	44.8%	63	13.1
12/8/2011	Simulated	Clear	Winter	4800	15360	75.0%	4800	15360	38.4%	73	15.2
12/9/2011	Real	Clear	Winter	6400	20480	100.0%	7200	23040	57.6%	80	16.6
12/9/2011	Simulated	Clear	Winter	6400	20480	100.0%	6400	20480	51.2%	72	15.0
12/20/2011	Real	Clear	Winter	7200	23040	112.5%	8800	28160	70.4%	70	14.6
12/20/2011	Simulated	Clear	Winter	6400	20480	100.0%	6400	20480	51.2%	47	9.8

Due to the ease of predictability during these days, the required inverter size ranges from 26% to 58% (see Fig 5.7) with an average of 39%. This range is extremely small, considering the wide variations of capacity requirements (10.2 - 48 kWh), but also confirms the theory that sunny days are easily predictable and require less error correction in predictions. Also it is important to note that an inverter size of at least 25% of the rated PV power is required to run the solar dispatch algorithm effectively (see Fig 5.7). This is important because the FREEDM PV System is rated at 40 kW and the Greensmith DESD has an inverter rating of 6 kW, giving us only 15% of the rated PV power. Actual real-time implementations of the algorithm will need to be adjustd for this fact. The maximum battery capacity needed was observed at 48 kWh with an average of 22.941 kWh. The maximum being 121% of the PV rated power and the average being 55% of the rated PV power.

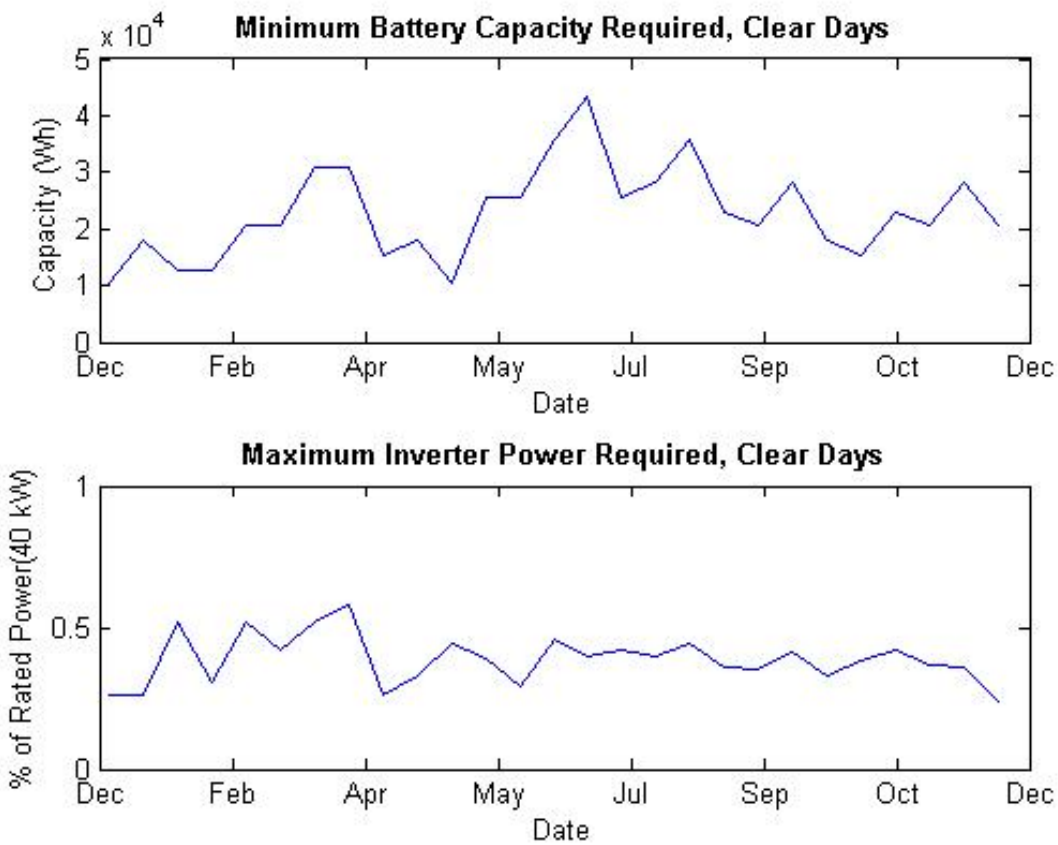

Figure 5.7: Similar Patterns Between The Simulated Data and Actual Data on a Cloudy Weather Day in April

A typical clear day's graphical output is shown in Figure 5.8. As with most clear sky days during dispatchable solar simulations, predictions are generally on target. There are some over predictions during the beginning and end of days due to sharp rises or declines in solar power, but these only last for short periods of time. In summer months, these larger errors will decrease SOC % more than winter months. Though, the largest capacity needed for any clear sky day observed in my simulations was only 850 aH.

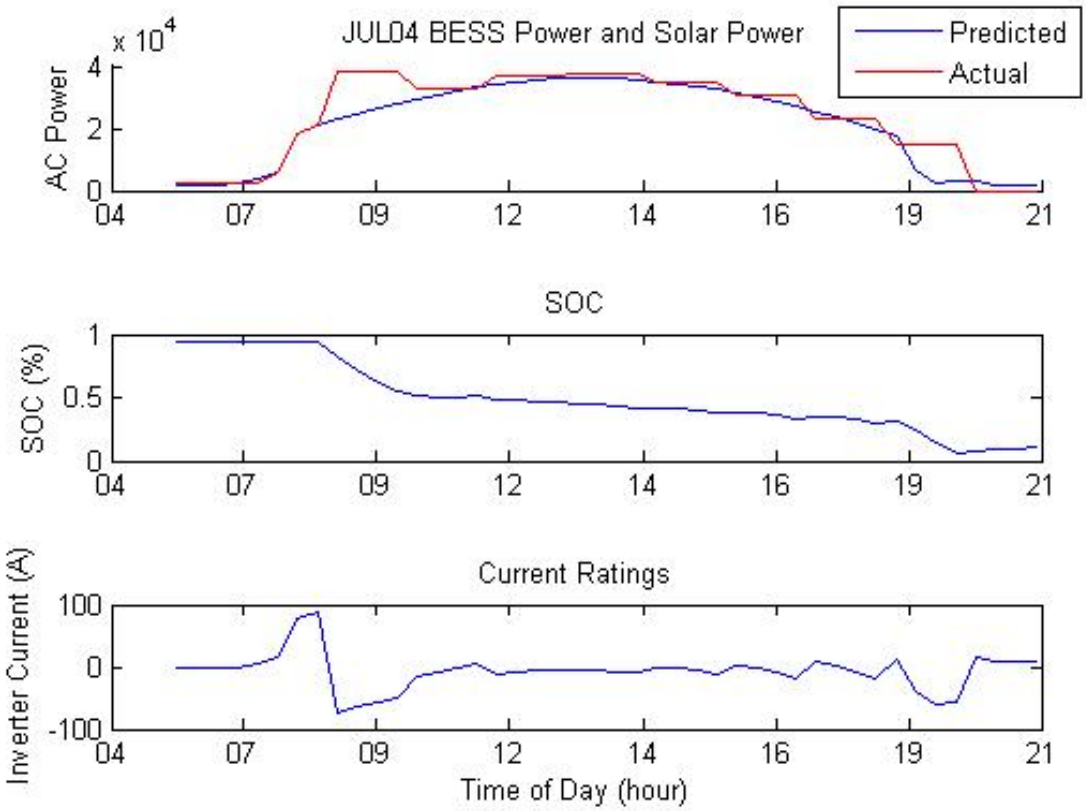

Figure 5.8: A Typical Clear Sky Day Dispatchable Solar. Predictions are Generally On Target and Current Ratings are Below 100

Simulation Results for Cloudy Days

For days where there moderate to extreme cover, the PV power output exhibited its non-typical parabolic output due to the sharp dips and rises due to cloud cover limiting solar irradiance

for short periods of time (typically 10 seconds to one minute). During these cloudy days, a minor trend could be detected in the peak inverter power needed to absorb or compensate errors between predicted values and actual values (see Table 5.5). Peak inverter power typically increased during Spring and Summer months (April to August) when sunshine and solar irradiance is stronger, and cloud cover is still prevalent. Sharp dips and rises during these months are much larger than in winter and fall months, when the peak irradiance is not as high.

The required inverter size ranges from extreme lows of 3% during winter months with extreme cloud cover, extreme highs of 88% during spring months when cloud cover is most extreme (see Table 5.5). These results confirm the unpredictability of cloudy days or days in which precipitation falls. One of the only noticeable trends is in peak inverter power, which is a direct result of the peak power observered in a day or season.

Table 5.5: Dispatchable Solar Simulation Results for Cloudy Days. Similar Capacity Results Prove Simulated Data is Comparable to Actual Data. Also, Noticeable Trends Exist Seasonally in Peak Power Requirements.

Date	Data Type	Weather	Season	Min aH	Wh	% GSmith	No Lim	Wh	%Solar	Max Amp	Max kW	Peak % Solar
1/2/2011	Real	Cloudy	Winter	1600	5120	25.0%	1600	5120	12.8%	20	4.2	0.10
1/9/2011	Real	Cloudy	Winter	4800	15360	75.0%	5600	17920	44.8%	100	20.8	0.52
1/11/2011	Simulated	Cloudy	Winter	14400	46080	225.0%	15200	48640	121.6%	100	20.8	0.52
1/21/2011	Simulated	Cloudy	Winter	800	2560	12.5%	800	2560	6.4%	5	1.0	0.03
2/4/2011	Real	Cloudy	Winter	2400	7680	37.5%	2400	7680	19.2%	10	2.1	0.05
2/5/2011	Simulated	Cloudy	Winter	800	2560	12.5%	800	2560	6.4%	5	1.0	0.03
2/27/2011	Real	Cloudy	Winter	3200	10240	50.0%	4000	12800	32.0%	80	16.6	0.42
3/11/2011	Real	Cloudy	Spring	3200	10240	50.0%	3200	10240	25.6%	70	14.6	0.36
3/15/2011	Simulated	Cloudy	Spring	4800	15360	75.0%	8800	28160	70.4%	157	32.7	0.82
4/5/2011	Real	Cloudy	Spring	4800	15360	75.0%	8000	25600	64.0%	170	35.4	0.88
4/14/2011	Simulated	Cloudy	Spring	5600	17920	87.5%	11200	35840	89.6%	110	22.9	0.57
4/20/2011	Real	Cloudy	Spring	6400	20480	100.0%	12000	38400	96.0%	116	24.1	0.60
5/3/2011	Real	Cloudy	Spring	2400	7680	37.5%	3200	10240	25.6%	104	21.6	0.54
5/5/2011	Simulated	Cloudy	Spring	13600	43520	212.5%	21600	69120	172.8%	115	23.9	0.60
5/13/2011	Real	Cloudy	Spring	6400	20480	100.0%	11200	35840	89.6%	125	26.0	0.65
5/25/2011	Simulated	Cloudy	Spring	10400	33280	162.5%	16000	51200	128.0%	67	13.9	0.35
6/1/2011	Real	Cloudy	Summer	5600	17920	87.5%	6400	20480	51.2%	107	22.3	0.56
6/5/2011	Real	Cloudy	Summer	10400	33280	162.5%	11200	35840	89.6%	140	29.1	0.73
6/5/2011	Simulated	Cloudy	Summer	10400	33280	162.5%	11200	35840	89.6%	140	29.1	0.73
6/15/2011	Simulated	Cloudy	Summer	9600	30720	150.0%	17600	56320	140.8%	114	23.7	0.59
6/25/2011	Simulated	Cloudy	Summer	9600	30720	150.0%	12000	38400	96.0%	89	18.5	0.46
7/3/2011	Simulated	Cloudy	Summer	7200	23040	112.5%	11200	35840	89.6%	91	18.9	0.47
7/15/2011	Simulated	Cloudy	Summer	6400	20480	100.0%	9600	30720	76.8%	131	27.2	0.68
7/22/2011	Simulated	Cloudy	Summer	5600	17920	87.5%	5600	17920	44.8%	82	17.1	0.43
8/12/2011	Simulated	Cloudy	Summer	4800	15360	75.0%	7200	23040	57.6%	70	14.6	0.36
8/14/2011	Simulated	Cloudy	Summer	4800	15360	75.0%	7200	23040	57.6%	70	14.6	0.36
9/6/2011	Simulated	Cloudy	Summer	12000	38400	187.5%	16800	53760	134.4%	85	17.7	0.44
9/11/2011	Simulated	Cloudy	Summer	8000	25600	125.0%	16800	53760	134.4%	93	19.3	0.48
10/10/2011	Simulated	Cloudy	Fall	11200	35840	175.0%	13600	43520	108.8%	86	17.9	0.45
10/27/2011	Simulated	Cloudy	Fall	12000	38400	187.5%	22400	71680	179.2%	100	20.8	0.52
11/15/2011	Real	Cloudy	Winter	4800	15360	75.0%	6400	20480	51.2%	77	16.0	0.40
11/15/2011	Simulated	Cloudy	Winter	10400	33280	162.5%	13600	43520	108.8%	63	13.1	0.33
11/16/2011	Simulated	Cloudy	Winter	1600	5120	25.0%	1600	5120	12.8%	28	5.8	0.15
12/2/2011	Simulated	Cloudy	Winter	15200	48640	237.5%	20000	64000	160.0%	68	14.1	0.35

Due to the difficulty of predictability during these days, the required inverter size ranges from 3% to 88% (see Fig 5.7) with an average of 49%, up 10% from the clear day inverter size average. This range is extremely large, and confirms the theory that cloudy days are difficult to predict and require more steep error corrections. The maximum battery capacity needed was observed at 69.1 kWh with an average of 31.6 kWh, up almost 10 kWh from clear sky days (see Fig 5.7). The maximum being 173% of the PV rated power and the average being 79% of the rated PV power.

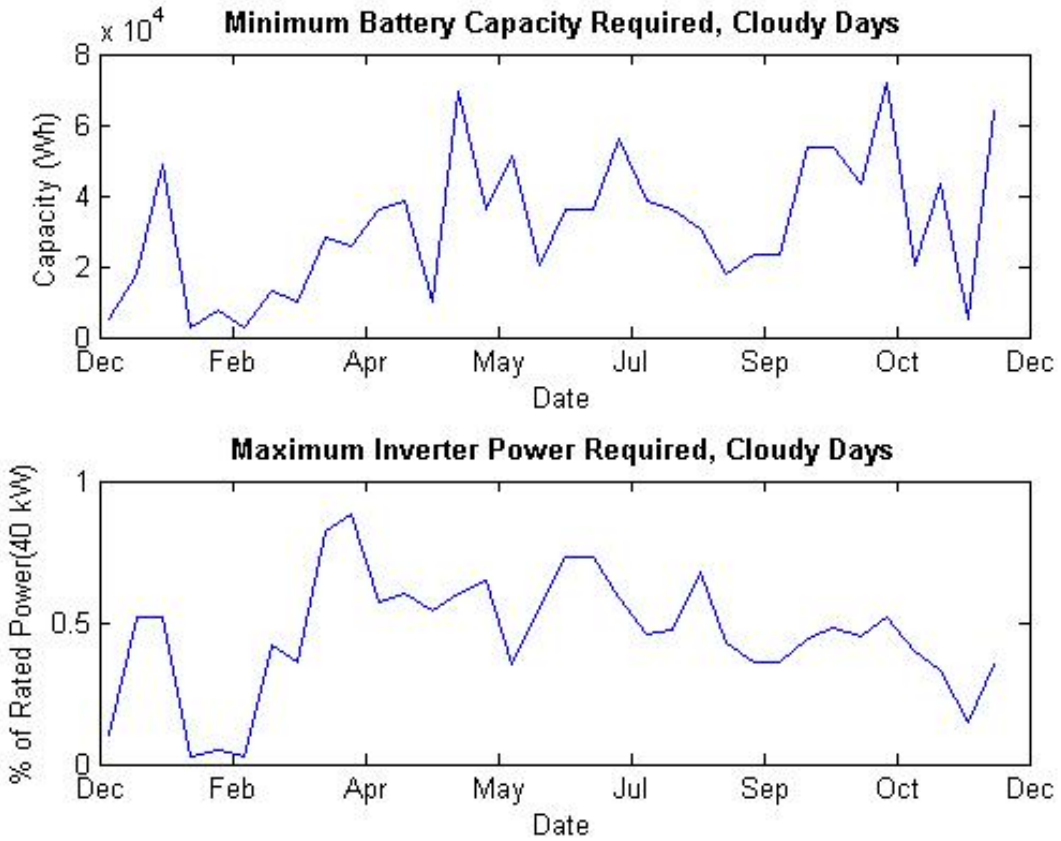

Figure 5.9: Similar Patterns Between The Simulated Data and Actual Data on a Cloudy Weather Day in April

A typical cloudy day's graphical output is shown in figure 5.10. As with most cloudy sky days during a dispatchable solar simulations, predictions can range from extremely high or extremely low compared to actual values. SOC incurs rapid decreases and increases, while

current limits, even for a low powered winter day, can peak at 100 A (comparable to a clear sky sunny day). In summer months, these larger errors will decrease SOC % more than winter months. Most days requiring a high battery capacity occurred between the months of May and October when the sun is brighter and the length of day is longer.

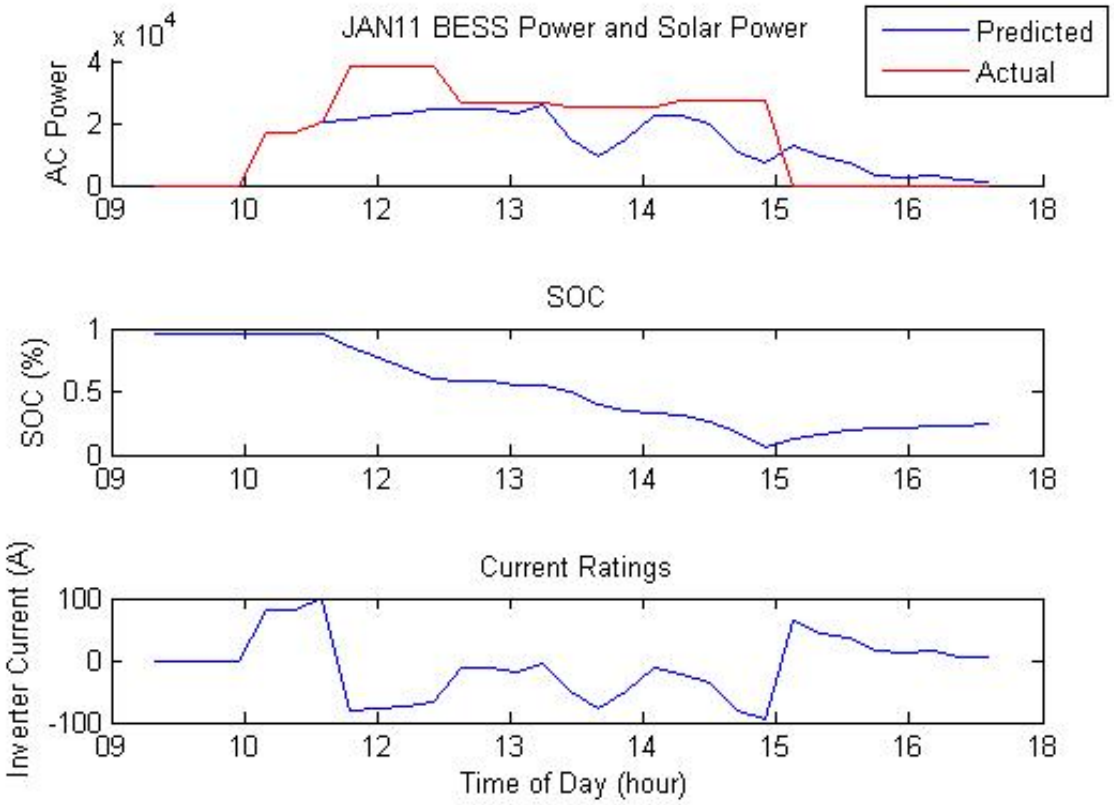

Figure 5.10: A Typical Cloudy Sky Day Dispatchable Solar

5.3 Dispatchable Solar Real Time Experiments

Real time Dispatchable Solar experiments were able to be conducted with the hardware mentioned in Section 5.1. Hardware was provided by funding and donations of AEG, the NSF, and industry sponsored donations from Progress and Duke Energy. Once again, LabVIEW was the preferred choice of program for integrating the Greensmith DESD and Fronius Inverters (see

Subsection 4.1.2. The real time experiment for Dispatchable Solar was almost an exact match logically to the Dispatchable Solar simulations conducted in Section 5.2 (see Fig A.9). Rule based control was used which took into account the DESD limitations as well as the inverter limitations.

5.3.1 Real Time Experiment Setup

Programming in LabVIEW was very similar to MATLAB simulations in terms of logic. The main differences were in the data acquisition. Simulations used already available data whereas experiments acquired data real time. Limitations on intervals were based on hardware limitations of the communication protocols of the inverters and DESD.

Due to the relatively low rating of the DESD inverter power (6 kW), only one fourth, or maximum 10 kW, of the total power acquired from the Fronius PV inverters was used in simulations. This would give a DESD rated inverter power of 60% of the total PV power, which better coincides with simulation results from Section 5.2.3. With a DESD inverter rating of 60% of the rated PV power, all clear days and most cloudy days should be able to be properly predicted and dispatched with no inverter size issues. Also, a clear cut number of 10 kW gives us insight into one aggregate inverter (rated 10 kW) for the total system. DESD size was not an issue. The rated 20 kWh of the Greensmith DESD batteries far exceeded any full day requirements even with the fully rated system, so no additional adjustments were needed.

Ethernet Communication with Greensmith DESD

The Greensmith DESD uses Ethernet protocols to communicate with a host computer or network. The DESD connects through secure web services which are modeled after the Department of Energy's 'Open Automated Demand Response'. Greensmith uses event-based asset management architecture which can easily integrate into systems [27]. LabVIEW incorporates multiple levels of Ethernet communication capability which made the integration of DESD communication very simple [32]. GreenSmith provided system integration summary documents which allowed easy access and decoding of data protocols. Variables obtained from the DESD included only SOC and total system power at the inverter level. This coincides with simulation requirements as well. System commands sent to the device only consisted of the commanded power, or P_{Diff}, which was the difference between the predicted solar output value and the prediction.

Data could be obtained from the DESD via UDP protocol every three to five seconds, which provided more than optimal results in terms of system monitoring on a real-time basis. Data monitoring on the simulation level was either at 5 or 15 minute intervals depending on the type of data used, so a five second interval was a vast improvement. SOC data in terms of available

amp-hours and maximum amp-hours was obtained for each of the 16 LiIon batteries, and then aggregated to a obtain total system SOC. Inverter power on the AC level and battery charger power on the AC level was monitored to give total DESD AC power at every time interval. AC power only mattered in terms of monitoring, which coincides with the inverter AC power monitored from the inverters (see Section A.4). AC grid power is also the most important variable in terms of Utility dispatchability, which is the primary motive of this experiment

Serial Communication with Fronius Interface Card

Fronius $10.0 - 1_{uni}$ inverters were originally installed with Fronius Datalogger Web for analysis and monitoring. This option allowed web-based access of data as well as historical data storage and analysis up to the five-minute level. For the real-time experiment, data needed to be obtained at much smaller intervals, down to the seconds level, to account for sudden changes in weather that do effect total system output.

Fronius also provides the Fronius Interface Card, which can monitor up to 100 inverters at once and provide real-time data to a PC or other data logging systems via RS-232 protocol (see Fig A.4). LabVIEW also has a VISA I/O protocol which can communicate with Serial ports as discussed in Section 4.1.2. Data could be observed at intervals at less than one second, which was more than optimal for monitoring real time changes in total system output power. For these reasons, the interface card was used as the data monitoring tool for the Fronius inverters. The only variable observed was total output power at each inverter, coinciding with simulation requirements. Though, the proprietary software allows access to dozens of variables including inverter current and power, irradiance, temperature, and others.

Serial communication had to be error checked to account for any erroneous values. An erroneous zero value for a single inverter's power output could heavily effect the P_{Diff} value and skew power commands to the DESD. For this reason, error checking existed as outlined in Equation 5.12.

$$IF P_{INV}(t) = 0, P_{INV}(t) = P_{INV}(t-1) \tag{5.12}$$

DESD and Inverter Integration

Overall, the logical flow of the Dispatchable Solar experiment was similar to the Dispatchable Solar Simulation (see Fig A.9). The main difference between the two was the addition of real time data acquisition (DAQ). DAQ took place on a 5 second interval in order to satisfy communication intervals of both the Fronius Interface Card and the Greensmith DESD UDP commands (see Sections 5.3.1 and 5.3.1). Therefore, the data acquisition horizon was 5 seconds, which was extremely small compared to the prediction horizon of 1 hour (720 per hour).

In order to find an optimal command horizon, which is the interval in between power commands to the DESD, a ramp time had to be determined for the inverters and battery chargers located in the Greensmith 6 kW DESD. After initial tests, I determined that a ramp time of 10-15 seconds was needed for the DESD to ramp up to its peak power of 6 kW. This ramp time was inconclusive due to the interval of status update messages from the UDP protocol (3-5 seconds). For this reason, the minimal command horizon used in my experiments was 20 seconds, in order to allow ample time for the DESD inverter and battery chargers to reach their commanded rate. Multiple command horizons were experimented with to determine the optimal length.

Finally, all relative data was stored in Excel files for optimal analysis. Values saved throughout the day in 5 second intervals included: Battery SOC, DESD Power, Fronius Inverter Power (1/4), and P_{Diff}.

5.3.2 Experiment Results

Overall, completely predictable solar on real-time hardware experiment results were not ideal. Due to sharp rises and falls of PV power output due to weather conditions, ramp rates of the Greensmith inverter were not ideal for compensating such large drop-offs with a command time of 20 seconds. Many PV power output dips would only last 5-15 seconds, and the inverter would attempt to firm these areas, and end up only over compensating the unaffected output after a dip. Experiments were run in the Summer of 2011 from May to August. Due to the timing of this research and availability of the systems in the FREEDM center, only these real time experiment results were obtained and further research should be done during other seasons of the year

Daily Specific Results

On June 3, almost perfect prediction results were achieved due to a clear sky day with near zero cloud interference. When minimal cloud cover occurred, the DESD could not keep up with the rapid changes in output power, and delayed ripples exist in total power (see Fig. 5.11). Sharp jumps in the total power output are due to this overcompensation with a command window of 20 seconds.

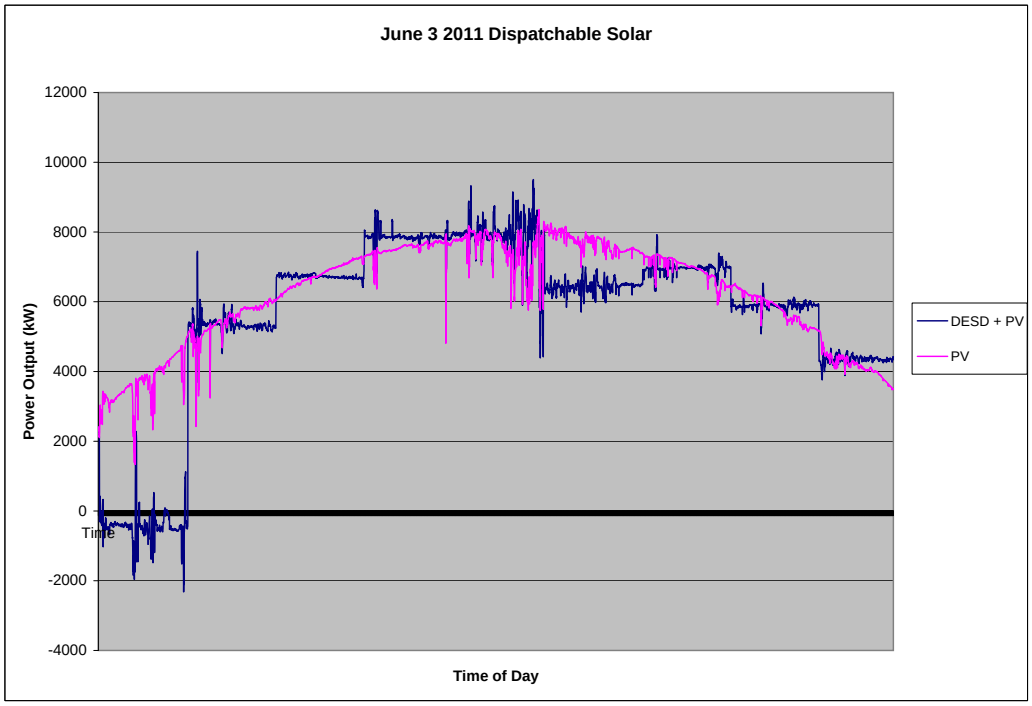

Figure 5.11: Experimental Results for an almost Cloudless Day. Most Predictions Are Achieved at the 20 Second Level, but Some Minimal Cloud Cover Causes Ripples

On June 26, almost perfect results were achieved due to a fairly predictable overcast day in which peak PV power output was well below rated power. Sharp changes in the PV output were minimal. It can be seen in after the daily peak that gradual PV power changes can be firmed quite well with the Greensmith system (see Fig. 5.12)

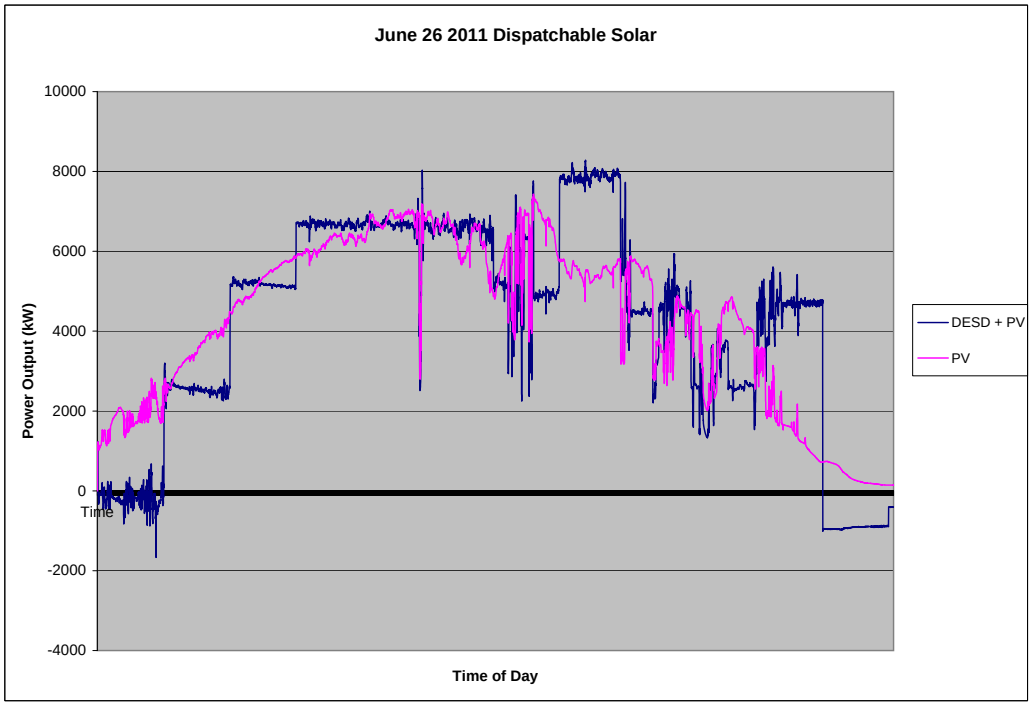

Figure 5.12: Experimental Results for an Overcast Day. Most Predictions Are Achieved at the 20 Second Level, but Some Minimal Cloud Cover Causes Ripples

On June 15, early and late hours were predictable due to minimal cloud cover with a basic gradual rise and fall of total PV power with relation to solar angle. Though during peak production hours, clouds were extremely prevalent and prevented proper dispatch of the solar power due to the ramp rate of the inverter, the provided command window, and extreme variation in cloud cover (see Fig. 5.13). Attempts to firm the output proved ineffective due to the random nature of the cloud cover.

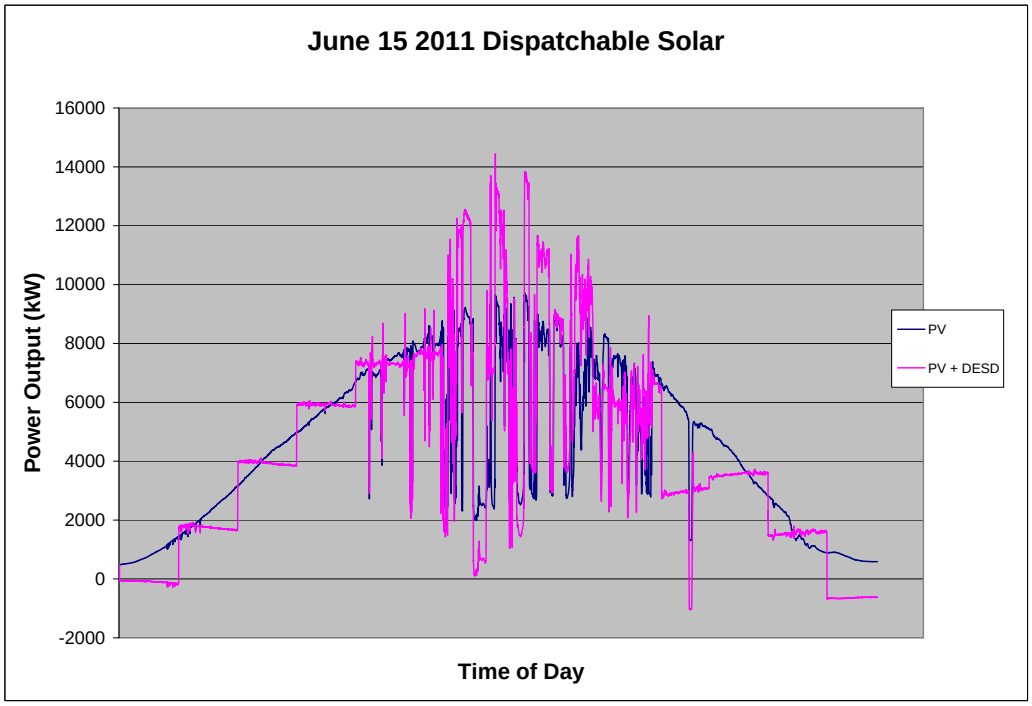

Figure 5.13: Experimental Results for a Cloudy Day During Peak Production Hours. Most Predictions Are Achieved at the 20 Second Level During Non Peak Hours. Proper Dispatch Was Not Achieved at Peak Hours due to Inverter Ramp Rates Much Lower than PV Power Slopes

On June 7, decent dispatch results were achieved for most of the day, but some cloud cover caused drastic changes in power around solar noon, in some cases on the magnitude of 5 kW on the seconds level, equating to half of the total potential PV power. Some positive results occurred towards the end of the day, when PV output power changed parabolically and the algorithm was able to dispatch the power based on predictions (see Fig. 5.14). The command window in this case was sufficient enough to account for the measuring window where changes were gradual.

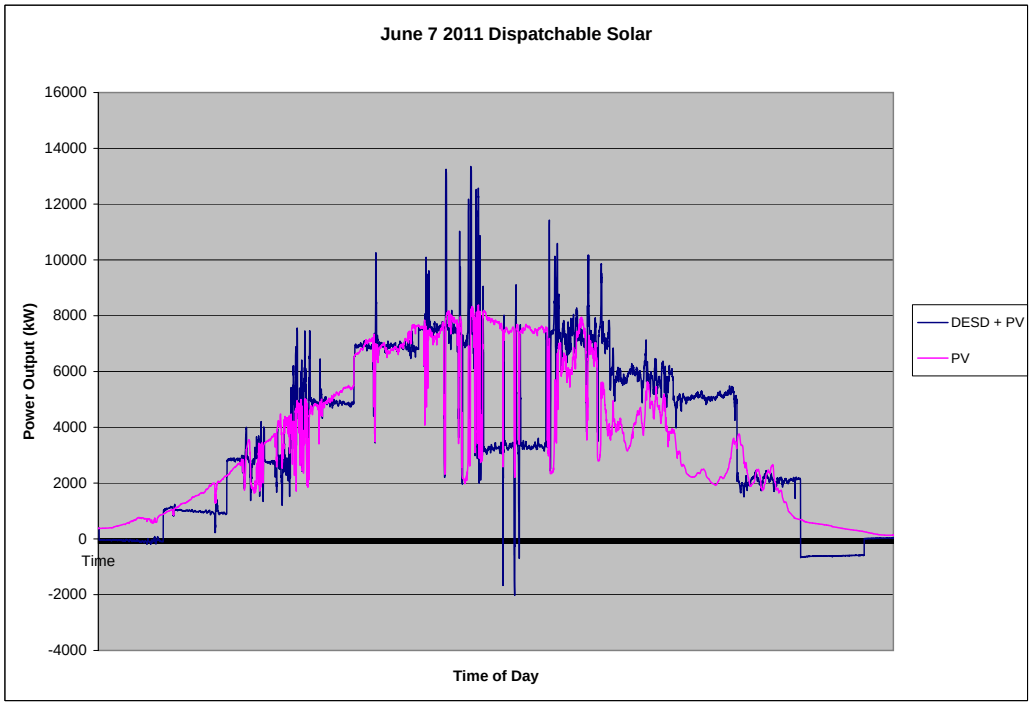

Figure 5.14: Experimental Results for a Sunny Day with Some Cloud Cover which Caused High Drops in Power. During These Times Dispatch Was Not Achieved. Positive Results Occurred in the Final Hours When Multiple Changing Slopes Were Firmed Properly

Compiled Results

Total results for all days were compiled, grouped into general types of days: mostly cloudy, cloudy, partly cloudy, and overcast. A ''Sunny Day" was left out because a complete sunny day was never recorded. Small amounts of cloud cover were seen during all measured days. In total, the experiment ran for 9 days during the months of May, June, July, and August of 2011.

Cloudy days typically required larger amounts of power to run the experiment, and also generated more prediction errors. As seen from the plotted results, the minimum required SOC to attempt to predict and firm solar power output hourly drops 15% depending on type of day (see Fig 5.15). Retained SOC, meaning the difference between the battery SOC at the beginning

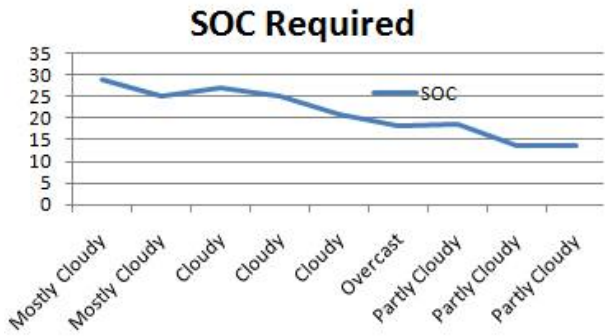

Figure 5.15: SOC Required to Perform Dipatchable Solar Under Different Conditions

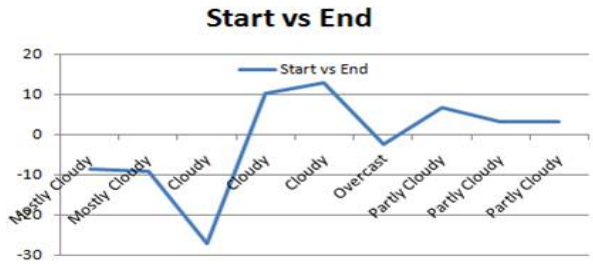

Figure 5.16: Start vs End SOC Required to Perform Dipatchable Solar Under Different Conditions.

of the day and end of the day after a firming experiment, is negative for cloudier days, up to 30% of the Greensmith SOC, and slightly positive for more clear or overcast days (see Fig 5.15). These two results show that cloudy days not only utilize a large amount of battery capacity, decreasing lifetime due to larger amounts of cycles utilized, but also on a day to day basis will not keep the SOC replenished. Back to back cloudy days, or periods of high precipitation, might gradually reduce battery SOC over time to a point where recharging is needed overnight, or firming experiments cannot be applied. This is important because large scale battery charging can be quite expensive, and becomes a cumbersome, large load introduced for the power grid to take on.

Relative, One Norm Error drops 30% from cloudy to partly cloudy days(see fig 5.17). This further confirms the idea that clouds cause unpredictable disturbances to solar power output due to their random shape, size, timing, and movement. Similarly, Relative Euclidean Norm between predicted and actual solar power output values drops 40%, and is not as linear a decline as the One Norm Relative Error (see Fig 5.18). This shows, based on the weight of errors for Euclidian Norms and the 10% increase in error from One Norm, that large prediciton errors are somewhat prevelant during the solar prediction and firming process. This was confirmed

Figure 5.17: Relative Error Incurred During Dipatchable Solar Under Different Conditions

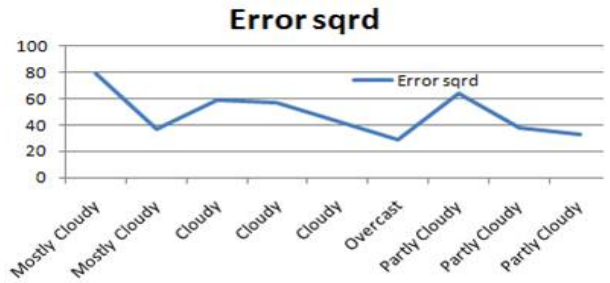

Figure 5.18: Euclidean Relative Error Incurred During Dipatchable Solar Under Different Conditions

for specific days, when sharp rises and falls of PV power occured up to 50% total solar power potential output (see Fig 5.14).

5.3.3 HMI

The final HMI is shown in Figure 5.19. Battery SOC, DESD Power, PV Power, and prediction errors are all plotted for easy experiment monitoring. Other functions are available for advanced users or administrators in the form of protocol error management, data monitoring before conversion, prediction calculations, and other features. All back end code links the Fronius Serial interface with the Greensmith BOS2, Ethernet based communication system. This cyber physical system utilizes an HMI for many reasons, please refer to the HMI section for further details (see Chapter 4).

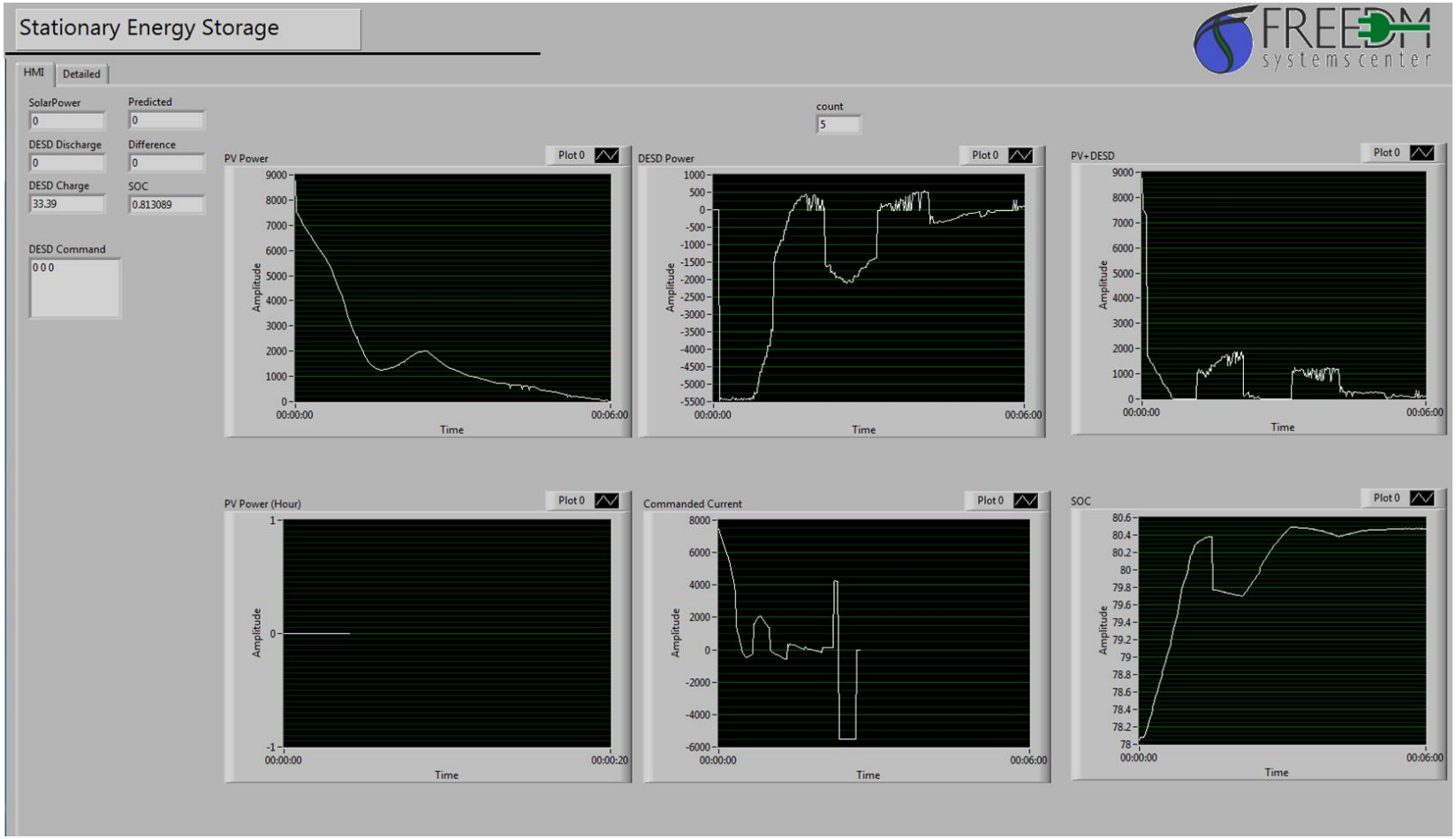

Figure 5.19: Dispatchable Solar Experiment HMI During Operation

5.4 Conclusion

Li-Ion batteries store energy via chemical reactions, and consequently have a chemically limited charge rate. DESD controls must prevent over/under voltage during charge/discharge cycles as well. Greensmith Control limits inverter ramp rate to 6 kW/ 20 sec, or 300 W/s, and therefore cannot follow rapid PV changes which are less than 20 seconds. This results in undershoot and consequent overshoot as seen in the results section. Batteries/Inverters cannot compensate by themselves and therefore a Super Capacitor or Flywheel is needed [36][37] to provide high stored power density over short periods of time where PV power fluctuates greatly.

Simulations proved successful, using simulated data from local PV generating farms and scaling due to size, only a 35% error was seen between actual data and simulated data. Cloudy days required some larger inverter sizes, and results were mostly random in correlation with time of year, with an average of 79% rated solar power. These values were much higher than in actual summer experiment results, showing that the less dynamic 15 minute command window causes unneccessary prediction errors. Cloudy days also had much higher minimum capacities due to the 15 minute command window, with an average of 39%, much higher than in the experimental data.

For clear sky days or overcast days, dispatchable solar is possible. For a 10 kW System, a DESD of 2.9 4.0 kWh, or 30-40% rated power, is needed. SOC stays relatively similar (-1%), or increases slightly during a day's operation.

For cloudy days, dispatchable solar needs more research and development in technology and software optimization. Results show that a 4.5 to 6.2 kWh system, or $\tilde{4}$5-60% Rated Power, is needed to attempt to dispatch solar power. Ending SOC is sporadic (-30% to +10%), making day to day SOC changes hard to determine, and might entail issues in the future for battery discharge over the course of a year.

Chapter 6

Conclusions and Future Work

Integration of BESS's and DESD's with Residential Households and PV Arrays via back end coding, cyber physical systems, and integrated HMI's, proved very successful in terms of development. HMI's were programmed with little technical difficulties, simulations included environmental variables and were tested for errors, and hardware systems were linked together via communication protocols to create fully functional cyber physical systems. Practically, there are limitations on the systems described in this experiment.

Conclusions:

- Cost cutting applied to residential and small scale commercial buildings with a BESS requires utility Peak/Off-Peak price adjustments
- Overall payback period for the initial cost of the BESS is less than 50 years with a 15 cent differential in peak and off peak rates
- Successful HMI's were built for the BDMF Charger and Solar Dispatch System with real time control and real time monitoring
- HMI's are aesthetically pleasing and functional
- BDMF charger has the infrastructure for multi-function ability built in
- Li-Ion batteries store energy via chemical reactions and consequently the charge rate is limited. This results in undershoot and consequent overshoot of PV prediction errors due to time delays brought on by the limitation
- For clear sky days or overcast days, dispatchable solar is possible
- For a 10 kW System, a DESD of 2.9 4.0 kWh, or 30-40%, rated power is needed

Future Work:

- Integration of a PV array for Free energy used for peak shaving
- Integrate the peak shaving study into a real time system (FREEDM Hardware) with real time demand monitoring via a smart-meter.
- HMI building process can be applied to other projects utilizing a DSP control approach
- For cloudy days, dispatchable solar needs more research. Results show a 4.5 6.2 kWh system, ~45-60% Rated Power, is needed
- Batteries/Inverters cannot compensate by themselves and therefore a Super Capacitor or Flywheel is needed [36] [37]

REFERENCES

[1] Renewable Energy Policy Network for the 21st Century (REN21), Renewables 2010 Global Status Report [Online]. Available http://www.ren21.net/Portals/97/documents/GSR/REN21_GSR_2010_full_revised%20Sept2010.pdf

[2] S. Teleke, "Rule-Based Control of Battery Energy Storage for Dispatching Intermittent Renewable Sources," *IEEE Transaction on Sustainable Energy*, Vol.1, No.3, October 2010

[3] S. Teleke.,*Control Methods for Energy Storage for Dispatching Intermittent Renweable Energy Resources,* MS Thesis, North Carolina State University, Raleigh, 2009.

[4] S. Telek, M. Baran, S. Bhattacharya, and A. Huang, "Optimal Control of Battery Energy Storage for Wind Farm Dispatching," *IEE Transactions on Energy Conversion*, Vol. 25, No. 3, Sept 2010, pp. 787-794.

[5] J. Dogger, B. Roossien, and F Nieuwenhout, "Characterization of Li-Ion Batteries for Intelligent Management of Distributed Grid-Connected Storage," *IEEE Transactions on Energy Conversions*, Vol. 26, No. 1, Mar. 2011, pp. 256-263.

[6] D.K. Maly and K.S. Kwan, "Optimal Battery Energy Storage System (BESS) Charge Scheduling with Dynamic Programming," *IEEE Proc.-Sci. Meas. Technol.*, Vol. 142, No 6., Nov. 1995, pp. 453-458

[7] R.E Bellman (1957). *Dynamic Programming.* Princeton, N.J: Princeton University Press.

[8] A Oudalov, R Cherkaoui, and A Beguin, "Sizing and Optimal Operation of Battery Energy Storage System for Peak Shaving Application," *Power TECH, 2007 IEEE Lausanne*, 2007, pp. 621-625

[9] A Whillier, "The Determination of Hourly Values of Total Solar Radiation from Daily Summations," *National Mechanical Engineering Research Institute, South African Council for Scientific and Industrial Research, Pretoria*, 1956, pp. 197-204

[10] P. C. Jain, "Estimation of Monthly Average Hourly Global and Diffuse Irradiation," *Solar & Wind Technology*, Vol. 5, No. 1, 1988, pp. 7-14

[11] P. C. Jain, "Comparison of Techniques for the Estimation of Daily Global Irradiation and a New Technique for the Estimation of hourly Global Irradiation," *Solar Wind Technol. 1*, 1984, pp. 123-134

[12] W Ji, C.K. Chan, J.W. Loh, F.H. Choo and L.H. Chen, "Solar Radiation Prediction Using Statistical Approaches," *Information, Communications, and Signal Processing 2009*, Dec 2009, pp. 1-5

[13] D. Gacek, O. Geynisman, D. Proudfoot, K. Minnick, "Migrating from SCADA to Automation," *Transmission and Distribution Conference and Exposition,"*, Vol 1., 2001, pp. 343-348.

[14] R. Reddi and A. Srivastava, "Real Time Test Bed Development for Power System Operation, Control, and Cyber Security," *North American Power Symposium (NAPS)*, Sept 2010, pp. 1-6

[15] X. Zhou and G. Wang, "Multi-Function Bi-Directional Battery Charger for Plug-in Hybrid Electric Vehicle Application," *Energy Conversion Congress and Exposition (ECCE)*, Sept 2009, pp. 2939-3936

[16] X. Zhou and G. Wang, "The Issue of Plug-In Hybrid Electric Vehicles' Grid-Integration and its Control Solution," *Energy Conversion Congress and Exposition (ECCE)*, Sept 2010, pp. 3596-3603

[17] Embedded Coder [Online]. MathWorks, 2011. Available http://www.mathworks.com/products/embedded-coder/

[18] Code Composer Studio (CCStudio) Integrated Development Environment (IDE) v3.3 [Online]. Texas Instruments Incorporated, 2011. Available http://focus.ti.com/docs/toolsw/folders/print/ccstudio3.html

[19] Charging The Lead-Acid Battery [Online]. Battery University and Cadex Electronics, 2011. Available http://batteryuniversity.com/learn/article/charging_the_lead_acid_battery

[20] NI LabVIEW Simulation Interface Toolkit (Link between LabVIEW and The MathWorks, Inc. Simulink ®. National Instruments Corporation, 2011. Available http://sine.ni.com/nips/cds/view/p/lang/en/nid/209048

[21] Creating GUIS with GUIDE [Online]. The MathWorks, Inc., 2011. Available http://www.mathworks.com/help/techdoc/creating_guis/bqz6p81.html

[22] NI LabVIEW DSP Test Integration Toolkit [Online]. National Instruments Corporation, 2011. Available http://zone.ni.com/devzone/cda/tut/p/id/5839

[23] Real Time Data eXchange (RTDX) [Online]. Texas Instruments Embedded Processors Wiki. Available http://processors.wiki.ti.com/index.php/Real_Time_Data_eXchange_-(RTDX)

[24] R. Brown (2010). *Business Essentials For Utility Engineers.* Boca Raton, FL: CRC Press.

[25] I. Ipsen (2009). *Numerical Matrix Analysis, Linear Systems and Least Squares.* Philadelphia, PA: Society for Industrial and Applied Mathematics.

[26] L. Xie and M. Ilic, "Model Predictive Economic/Environmental Dispatch of Power Systems with Intermittent Resources," *Power & Energy Society (PES) General Meeting*, 2009, pp 1-6.

[27] Greensmith Specification Sheet [Online]. Greensmith Energy Management Systems, LLC. 2010. Available http://greensmith.us.com/downloads/gs_specsheet.pdf

[28] Greensmith DESS 6kW Unit. Greensmith Energy Management Systems, LLC. 2010.

[29] REC AE-US High Performance Solar Modules [Online]. Renewable Energy Corporation ASA. Available http://www.recgroup.com/Global/REC_AE_series_US_version_E_WEB_-250110.pdf

[30] Fronius USA LLC [Online]. Fronius International GmbH. 2011. http://www.fronius.com/cps/rde/xchg/fronius_usa

[31] GRIDC Renewable Energy Data Acquisition System [Online]. GRIDC, Heliotronics. 2008. . Available http://www.gridc.net/

[32] Basic TCP/IP and UDP Communication in LabVIEW [Online]. National Instruments Corporation. 2011. Available http://zone.ni.com/devzone/cda/tut/p/id/4950 and http://zone.ni.com/devzone/cda/tut/p/id/2710

[33] Load Profiles [Online]. New Hampshire Electric Cooperative, Inc. 2011. Available http://www.nhec.com/rates_electricchoice_loadprofiles.php

[34] Residential Time Of Use Schedule [Online]. Progress Energy. 2011 Available https://www.progress-energy.com/assets/www/docs/company/NCScheduleR-TOUD.pdf

[35] Progress Energy Distribution Engineering Manual. Transformer section. Revised 1/31/2006. Protected information.

[36] N. Hasegwa, K. Fujimoto, T. Matsuyama, T. Ichikawa, K. Yukita, Y. Goto, and K. Ichiyangi. "Suppression of Power Variation for PV Using Flywheel and EDLC," *Transmission & Distribution Conference & Exposition: Asia and Pacific,*, 2009, pp 1-4.

[37] J. Cho and W. Hong. "Power Control and Modeling of a Solar-Ultra Capacitor Hybrid Energy System for Stand-Alone Applications," *2010 International Conference on Control Automation and Systems (ICCAS),*, 2010, pp 811-814.

APPENDIX

Appendix A

Appendix A - Datasheets

A.1 A First Section

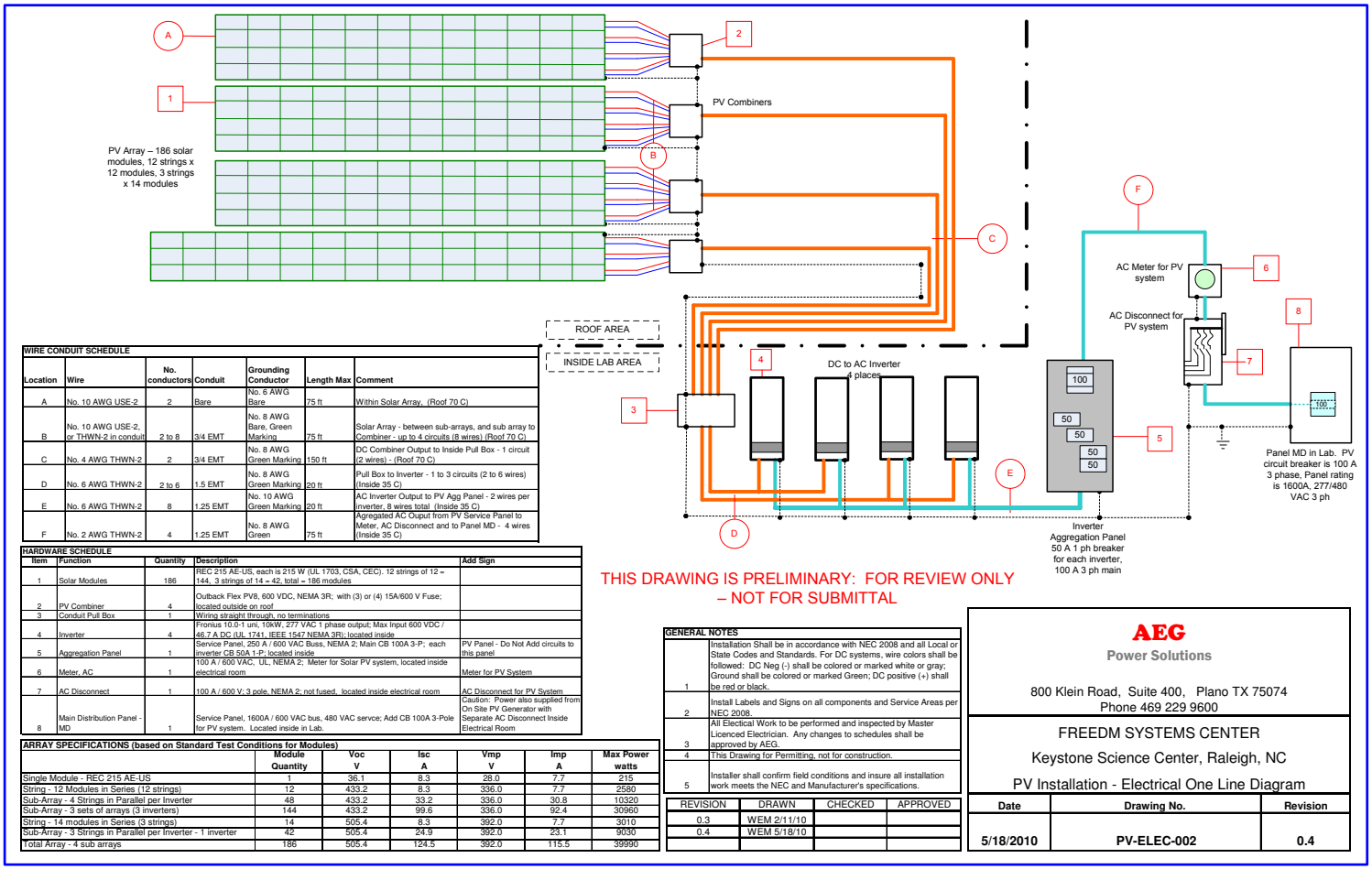

WIRE CONDUIT SCHEDULE

Location	Wire	No. conductors	Conduit	Grounding Conductor	Length Max	Comment
A	No. 10 AWG USE-2	2	Bare	No. 6 AWG Bare	75 ft	Within Solar Array, (Roof 70 C)
B	No. 10 AWG USE-2, or THWN-2 in conduit	2 to 8	3/4 EMT	No. 8 AWG Bare, Green Marking	75 ft	Solar Array - between sub-arrays, and sub array to Combiner - up to 4 circuits (8 wires) (Roof 70 C)
C	No. 4 AWG THWN-2	2	3/4 EMT	No. 8 AWG Green Marking	150 ft	DC Combiner Output to Inside Pull Box - 1 circuit (2 wires) - (Roof 70 C)
D	No. 6 AWG THWN-2	2 to 6	1.5 EMT	No. 8 AWG Green Marking	20 ft	Pull Box to Inverter - 1 to 3 circuits (2 to 6 wires) (Inside 35 C)
E	No. 6 AWG THWN-2	8	1.25 EMT	No. 10 AWG Green Marking	20 ft	AC Inverter Output to PV Agg Panel - 2 wires per inverter, 8 wires total (Inside 35 C)
F	No. 2 AWG THWN-2	4	1.25 EMT	No. 8 AWG Green	75 ft	Agregated AC Ouput from PV Service Panel to Meter, AC Disconnect and to Panel MD - 4 wires (Inside 35 C)

HARDWARE SCHEDULE

Item	Function	Quantity	Description	Add Sign
1	Solar Modules	186	REC 215 AE-US, each is 215 W (UL 1703, CSA, CEC). 12 strings of 12 = 144, 3 strings of 14 = 42, total = 186 modules	
2	PV Combiner	4	Outback Flex PV8, 600 VDC, NEMA 3R; with (3) or (4) 15A/600 V Fuse; located outside on roof	
3	Conduit Pull Box	1	Wiring straight through, no terminations	
4	Inverter	4	Fronius 10.0-1 uni, 10kW, 277 VAC 1 phase output; Max Input 600 VDC / 46.7 A DC (UL 1741, IEEE 1547 NEMA 3R); located inside	
5	Aggregation Panel	1	Service Panel, 250 A / 600 VAC Buss, NEMA 2; Main CB 100A 3-P; each inverter CB 50A 1-P; located inside	PV Panel - Do Not Add circuits to this panel
6	Meter, AC	1	100 A / 600 VAC, UL, NEMA 2; Meter for Solar PV system, located inside electrical room	Meter for PV System
7	AC Disconnect	1	100 A / 600 V; 3 pole, NEMA 2; not fused, located inside electrical room	AC Disconnect for PV System
8	Main Distribution Panel - MD	1	Service Panel, 1600A / 600 VAC bus, 480 VAC servce; Add CB 100A 3-Pole for PV system. Located inside in Lab.	Caution: Power also supplied from On Site PV Generator with Separate AC Disconnect Inside Electrical Room

ARRAY SPECIFICATIONS (based on Standard Test Conditions for Modules)

	Module Quantity	Voc V	Isc A	Vmp V	Imp A	Max Power watts
Single Module - REC 215 AE-US	1	36.1	8.3	28.0	7.7	215
String - 12 Modules in Series (12 strings)	12	433.2	8.3	336.0	7.7	2580
Sub-Array - 4 Strings in Parallel per Inverter	48	433.2	33.2	336.0	30.8	10320
Sub-Array - 3 sets of arrays (3 inverters)	144	433.2	99.6	336.0	92.4	30960
String - 14 modules in Series (3 strings)	14	505.4	8.3	392.0	7.7	3010
Sub-Array - 3 Strings in Parallel per Inverter - 1 inverter	42	505.4	24.9	392.0	23.1	9030
Total Array - 4 sub arrays	186	505.4	124.5	392.0	115.5	39990

GENERAL NOTES

1	Installation Shall be in accordance with NEC 2008 and all Local or State Codes and Standards. For DC systems, wire colors shall be followed: DC Neg (-) shall be colored or marked white or gray; Ground shall be colored or marked Green; DC positive (+) shall be red or black.
2	Install Labels and Signs on all components and Service Areas per NEC 2008.
3	All Electical Work to be performed and inspected by Master Licenced Electrician. Any changes to schedules shall be approved by AEG.
4	This Drawing for Permitting, not for construction.
5	Installer shall confirm field conditions and insure all installation work meets the NEC and Manufacturer's specifications.

REVISION	DRAWN	CHECKED	APPROVED
0.3	WEM 2/11/10		
0.4	WEM 5/18/10		

Figure A.1: FREEDM 40 kW Solar Array Single Line Diagram

REC AE-US SERIES

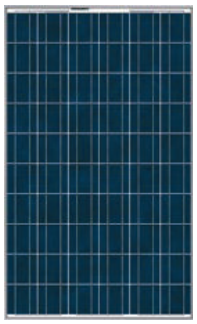

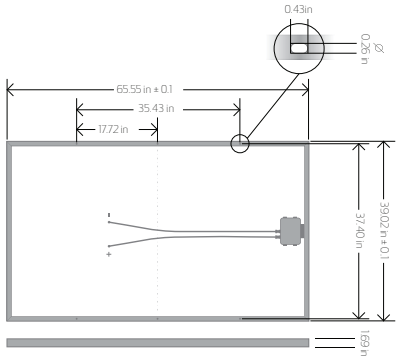

IV CHARACTERISTICS 215W MODULE

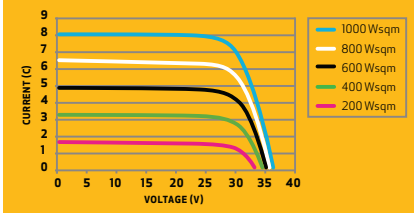

13.9 EFFICIENCY

63 MONTHS WORKMANSHIP WARRANTY

25 YEAR POWER OUTPUT WARRANTY

ELECTRICAL DATA @ STC	REC205 AE-US	REC210 AE-US	REC215 AE-US	REC220 AE-US	REC225 AE-US	REC230 AE-US
Peak Power Watts - P_{MAX} (Wp)	205	210	215	220	225	230
Watt Class Tolerance - P_{TOL} (W)	0/+5	0/+5	0/+5	0/+5	0/+5	0/+5
Watt Class Tolerance - P_{TOL} (%)	0/+2	0/+2	0/+2	0/+2	0/+2	0/+2
Maximum Power Voltage - V_{MPP} (V)	27.6	27.9	28.2	28.5	28.7	29.0
Maximum Power Current - I_{MPP} (A)	7.5	7.6	7.7	7.8	7.9	8.0
Open Circuit Voltage - V_{OC} (V)	35.8	36.1	36.3	36.5	36.7	36.9
Short Circuit Current - I_{SC} (A)	8.2	8.3	8.3	8.4	8.5	8.6
Module Efficiency (%)	12.4	12.7	13.0	13.3	13.6	13.9

Values at Standard Test Conditions STC (Air Mass AM 1.5, Irradiance 1000 W/m², Cell temperature 25 °C)

GENERAL DATA

Cell Type	156 x 156 mm multi-crystalline cells 60 cells in series - 3 strings of 20 cells
Glass	High-transparency solar glass with antireflection surface treatment by Sunarc Technology
Back sheet	Double layer high performance polyester
Frame	Anodized aluminium
Connectors	2 x 61 in (1.55m) solar cables with MC4 connectors

TEMPERATURE RATINGS (230W RATED MODULE)

Nominal Operating Cell Temperature (NOCT)	48.6°C (±2°C)
Temperature Coefficient of P_{MPP}	-0.497%/°C
Temperature Coefficient of V_{OC}	-0.370%/°C
Temperature Coefficient of I_{SC}	0.109%/°C

WARRANTY

10 years limited warranty of 90% power output
25 years limited warranty of 80% power output
63 months limited product warranty

CERTIFICATION

C US

Certified according to UL 1703 - 3rd edition
CEC/CSI listed

MECHANICAL DATA

Dimensions	65.55" x 39.02" x 1.69"
Area	17.76 ft²
Weight	48.50 lbs

MAXIMUM RATINGS

Operational Temperature	-40 ... +176°F [-40 ... +80°C]
Maximum System Voltage (UL 1703)	600V
Maximum Load (IEC 61215)	112 lbs/ft² (5400 Pa)
Design Load (UL 1703)	75.2 lbs/ft² (3600 Pa)
Wind Speed	122 mph (safety factor 3, 197 km/h)
Max Series Fuse Rating	15A
Max Reverse Current	15A

Note! Specifications subject to change without notice.

REC is the leading vertically integrated player in the solar energy industry. REC Silicon and REC Wafer are among the world's largest producers of polysilicon and wafers for solar applications. REC Solar is a rapidly growing manufacturer of solar cells and modules, and are also engaging in project development activities in selected segments of the PV market. REC had revenues of NOK 8 191 million and an operating profit of NOK 2 529 million in 2008. Close to 3 000 employees work in REC's worldwide organization.

For further information, contact your local distributor or visit our web site: **www.recgroup.com**

January 2010, version E

REC

REC Solar AS
Kjørboveien 29
1302 Sandvika
Norway

www.recgroup.com

Figure A.2: REC Solar Panel Datasheet [29]

INPUT DATA Fronius IG Plus V	3.0-1 UNI	3.8-1 UNI	5.0-1 UNI	6.0-1 UNI	7.5-1 UNI	10.0-1 UNI	11.4-1 UNI	11.4-3 Delta	12.0-3 WYE277
Recommended PV-Power (Wp)	2500-3450	3200-4400	4250-5750	5100-6900	6350-8600	8500-11500	9700-13100	9700-13100	10200-13800
MPPT-Voltage Range	230 ... 500 V								
DC Startup Voltage	245 V								
Max. Input Voltage (at 1000 W/m² 14°F (-10°C) in open circuit operation)	600 V								
Nominal Input Current	8.3 A	10.5 A	13.8 A	16.6 A	20.7 A	27.6 A	31.4 A	31.4 A	33.1 A
Max. usable Input Current	14.0 A	17.8 A	23.4 A	28.1 A	35.1 A	46.7 A	53.3 A	53.3 A	56.1 A
Admissible conductor size (DC)	No. 14 - 6 AWG								
Number of DC Input Terminals	6								
Max. Current per DC Input Terminal	20 A; Bus bar available for higher input currents								

OUTPUT DATA Fronius IG Plus V		3.0-1 UNI	3.8-1 UNI	5.0-1 UNI	6.0-1 UNI	7.5-1 UNI	10.0-1 UNI	11.4-1 UNI	11.4-3 Delta	12.0-3 WYE277
Nominal output power ($P_{AC\ nom}$)		3000 W	3800 W	5000 W	6000 W	7500 W	10000 W	11400 W	11400 W	12000 W
Max. continuous output power 104°F (40°C) 208 V / 240 V / 277 V		3000 W	3800 W	5000 W	6000 W	7500 W	10000 W	11400 W	11400 W	12000 W
Nominal AC output voltage		208 V / 240 V / 277 V							208 V / 240 V	277 V
Operating AC voltage range (default)	208 V	183 - 229 V (-12 / +10 %)								
	240 V	211 - 264 V (-12 / +10 %)								
	277 V	244 - 305 V (-12 / +10 %)								
Max. continuous output current	208 V	14.4 A	18.3 A	24.0 A	28.8 A	36.1 A	48.1 A	54.8 A	31.6 A*	n.a.
	240 V	12.5 A	15.8 A	20.8 A	25.0 A	31.3 A	41.7 A	47.5 A	27.4 A*	n.a.
	277 V	10.8 A	13.7 A	18.1 A	21.7 A	27.1 A	36.1 A	41.2 A	n.a.	14.4 A*
Admissible conductor size (AC)		No. 14 - 4 AWG								
Max. continuous utility back feed current		0 A								
Nominal output frequency		60 Hz								
Operating frequency range		59.3 - 60.5 Hz								
Total harmonic distortion		< 3 %								
Power factor		1								

GENERAL DATA Fronius IG Plus V		3.0-1 UNI	3.8-1 UNI	5.0-1 UNI	6.0-1 UNI	7.5-1 UNI	10.0-1 UNI	11.4-1 UNI	11.4-3 Delta	12.0-3 WYE277
Max. Efficiency		96.2 %								
CEC Efficiency	208 V	95.0 %	95.0 %	95.5 %	95.5 %	95.0 %	95.0 %	95.0 %	95.0 %	n.a.
	240 V	95.5 %	95.5 %	95.5 %	96.0 %	95.5 %	95.5 %	95.5 %	96.0 %	n.a.
	277 V	96.0 %	96.0 %	96.0 %	96.0 %	96.0 %	96.0 %	96.0 %	n.a.	96.0 %
Consumption in standby (night)		< 1.5 W								
Consumption during operation		8 W		14 W			20 W			
Cooling		Controlled forced ventilation, variable fan speed								
Enclosure Type		NEMA 3R								
Unit Dimensions (W x H x D)		17.1 x 26.5 x 9.9 in.		17.1 x 38.1 x 9.9 in.			17.1 x 49.7 x 9.9 in.			
Power Stack Weight		31 lbs. (14 kg)		57 lbs. (26 kg)			82 lbs. (37 kg)			
Wiring Compartment Weight		24 lbs. (11 kg)		26 lbs. (12 kg)			26 lbs. (12 kg)			
Admissible ambient operating temperature		-4 ... 122°F (-20 ... +55°C)								
Compliance		UL 1741-2010, IEEE 1547-2003, IEEE 1547.1, ANSI/IEEE C62.41, FCC Part 15 A& B, NEC Article 690, C22. 2 No. 107.1-01 (Sept. 2001)								

PROTECTION DEVICES Fronius IG Plus V	3.0-1 UNI	3.8-1 UNI	5.0-1 UNI	6.0-1 UNI	7.5-1 UNI	10.0-1 UNI	11.4-1 UNI	11.4-3 Delta	12.0-3 WYE277
Ground fault protection	Internal GFDI (Ground Fault Detector/Interrupter); in accordance with UL 1741-2010 and NEC Art. 690								
DC reverse polarity protection	Internal diode								
Islanding protection	Internal; in accordance with UL 1741-2010, IEEE 1547-2003 and NEC								
Over temperature	Output power derating / active cooling								

* per Phase

Fronius USA LLC Solar Electronic Division
10421 Citation Drive, Suite 1100, Brighton, Michigan, 48116
E-Mail: pv-us@fronius.com
www.fronius-usa.com

40,0006,2981,AE v02 2010

Figure A.3: Fronius 10.0.1 Inverter Datasheet [30]

FRONIUS IG INTERFACE CARD / BOX
FRONIUS IG DATALOGGER & INTERFACE

FRONIUS IG INTERFACE CARD / BOX

The FRONIUS IG Interface Card / Box has a **serial interface with an open data protocol** that enables the latest PV data to be downloaded from the inverter and processed. This will have the following advantages:

- Integration of system data in other IT systems (building control, alarm systems, etc.)
- Data transfer to PC for other visualisation purposes (e.g. to include PV data on a homepage)
- Interface to other data logging systems

Configuring the Interface Card / Box as a serial interface enables a PC or other devices to be connected. - As normal with FRONIUS IG DatCom components, power for the FRONIUS IG Interface Card (Box) is supplied by an inverter or a plug-in power pack.

The new standard interface from Fronius is compatible with all FRONIUS IG inverters. The only prerequisite is that a datalogger be present.

TECHNICAL DATA

Supply Voltage	12 V DC
Power consumption	**Card:** 1,2 W **Box:** 1,6 W
Protection class	**Card:** equal to the FRONIUS IG, in which the Card is installed **Box:** IP 20
Dimensions	**Card:** 140 x 100 x 26 mm (l x w x h) **Box:** 197 x 110 x 57 mm (l x w x h)
Connection area Interface Card / Box	RS 232-interface, 9-pole submin-socket „Data“
Additional pins Interface Box	RS 485-interface, RJ 45-socket „IN“ RS 485-interface, RJ 45-socket „OUT“
Adjustable baudrates	2400, 4800, 9600, 14400, 19200
Fronius Article-Numbers	**Card integrated: 4,240,009** **Card retrofit: 4,240,009,Z** **Box: 4,240,109**

01/2006 1

Figure A.4: Fronius Interface Card Datasheet [30]

GREENSMITH energy management systems

DESS 6kW Unit

DESS 6kW Unit Specifications	
Maximum Input Power	6 kW at 220/240 VAC, 50/60 Hz, 30 Amp
Maximum Output Power	6 kW at 220/240 VAC, 50/60 Hz, 30 Amp
Energy Storage Capacity	21kWh
Dimensions	5 ft x 3 ft x 4.6 ft
Weight	1,200 lbs
Operating Temperature	Standard -10° C to 40° C Optional -10° C to 70° C
Storage Temperature	-20° C to 60° C
Protection - Charger	High temperature, high current, reverse polarity
Protection - Inverter	Short-circuit, low voltage, high voltage, over frequency, under frequency, high temperature, reverse polarity

6701 Democracy Boulevard, Suite 300, Bethesda, MD 20817
Phone 888.882.7430 (US & Canada) 415.684.7746 (International)
Email info@greensmith.us.com

Figure A.5: Greensmith DESS 6 kW Unit Datasheet (1 of 2) [28] [27]

DESS 6kW Unit Specifications		
Protection - BMS	Battery over-discharge, over-charge, high & low voltage, high & low temperature, over & under-SOC, recalibration	
Overall BOS/SCADA	Overall real-time control & monitoring of both AC & DC voltage, current, temperature, frequency, battery SOC, battery calibration, and event management	
Network Communications	Direct Ethernet; XML/HTTP; Custom options available	
Batteries	Lithium-Ion Iron Phosphate (LiFePO4)	
Number of Battery Cells	16	
Cell Nominal Capacity	400Ah	
Cell Voltage Limits	Charge Discharge	4.0V 2.8V
Maximum Discharge	3C	
Maximum Charge	Constant Current Impulse Charge	3C 20C
Standard Charge/Discharge	0.5C	
Cycle Life, Cycles	80DOD% 70DOD%	>3,000 >5,000
Operating Temperatures	-45°C-85°C	
Self Discharge Rate	<3% Monthly	
Individual Cell Weight	30 lbs	
Software	BOSII direct operating environment Access to DESS Server for battery management Custom drop in control module optional	

6701 Democracy Boulevard, Suite 300, Bethesda, MD 20817
Phone 888.882.7430 (US & Canada) 415.684.7746 (International)
Email info@greensmith.us.com

Figure A.6: Greensmith DESS 6 kW Unit Datasheet (2 of 2) [28] [27]

GREENSMITH
energy management systems

One of the electric industry's first commercially available Smart Storage solutions, the ***Greensmith Distributed Energy Storage System (DESS)*** harnesses advanced lithium-ion battery technology to deliver numerous benefits to utilities and consumers alike. Proprietary advances in intelligent control allow Greensmith's Smart Storage Systems to interact with both advanced environments utilizing Smart Meters and the Smart Grid, and legacy environments not yet upgraded.

Two primary components of the DESS system, the DESS Client and the DESS Server, work together to improve overall system performance.

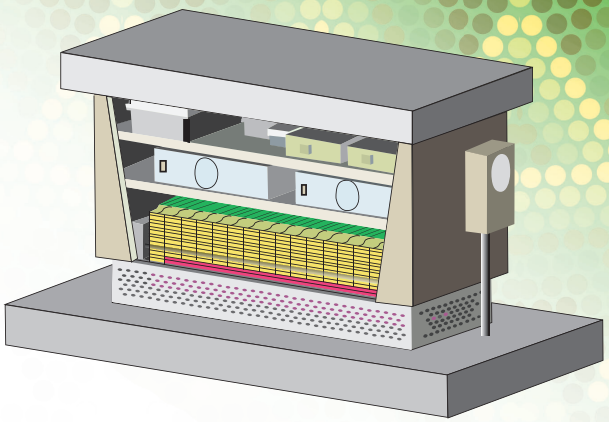

DESS CLIENT ENCLOSURE: Weatherproof, tamper-resistant metal enclosure suitable for mounting outdoors. Horizontal design model presented with an open front-facing view of the internal components.

Safe & Reliable Technology

Greensmith's highly durable Advanced Lithium-Ion Iron Phosphate Battery and proprietary Battery Management System perform at high efficiency for *at least 3000 life cycles*, and their real-time monitoring capabilities ensure *safety and compliance* within operating parameters.

Each unit connects through secure, platform-independent web services to optimize complex and comprehensive relationships. Modeled after the Department of Energy approved 'Open Automated Demand Response,' the Greensmith DESS leads the industry with its event-based asset management architecture and easily integrates into any utility framework.

Lithium-Ion Iron Phosphate (LiFePO4) Battery Pack	
Number of Battery Cells	16
Individual Cell Nominal Capacity	400 Ah
Individual Cell Operating Voltage	
Charge	4.25 V
Discharge	2.5 V
Max Charge Current	<-2
Max Discharge Current	
Constant current	<-2 ca
Impulse current	<-10
Standard Charge/Discharge Current	0.3 ca
Cycle Life, Cycles	
80% DOD	>=2000 times
70% DOD	>=3000 times
Temperature Durability of Case	<=250
Operating Temperature	
Charge	-25°_~75°_
Discharge	-25°_~75°_
Self Discharge Rate	<=3% (Monthly)
Individual Cell Weight	13.5 kg

GREENSMITH SMART STORAGE UNIT

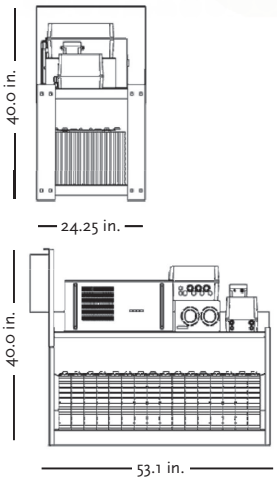

6701 Democracy Boulevard, Suite 300 | Bethesda, MD 20817
www.GREENSMITH.us.com | info@GREENSMITH.us.com

Figure A.7: reensmith 20 kWh Unit Specifications [27] (1 of 2)

Inverter Specifications, Model SC48-60 (Two per DESS Unit)

DC Input	
Input rated voltage (VDC)	48
Range of DC voltage (VDC)	40~60
Range discharging current (A)	60
DC current ripple (A)	<5%
AC Grid	
Rated grid voltage (Vac)	220
Range of grid voltage (Vac)	180-260
Rated grid current (A)	12
Distortion of grid current (THD)	<4%
Frequency range	48~52 (or 58~62 for 60Hz grid)
Grid-connected power factor (PF)	0.99
Efficiency	88%
Environmental Condition	
Installation environment	Indoor
Operating temperature	-10°C to 40°C
Storage temperature	-20°C to 60°C
Safety Insulation (M 'Ω)	
Insulating resistance	>5
Insulation strength	1500Vac per minute
Mechanical Parameters	
Size (L x W x H)	465 x 609.6 x 132.5
Weight (Kg)	17
Noise	<45
Grade of protection	IP21
Cooling method	Air cooling

Charger Specifications (Two per DESS Unit)

Input voltage	
AC	70. . .264 Vac 1-phase
DC	70. . .369Vdc
Efficiency	89% at full load, >90% at 50% load
Input Current	16 A (max)
Frequency	47-63Hz
Power Factor	>0.98
Inrush Current	Soft start
Output Ripple	<300mVrms
Mechanics	Wall mounting
Connectors	
Input	Input power cord
Output	Models 12V, 24V, 36V, 48V: copper bus-bar terminals
	Models 110V, 160V, 220V: 6mm2 1.5m output calbes
Enclosure	Aluminum case, IP20
Weight	7.1 kg without cables
Output Grounding	Floating
Ambient Temperature Range	-20°C. . .+40°C at full load
Over-Temperature Protection	Processor controlled
Over-Current Protection	Electrical current limit
Reverse Polarity Protection	With fuse
Standards Safety	Class 1
EMC	EN55022 Class A

GREENSMITH
energy management systems

How does Distributed Storage function like Centralized Storage?

An integrated modular unit, the DESS Client combines a Lithium-Ion Iron Phosphate (LFP) battery pack, a proprietary Battery Management System (BMS), a power conversion system, a remote communication layer, and an enclosure. Installed at the edges of the networks (220 V-240 V), the DESS Client provides local energy storage, available for variable power-level charge and discharge cycles, within the operating constraints of the battery management system. Depending on consumer needs, they deliver power of at least 5kW with total nominal and available energy of at least 20kWh and 15kWh, respectively.

Through a secure web-based user interface designed for either human interaction or automated machine-to-machine integration, the DESS Server remotely manages one or many DESS Clients through an event-based application with administrative configuration and reporting capabilities.

The highly flexible and reliable DESS executes charge/discharge under multiple parameters, and the open information architecture supports extended logic/application at both local and server levels. Greensmith's optimization of deployment allows a utility to tailor different groups of DESS clients to specific needs, while retaining the ability to centrally control any or all units. Additionally, the DESS allows for less specialized installation personnel due to lower voltage and turn-key solutions.

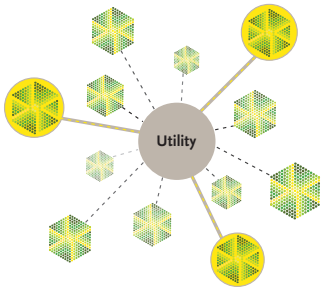

*The **Greensmith** DESS allows for centralized remote monitoring, control, and reporting, enabling the utility to not only respond to demand and grid events, but also to dispatch power across some or all of the deployed units.*

Printed on 100% recycled paper

Figure A.8: reensmith 20 kWh Unit Specifications [27]t (2 of 2)

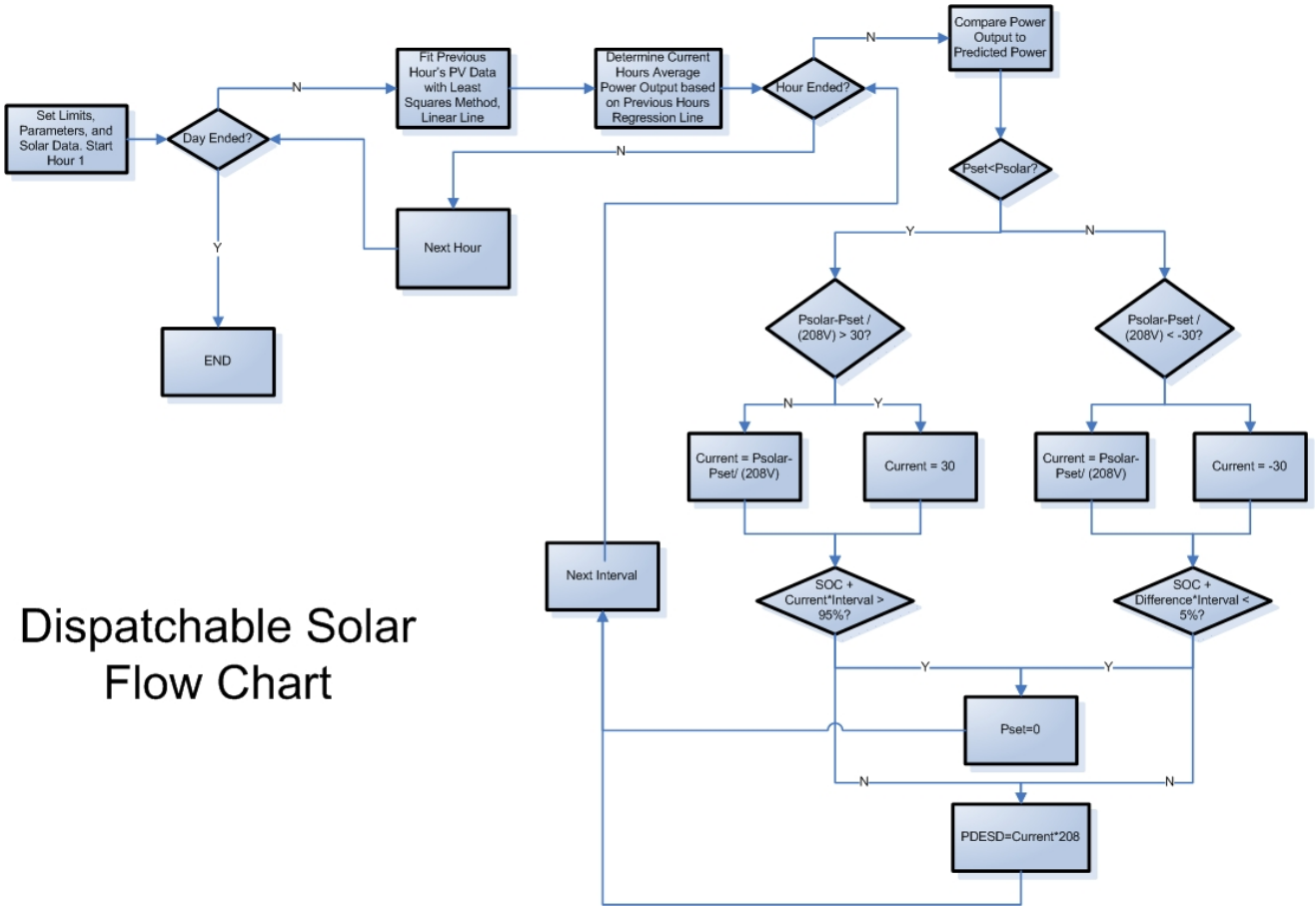

Figure A.9: Dispatchable Solar Simulations Flow Chart

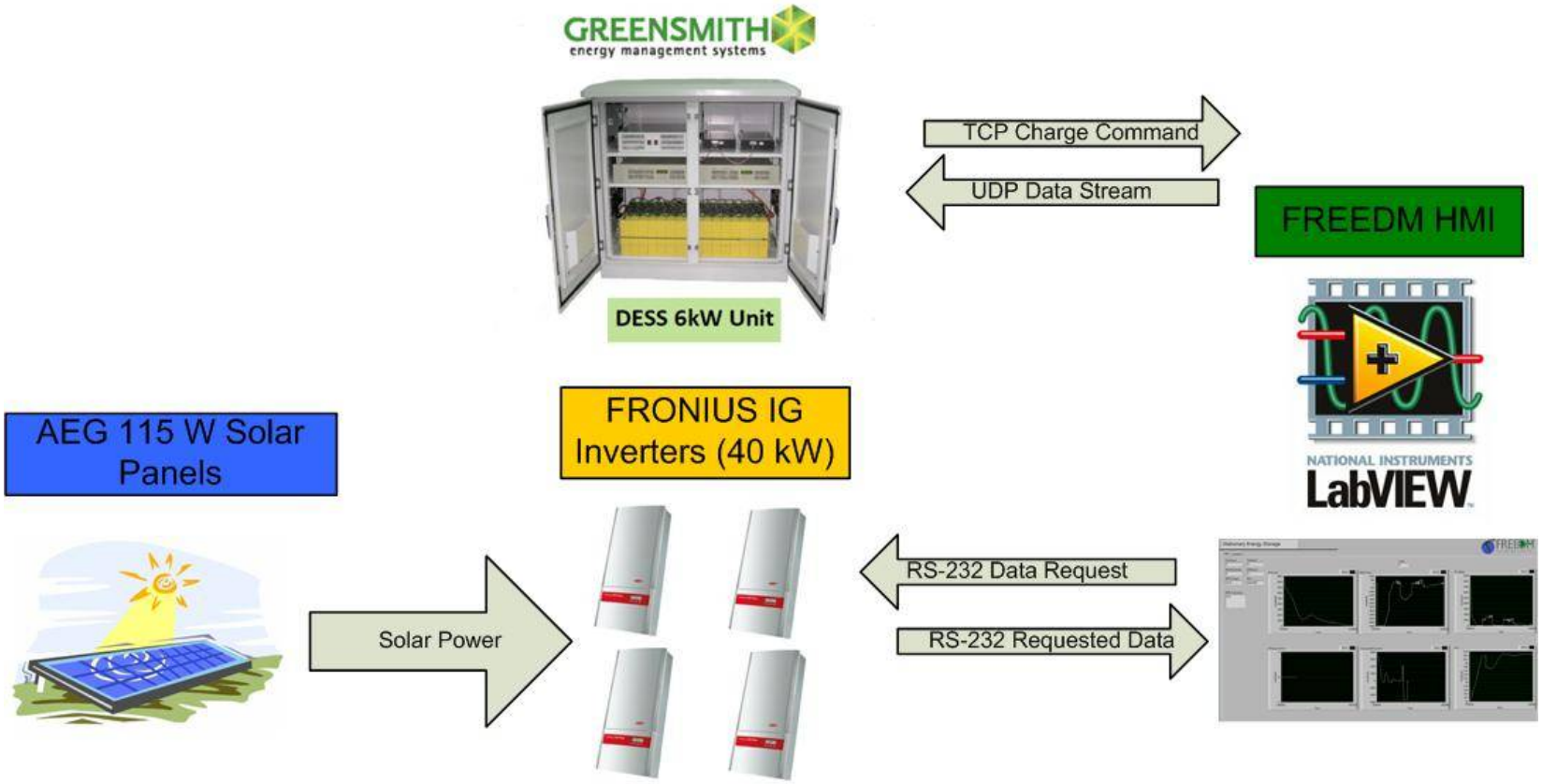

Figure A.10: Dispatchable Solar Experiment Hardware/Software Integration Flow Chart

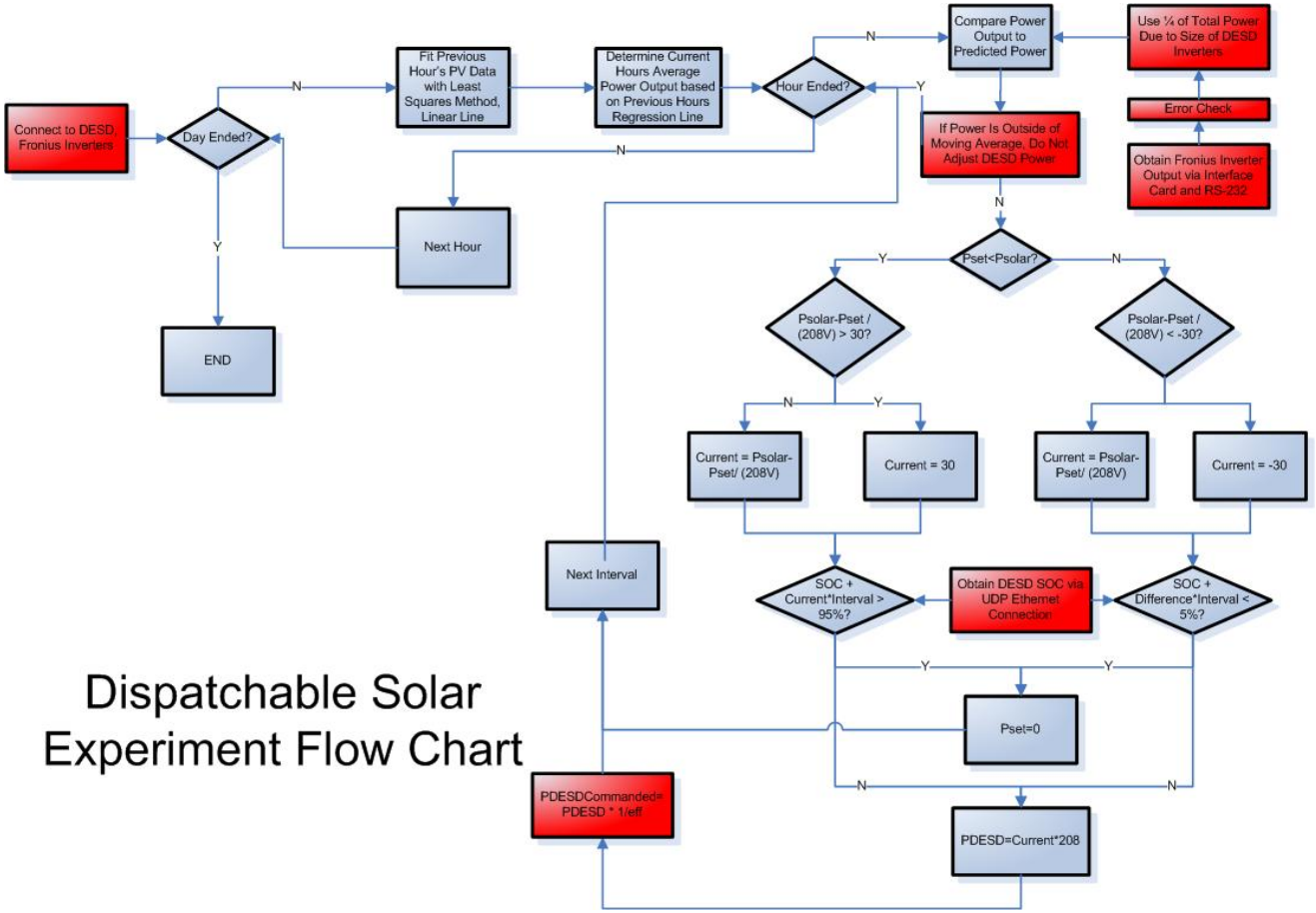

Figure A.11: Dispatchable Solar Experiment Flow Chart. Differences from Simulation are Highlighted in Red

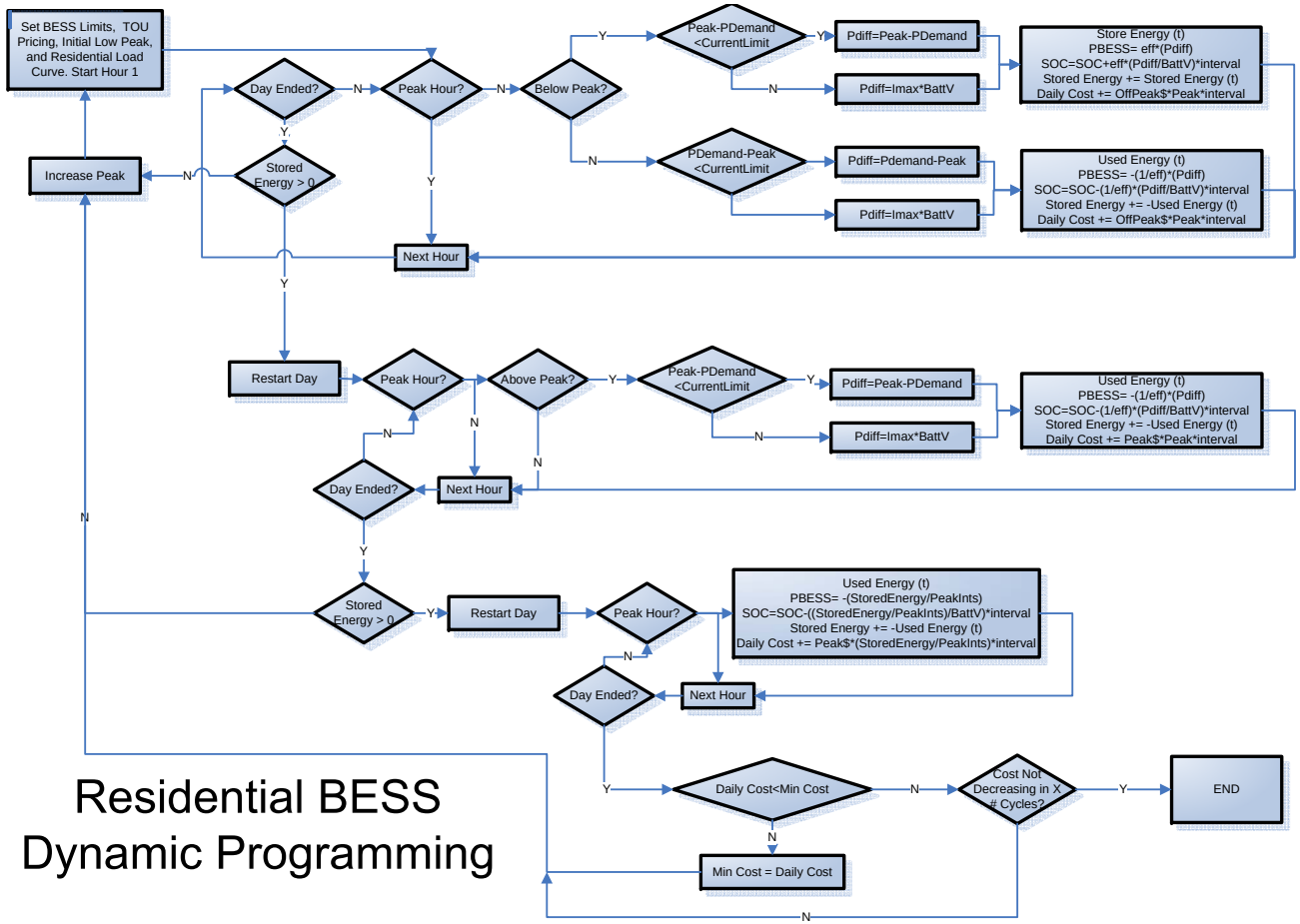

Figure A.12: Residential BESS Dynamic Code Flow Chart

RESIDENTIAL SERVICE
TIME-OF-USE
SCHEDULE R-TOUD-17

AVAILABILITY

This Schedule is available on a voluntary basis when electric service is used for domestic purposes in and about (1) a residential dwelling unit, including electric service used on a farm and in the preparation of the farm products for market, or (2) a family care home. A residential dwelling unit served under this Schedule may be used as a boarding house, fraternity house, tourist home, or like establishment, provided such residential dwelling unit is one which ordinarily would be used as a private residence. A family care home is defined as a home with support and supervisory personnel that provides room and board, personal care and habilitation services in a family environment for not more than six resident handicapped persons.

This Schedule is also available to customers served under the Residential Service Load Control Rider with applicable billing credits. Billing demands established and energy consumed by the load subject to control will be billed in accordance with this Schedule.

Service under this Schedule is not available: (1) for processing (or handling) for market of farm products produced by others; (2) for separately metered domestic or farm operations; (3) for individual motors in excess of 10 HP (in exceptional cases, motors as large as 15 HP may be served upon approval by the Engineering Department); (4) for commercial or industrial purposes; (5) for other uses not specifically provided for by the provisions herein; or (6) for resale service.

Nonfossil energy sources caused by acts of nature such as wind or solar are permitted as supplement to Customer's energy requirement provided Company is granted the right to install, operate, and monitor special equipment at Company's expense to measure Customer's load or any part thereof and to obtain any other data necessary to determine the operating characteristics and effects of the installation. In situations where special equipment is needed to assure safety, reliability, or metering accuracy, the installation of such equipment shall be at the Customer's expense.

APPLICABILITY

This Schedule is applicable to all electric service of the same type supplied to Customer's premises at one point of delivery through one meter.

TYPE OF SERVICE

The types of service to which this Schedule is applicable are alternating current, 60 hertz, either single-phase 2 or 3 wires, or three-phase 4 wires, at Company's standard voltages of 240 volts or less.

Figure A.13: Progress Energy TOU Rate Tarriff [34] (1 of 3)

MONTHLY RATE

I. For Single-Phase Service:

A. Service used during calendar months of June through September:

1. Basic Customer Charge: $9.85

2. On-Peak kW Demand Charge: $5.02 per kW for all on-peak Billing Demand

3. kWh Energy Charge: 6.377¢ per on-peak kWh 5.003¢ per off-peak kWh

B. Service used during calendar months of October through May:

1. Basic Customer Charge: $9.85

2. On-Peak kW Demand Charge: $3.73 per kW for all on-peak Billing Demand

3. kWh Energy Charge: 6.377¢ per on-peak kWh 5.003¢ per off-peak kWh

Minimum Bill

The minimum monthly charge shall be the Basic Customer Charge plus the REPS Adjustment.

II. For Three-Phase Service:

The bill computed for single-phase service plus $9.00.

III. Renewable Energy Portfolio Standard (REPS) Adjustment:

The monthly bill shall include a REPS Adjustment based upon the revenue classification:

Residential Classification - $0.58/month

Upon written request, only one REPS Adjustment shall apply to each premise serving the same customer for all accounts of the same revenue classification. If a customer has accounts which serve in an auxiliary role to a main account on the same premise, no REPS charge should apply to the auxiliary accounts regardless of their revenue classification (see Annual Billing Adjustments Rider BA).

BILLING DEMAND

The on-peak Billing Demand shall be the maximum demand used in the on-peak hours of the current month during any 15-minute interval.

DETERMINATION OF ON-PEAK AND OFF-PEAK HOURS

I. On-Peak Hours:

A. Service used beginning at 12:00 midnight March 31 and ending at 12:00 midnight September 30:

The on-peak hours are defined as the hours between 10:00 a.m. and 9:00 p.m., Monday through Friday, excluding holidays considered as off-peak.

R-TOUD-17 Sheet 2 of 3

Figure A.14: Progress Energy TOU Rate Tarriff [34] (2 of 3)

B. Service used beginning at 12:00 midnight September 30 and ending at 12:00 midnight March 31:

The on-peak hours are defined as those hours between 6:00 a.m. and 1:00 p.m., plus 4:00 p.m. through 9:00 p.m., Monday through Friday, excluding holidays considered as off-peak.

II. Off-Peak Hours:

The off-peak hours in any month are defined as all hours not specified above as on-peak hours. All hours for the following holidays will be considered off-peak: New Year's Day, Good Friday, Memorial Day, Independence Day, Labor Day, Thanksgiving Day and the day after, and Christmas Day. When one of the above holidays falls on a Saturday, the Friday before the Holiday will be considered off-peak; when the holiday falls on a Sunday, the following Monday will be considered off-peak.

SALES TAX

To the above charges will be added any applicable North Carolina Sales Tax.

PAYMENTS

Bills are due when rendered and are payable within 25 days from the date of the bill. If any bill is not so paid, Company has the right to suspend service in accordance with its Service Regulations. In addition, any bill not paid on or before the expiration of twenty-five (25) days from the date of the bill is subject to an additional charge of 1% per month as provided in Rule R12-9 of the Rules and Regulations of the North Carolina Utilities Commission.

CONTRACT PERIOD

The Contract Period shall be on a monthly basis. For a Customer who has previously received service under this Schedule or its predecessor, at the current location, the Contract Period shall not be less than one year.

GENERAL

Service under this Schedule is subject to the Company's Service Regulations, and any changes therein, substitutions therefore, or additions thereto lawfully made.

ADDITIONAL CHARGES

The Monthly Rate, shown above, includes the following approved charges as set forth in Annual Billing Adjustments Rider BA:

a) Fuel Adjustment Rate
b) Fuel Adjustment Experience Modification Factor
c) DSM/EE Rate
d) DSM/EE Experience Modification Factor

Supersedes Schedule R-TOUD-15
Effective for service rendered on and after December 1, 2010
NCUC Docket No. E-2, Subs 974, 976 and 977

R-TOUD-17 Sheet 3 of 3

Figure A.15: Progress Energy TOU Rate Tarriff [34] (3 of 3)